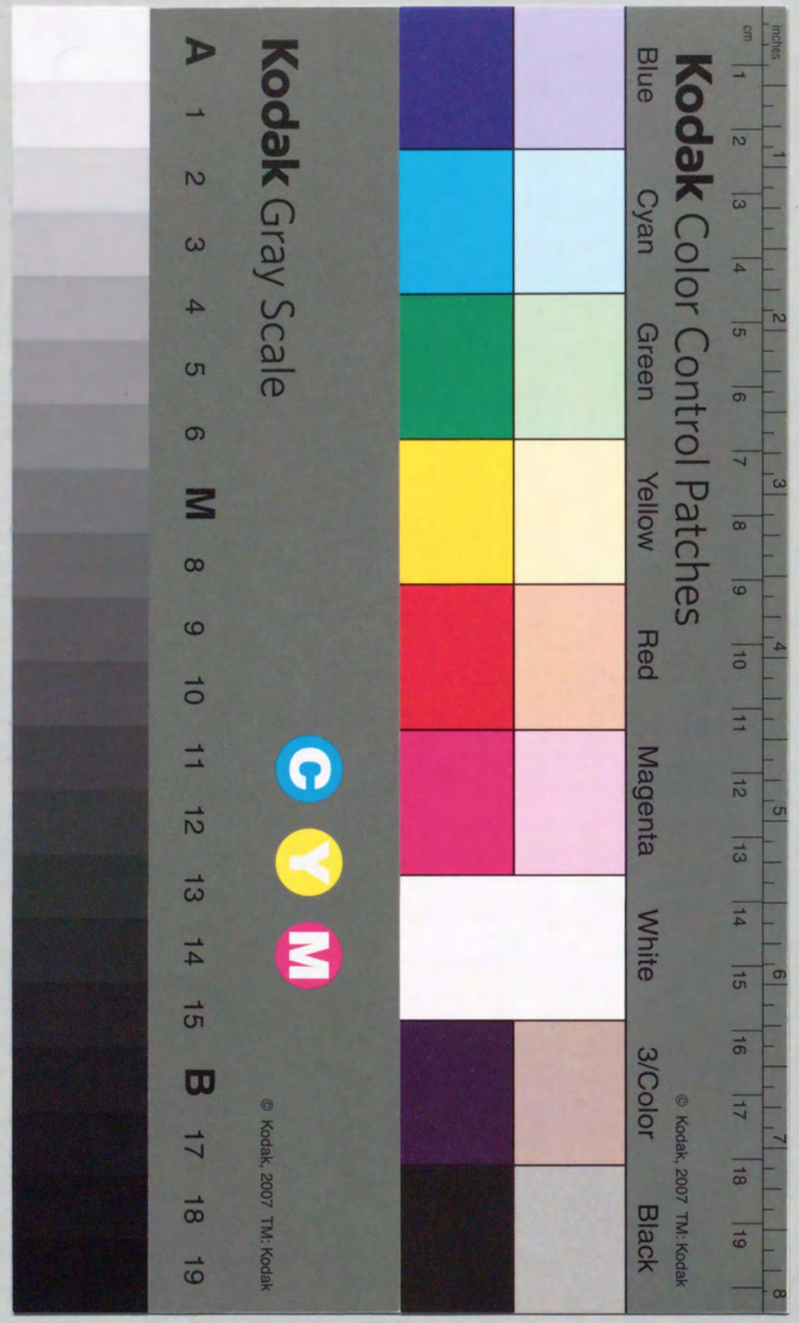

(1)

Effects of Molecular Orientation on the Rates of Formation of Excited CN Radicals in the Reactions of $Ar(^3P)$ with CX_3CN(X= H, D) and CF_3CN

Doctoral Dissertation

by

Dock-Chil CHE

Faculty of Science

Osaka University

1993

Effects of Molecular Orientation on the Rates of Formation of Excited CN Radicals in the Reactions of $Ar(^3P)$ with CX_3CN(X= H, D) and CF_3CN

Doctoral Dissertation

by

Dock-Chil CHE

Faculty of Science

Osaka University

1993

Abstract

Effects of molecular orientation on the rates of formation of the electronically excited CN radicals in the reactions of the $Ar(^3P)$ atoms with the oriented CX_3CN (X=H, D) and CF_3CN molecules were studied by use of a hexapole orienting field. The CN-end attack was more favorable for the formations of the excited CN radicals than the methyl-end attack in these reactions. However, the stereoanisotropies of the formations of the excited CN radicals in these reactions were dissimilar in each reaction.

In the reactions of $Ar(^3P)$ with acetonitrile and acetonitrile-d_3, the intensities of the CN(B→X) emission as a function of the collisional geometry, that is the CN-end to the methyl-end attack, were analyzed by the hard-sphere model, and it was found that the ratio of the reaction probability for the CN-end to that for the methyl-end attacks in the CH_3CN + Ar* reaction was about three. In the reaction of CD_3CN + Ar*, however, the stereoanisotropy became smaller than that in the CH_3CN reaction and the reaction cross-section for the formation of CN(B) increased. It reveals that the reaction branching of the formation of CN(B) is affected by the heavy atom substitution. The difference in stereoanisotropy suggests that the formation of CN(B) has at least two reaction processes which are relevant to anisotropic and isotropic molecular orbitals of acetonitrile. The effect of this molecular orientation in reaction was explained in terms of the spatial distribution of the molecular orbitals of molecule.

In order to investigate the relationship between the branching of the radical formation and the heavy atom substitution, the orientation dependence of the formation of CN(B) in the reaction of $Ar(^3P)$ with CF_3CN was studied. The effects of molecular orientation for the formations of CN(A) and CF_3* were also observed, and it was found the branching ratio of the formation of CF_3* is very small as compared to that of the formations of the excited CN radicals. The stereoanisotropies for both formations of CN(B) and CN(A) in reaction were almost equal to each other. The values were found to be 1.6 ± 0.2 in the

formation of CN(B), and 1.5 ± 0.2 in the formation of CN(A). These values are close to the $CD_3CN + Ar(^3P)$ reaction, but smaller than the $CH_3CN + Ar(^3P)$ reaction. In order to discuss the contributing molecular orbital in reaction, the opacity functions of the formations of CN(B) and CN(A) were obtained by the Legendre expansion technique, and these opacity functions are similar to each other was found. The shape of the opacity function was attributed to the molecular orbitals of the $7a_1$ which is localized at the CN-end and the 2e which is rather isotropic in the spatial distribution of electron. It shows the $7a_1$ and the 2e molecular orbitals contribute to the formations of the excited CN radicals. The similar orientation dependence of the formation of CN(B) and CN(A) indicates that both radicals originate from the same electronically excited state of CF_3CN. The reaction mechanism for both radical formations was discussed in terms of the electron exchange between the molecular orbitals and the atomic orbital of Ar* at the stage of the energy transfer from Ar*.

The emission spectra of the excited CN radicals were observed using a randomly oriented molecular beam to investigate the relationship between the the weight of the methyl group and the energy disposal of the formed radicals. The total emission cross-section and the vibrational energy disposal of the CN(B) radical were found to increase as the weight of the methyl group increases.

Contents

I. General Introduction

I-1. Oriented Molecular Beam

The idea that chemical reaction depends on the orientation of reagent molecule is one of the most intuitive concepts for chemists. Measurements of the steric effects in atom-molecule reactions can provide insight into anisotropies of interaction potential and the reaction dynamics.[1-4] However, because of the inherent difficulty in controlling the collisional geometry in the laboratory, only a handful of such experiments have been done to date.[5,6]

Several molecular beam methods to control molecular orientation or alignment have been reported.[6] To clarify the distinction between the oriented molecular beam and the aligned molecular beam, the schematic distributions of $\cos\theta$ using three type of the molecular beams are shown in figure I-1, where θ is the angle between the molecular axis and the fixed axis in laboratory frame. (Fig. a) For a randomly oriented molecular beam, the distribution of $\cos\theta$ is equally populated with $\cos\theta$. (Fig. b) The distribution of $\cos\theta$ for the aligned molecular beam has even symmetry with $\cos\theta$. It means that one end of molecule cannot be distinguished from another. For example, the aligned molecular beam can be obtained by removing the molecule of the unwanted aligned molecule from the beam by the photodissociation using the polarized laser.[7,8]

(Fig. c) The distribution of $\cos\theta$ for the oriented molecular beam has the asymmetric population with $\cos\theta$. The intuitive method for the molecular orientation is the "brute force" method which is merely applied a strong field on the polar molecule.[9,10] But this method is highly restrictive. It requires either very cold molecules or very high fields. The ensemble average of the orientational distribution in the reported experiments has been poor.

The most powerful method for elucidating the effect of the molecular orientation in reaction is the application of the hexapole electric field. In this

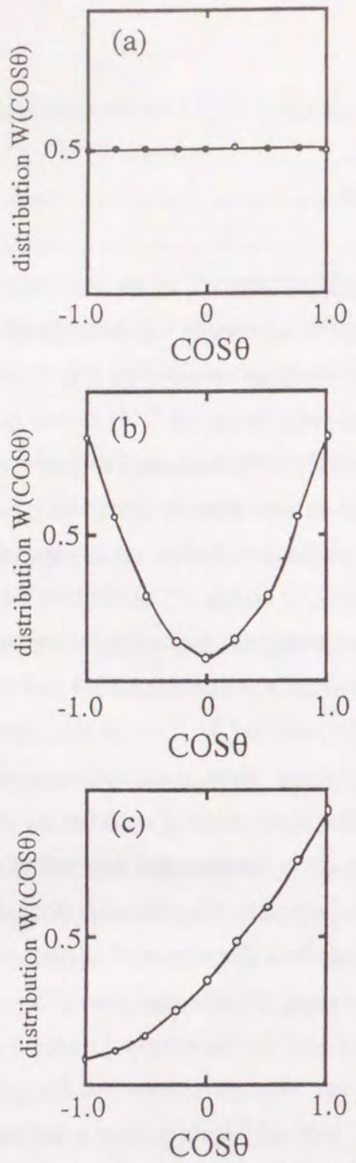

Figure I-1. Various possible distributions of cosθ using the molecular beam. θ is defined as the angle between the molecular axis and the direction of the electric field. (a) Distribution of the randomly oriented molecular beam. (b) Distribution of the aligned molecular beam. (note symmetry with respect to cosθ = 0) (c) Distribution of the oriented molecular beam.

method, the symmetric-top molecules, such as CF_3H, NH_3, and so on, can be easily oriented in the laboratory frame by the first-order Stark effect. The pioneering work in the field of the reactant orientation by use of the hexapole electric field has been carried out by the groups of Brooks and of Bernstein.[11,12] The first experiments for the effect of molecular orientation in reaction were performed on the reactions K + CH_3I and Rb + CH_3I. The results have shown that the KI and Rb products are formed preferentially when the alkali atom approaches the iodine end of the molecule. Stolte and co-workers have studied the O_3 + NO[13], N_2O + Ba[14], and Ca($^1D_2$) + CH_3F[15] reactions. In the O_3 + NO reaction system, the evidence was found for two distinct reaction mechanisms corresponding to different approach geometries. The orientation dependences of the chemiluminescent channel in the reaction of the metastable argon atom with molecule have been studied in our laboratory. The considerable orientation dependence of the formation of the excited radical have been observed in the reaction of CF_3H + Ar(^3P) and NH_3 + Ar(^3P).[16,17]

These experimental results tell us that chemical reaction considerably depends on the molecular orientation.

I-2. Orientation dependence in the reaction of metastable argon atom with molecule

The reactions of metastable rare-gas atoms such as Ar(3P) or Ar* with molecules have explicitly shown key roles of the molecular orientation because this type of reaction is likely to be initiated by an electron exchange in the energy transfer.[18] If the oriented molecular beam is used in the study of the reaction of Ar* with molecule, the molecular orbitals which contribute in reaction can be selected at the stage of the energy transfer. Especially, the reaction cross-section of the formation of the excited radical is a few $Å^2$[19], thus it is expected that only the trajectories with small impact parameter contribute in the radical

formation and the reaction occurs at the short-range part between Ar* and molecule.[16] Additionally, the emission from the excited radical can be sensitively detected by the photon-counting system, and the initial energy distribution of the formed radical can be determined by the measurement of the emission spectrum and the simulation of the spectrum.

In earlier work, the orientation dependence of the CF_3* formation in the reaction of CF_3H + Ar* has been observed, and it was found the shape of the opacity function of the formation of CF_3* can be attributed to the exchange interaction between the $6a_1$ molecular orbital of CF_3H and the atomic orbital of Ar*.[16] In the reaction of ammonia with Ar*, it has been shown that the $3a_1$ and 1e molecular orbitals of ammonia related to the alignment dependence of the NH_2* formation.[17]

The CN containing molecules such as CH_3CN has a nonbonding orbital which is localized at the CN-end. A large orientation dependence of the radical formation is expected in the reaction of the metastable argon atom because it has been shown the nonbonding orbital is more favorable than the sigma orbital in the electron exchange between the Ar* atom and molecule in the study of the Penning ionization electron spectroscopy (PIES).[20]

The electronic state of molecule should be unchanged by the deuterium substitution.[21] However, an enhanced CN(B) emission of the B→X transition for the CD_3CN + Ar* reaction as compared with the CH_3CN + Ar* reaction has been observed.[19] It has been explained that the branching ratio of the hydrogen atomization was decreased by the deuterium substitution and that of the formation of CN(B) increased. To investigate the relationship between the branching either to the formation of CN(B) or to the hydrogen atomization and the excitation of the molecular orbital by the electron exchange, the orientation dependences of the formations of the CN(B) radicals were studied in the reactions of the metastable argon atom with acetonitrile and acetonitrile-d_3. The experimental results were analyzed by a hard-sphere model and discussed in

terms of the spatial distribution of the molecular orbitals.

I-3. Effect of molecular orientation on the reaction branching

When the several products are formed simultaneously in a reaction, orientation of the reactant molecule is one of the dominant factors to determine the branching of reaction because the chemical reaction considerably depends on the molecular orientation. The dissimilar alignment dependence between the formations of the CS^+ ion and the CS*(A) radical have been observed in the reaction of metastable atom Ar(^{3}P), or Ar*, with the aligned CS_2 molecule. This result shows the reaction branching between the formations of the CS^+ ion and the CS*(A) radical depends on the molecular alignment.[22]

The reaction of the metastable argon atoms with molecules seems to be suitable for the study of the orientation dependence of the reaction branching because of the variety of the reaction channels such as dissociative excitation, fragmentation, excimer formation and so on.[18,23-25] The propensity rule of the orbital selection in the various reaction channels is of central interest in the reaction dynamics.

The reaction of Ar* with CF_3CN seems to suitable for the study of the relationship between the reaction branching and the selected molecular orbital because the formations of the CN(B), the CN(A), and the CF_3*($2A''_2$, 1E', and $2A''_1$) radicals are energetically accessible in this reaction and these radicals are directly detected by the emissions from the excited radicals.[26] Additionally, this reaction closely relates to the reaction of Ar* with acetonitrile, and is considered to be suitable for the study of the effect of the heavy mass substitution on the formation of CN(B). In the reaction of the metastable argon atom with CF_3CN, the orientation dependences of the formations of CN(B), CN(A) and CF_3* were studied, and the results were analyzed by the hard-sphere model in order to compare with the reaction of Ar* with acetonitrile. The opacity functions of these

radical formations were obtained by the Legendre polynomial expansion.[27] The reaction mechanism of the radical formations are discussed in terms of the exchange interaction between the molecular orbitals of molecule and the atomic orbital of $Ar(^3P)$.

This thesis consists of five chapters. In section II the theory and experimental setup for the oriented molecular beam are presented. In section III the initial energy distributions of the excited CN radicals in the reactions of Ar* with CX_3CN and CF_3CN using a randomly oriented molecular beam are given. In addition, the relationship between the weight of the methyl group and the reaction cross-section of the formation of CN(B) is discussed. Section IV gives the deuterium isotope effect on the orientation dependence of the formation of CN(B) in the reactions of Ar* with acetonitrile and its deuterate. In the section V, the opacity functions of the formation of CN(B) and CN(A) are given and the reaction mechanism of the branching between the these radicals is discussed.

References

[1] Dynamical Stereochemistry Issue, *J. Phys. Chem.* **91** (1987) ; Bernstein Memorial Issue, *J. Phys. Chem.* **95** (1991)

[2] R.B. Brooks, *Sience*. **193** (1976) 11

[3] R.B. Bernstein, D.R. Herschbach, R.D. Levine, *J. Phys. Chem.* **91** (1987), 5365; D.H. Parker, R.B. Bernstein, *Annu. Rev. Phys. Chem* **40** (1989) 561

[4] S. Stolte, *Ber. Bunsenges. Phys. Chem.* **86** (1982) 413

[5] G. Scoles, ed., *Atomic and Molecular Beam Methods*. **Vol 1** (Oxford Univ. Press, Oxford, 1988)

[6] R.D. Levine and R.B. Bernstein, *Molecular Reaction Dynamics and Chemical Reactivity*. (Oxford Univ. Press, Oxford, 1987)

[7] M.S. de Vries, V.I. Scdanov, C.P. Hanrahan, R.M. Martin, *J. Chem. Pyhs.* **77** (1982) 2688

[8] R.C. Estler, R.N. Zare, *J. Am. Chem. Soc.* **100** (1978) 1323; Z. Karney, R.C. Estler, R.Z. Zare, *J. Chem. Phys.* **69** (1978) 5199

[9] H.J. Loesch, A. Remscheod, *J. Chem. Phys.* **94** (1990) 4779; **95** (1991) 8194

[10] J.M. Rost, J.C. Griffin, B. Friedrich, D.R. Herschbach, *Phys. Rev. Lett.* **68** (1992) 1299; P.A. Block, E.J. Bohac, R.E. Miller, *Phys. Rev. Lett.* **68** (1992) 1302; B. Friedrich, H.-G. Rubahn, N. Sathyamurthy, *Phys. Rev. Lett.* **69** (1992) 2487

[11] R.B. Brooks, E.M. Jones, *J. Chem. Phys.* **45** (1966) 3449; R.B. Brooks, J.S. McKillop, H.G. Pippin, *Chem. Phys. Lett.* **66** (1980) 13; P. W. Harland, H.S. Carman, Jr, L.F. Phillips, P.R. Brooks, *J. Chem. Phys.* **95** (1991) 8137

[12] R.J. Beuhler, R.B. Bernstein, K.H. Kramer, *J. Am. Chem. Soc.* **88** (1966) 5331

[13] D. van de Ende, S. Stolte, *Chem. Phys.* **45** (1980); *Chem. Phys. Lett.* **76** (1980) 13; *Chem. Phys.* **89** (1984) 121

[14] H. Jalink, F. Harren, D. van de Ende, S. Stolte, *Chem. Phys.* **108** (1986)

391; H. Jalink, D.H. Parker, S. Stolte, *J. Chem. Phys.* **85** (1987) 5372; H. Jalink, S. Stolte, D.H. Parker, *Chem. Phys. Lett.* **140** (1987) 215
[15] M.H. Janssen, D.H. Parker, S. Stolte, *J. Phys. Chem.* **95** (1991) 8142
[16] H. Ohoyama, T. Kasai, K. Ohashi, K. Kuwata, *Chem, Phys. Lett.* **136** (1987) 236; H. Ohoyama, T. Kasai, K. Ohashi, K. Kuwata, *Chem. Phys.* **165** (1992) 155
[17] K. Ohashi, T. Kasai, D.-C. Che, K. Kuwata, *J. Phys. Chem.* **93** (1989) 5484
[18] D.H. Stedman, D.W. Setser, *Prog. React. Kinet.* **6** (1971) 4; D.W.Setser, *Annu. Rev. Phys. Chem.* **27** (1976) 407; J.A. Coxon, D.W. Setser, W.H. Duewer, *J. Chem. Phys.* **6** (1973) 2244
[19] K. Tabayashi, K. Shoubatake, *J. Chem. Phys.* **87** (1987) 2404
[20] K. Ohno, S. Matsumoto, K. Imai, Y. Harada, *J. Phys. Chem.* **88** (1984) 246
[21] M.N.R. Ashford, J.P. Simons, *Trans. Faraday. Soc. 2.* **74** (1978) 1263
[22] M.S. de Veries, G.W. Tyndall, C.L. Cobb, R.M. Martin, *J. Chem. Phys.* **86** (1987) 2653
[23] K. Johnson, J.P. Simons, P.A. Washington, A. Kvaran, *Mol. Phys. 57* (1986) 255
[24] T. Krumpelmann, T. Ottinger, *J. Chem. Phys.* **88** (1988) 5245
[25] T, Nagata, T. Kondow, K. Kuchitsu, K. Tabayashi, S. Ohshima, K. Shoubatake, *J. Chem. Phys.* **89** (1985) 2916
[26] M. Sut, N. Washida, *J. Chem. Phys.* **78** (1983) 1007; M. Suto, N. Washida, H. Akimoto, M. Nakamura, *J. Chem. Phys.* **78** (1983) 1019
[27] S. Stolte, K.K. Chakravorty, R.B. Bernstein, D.H. Parker, *Chem. Phys.* **136** (1982) 353

II. Orientation of Molecules

In this section, the theory and the experiment of the oriented molecular beam are described. In order to determine the orientation dependence of reaction, the orientational distribution of molecules of the molecular beam should be known. The orientational distribution of molecules is understood in a qualitative way from classical mechanics, although any detailed understanding of that require a quantum mechanical approach. The classical treatment for the molecular orientation is described first, and the detailed expression of the orientational distribution is discussed by the quantum treatment. In section II-2, the apparatus for orienting molecules and the measurement of the emission from the exited CN radical are described.

II-1. Theory of Oriented Molecular Beam

A. Energy of the Symmetric Top Molecule

In this thesis, the reactions of the metastable argon atoms with the symmetric-top molecules, such as CX_3CN, are studied. The symmetric-top molecules which has a electric dipole moment are oriented by use of the hexapole electric field, and the orientational distributions of the molecular beams are determined by the trajectory calculation.

In order to obtain the orientational distribution of molecules, the rotational energy distribution of the symmetric-top molecule is needed to be calculated. The behavior of the symmetric top is deduced from the classical mechanics.[1] Figure II-1 illustrated the classical motion of the symmetric-top molecule. The axis of molecule rotates around the total angular momentum P with the frequency that can be shown to be $\omega/2\pi = P/2\pi I_B$. At the same time the molecular axis may spin about its axis.[2]

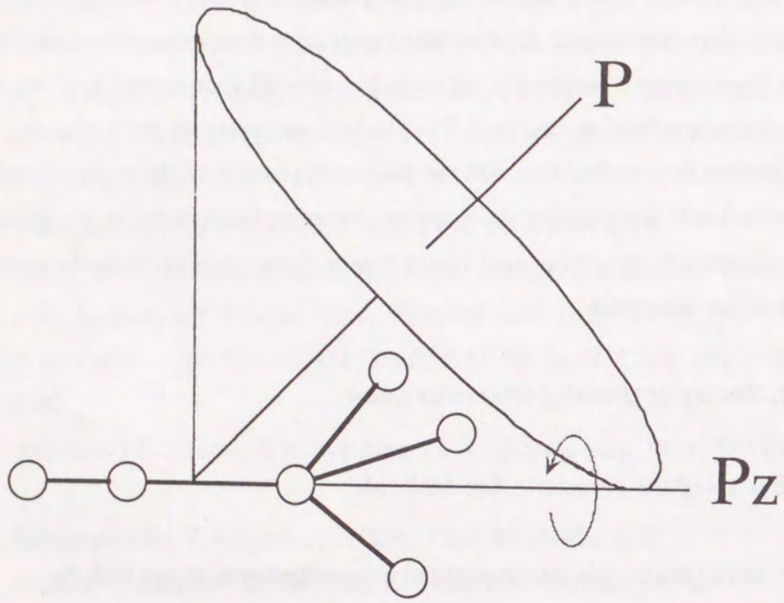

Figure II-1. Classical motion of a symmetric-top molecule. This is a combined rotation around the molecular axis associated with P_z and a precession of this axis around the total angular momentum P.

The energy of the rotation would be given by

$$W = \frac{1}{2}(I_x\omega_x^2 + I_y\omega_y^2 + I_z\omega_z^2) \qquad \text{(II-1)}$$

$$= \frac{1}{2}(\frac{P_x^2}{I_x} + \frac{P_y^2}{I_y} + \frac{P_z^2}{I_z}), \qquad \text{(II-2)}$$

where x, y, and z are directions along the principal axes of inertia, z being the symmetry axis of the molecule.

Because of the symmetric-top molecule, I_x and I_y are equal and will be both called as I_B, I_z will be designated as I_C. Using this fact, equation II-2 becomes

$$W = \frac{P^2}{2I_B} + P_z^2(\frac{1}{2I_C} - \frac{1}{2I_B}) \; . \qquad \text{(II-3)}$$

The square of the total angular momentum P^2 is quantized and equal to $J(J+1)h^2/4\pi^2$, where J is an integer. Similarly, the component of the angular momentum along some direction is quantized, so that $P_z^2 = K^2h^2/4\pi^2$, where K is an integer. Hence equation (II-3) becomes

$$W = \frac{J(J+1)h^2}{8\pi^2 I_B} + (\frac{h^2}{8\pi^2 I_C} - \frac{h^2}{8\pi^2 I_B})\,K^2 \qquad \text{(II-4)}$$

or

$$\frac{W}{h} = BJ(J+1) + (C-B)\,K^2$$

$$B = \frac{h}{8\pi^2 I_B}$$

$$C = \frac{h}{8\pi^2 I_c} \quad , \qquad \text{(II-5)}$$

where B and C are the rotational constants of the molecule.

Equation (II-5) gives the energy levels for a symmetric-top molecule. From this results, the fraction of molecules in a particular J, K state is expressed as

$$f_{JK} = \frac{(2J+1)e^{-[BJ(J+1)+(C-B)K^2]h/kT}}{\sum_{J=0}^{\infty}\sum_{K=-J}^{J}(2J+1)e^{-[BJ(J+1)+(C-B)K^2]h/kT}} . \qquad \text{(II-6)}$$

The more detailed discussion of the energy level of symmetric-top must take into consideration the nuclear effect. The usual type of symmetric-top has threefold symmetry about axis and the separation between inversion levels is negligible. In that case according to the reference,[2] the degeneracy due to the spin and inversion levels for each value of J and K is proportional to

$$S(I, K) = 2(4I^2 + 4I + 3) \text{ , when K is a multiple of 3, but not 0;}$$

$$S(I, K) = (4I^2 + 4I + 3), \text{ when K = 0.} \qquad \text{(II-8)}$$

Allowing for this degeneracy, equation (II-6) becomes

$$f_{JK} = \frac{S(I, K)(2J+1)e^{-[BJ(J+1)+(C-B)K^2]h/kT}}{\sum_{J=0}^{\infty}\sum_{K=-J}^{J}S(I, K)(2J+1)e^{-[BJ(J+1)+(C-B)K^2]h/kT}} . \qquad \text{(II-9)}$$

This is the expression of the fraction of the symmetric-top molecule in a particular J, K rotational state.

B. Stark Effects

When the molecule which has an electric dipole moment is in an electric field, the rotational energy of molecule is changed since the field exerts torques

on the molecular dipole moment. This type of effects can be understood in a qualitative way from the classical mechanics, although the detailed explanation about this effects requires a quantum mechanical approach.

Figure II-2 illustrated the case when the molecule is in a free field (a), and the case when the molecule is in an electric field (b). The dipole moment of molecule is defined by $\mu = ql$. In an electric field, the field exerts a torque on molecule as shown fig (b). The force from the field is $qE\sin\theta = \mu E\sin\theta$. Therefore, the energy W' which is required to rotate about θ from the equilibrium position, can be calculated equation (II-10)

$$W' = \int \mu E\sin\theta \, d\theta = -\mu E\cos\theta \ , \qquad \text{(II-10)}$$

where θ is defined by the angle between the dipole moment and the electric field.

For the quantum mechanical treatment, this energy should be solved according to the perturbation theory.[3] The quantum mechanical treatment of the Stark effect starts with the Hamiltonian and the wave equation.[4]

The rotational behavior of a symmetric-top molecule in the electric field is completely described by three angular momenta, J, K, and M. The rotational wave function Ψ_{JKM} of a symmetric-top molecule is characterized by the total angular momentum J, its projection K on the molecular axis, and its projection M on the space fixed axis of quantization, the electric field E as shown in figure II-3. The axis of molecule precesses around the total angular momentum J, and J precesses around the space fixed axis, that is Z axis.

When the center of mass is chosen as the origin of the space-fixed system, the relationship between the body-fixed and the space-fixed frames can be expressed by the Eulerian angle (ψ,ϕ,γ). Definitions of angles are given in reference. [4] The normalized rotational wave function Ψ_{JKM} has the explicit form

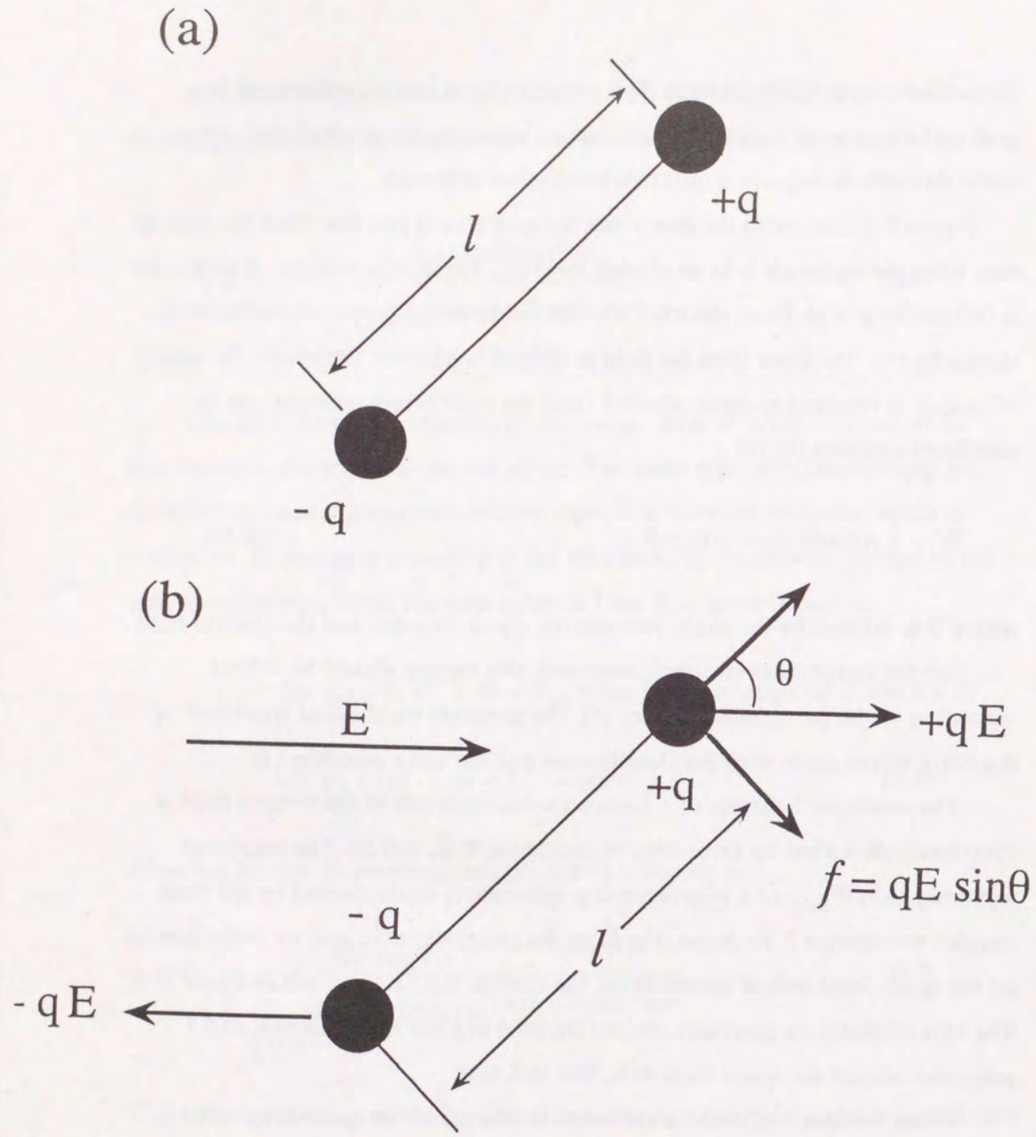

Figure II-2. The interaction between the electric field and the polar molecule. (a) The case when the molecule is in a free field (b) The case when the molecule is in a electric field.

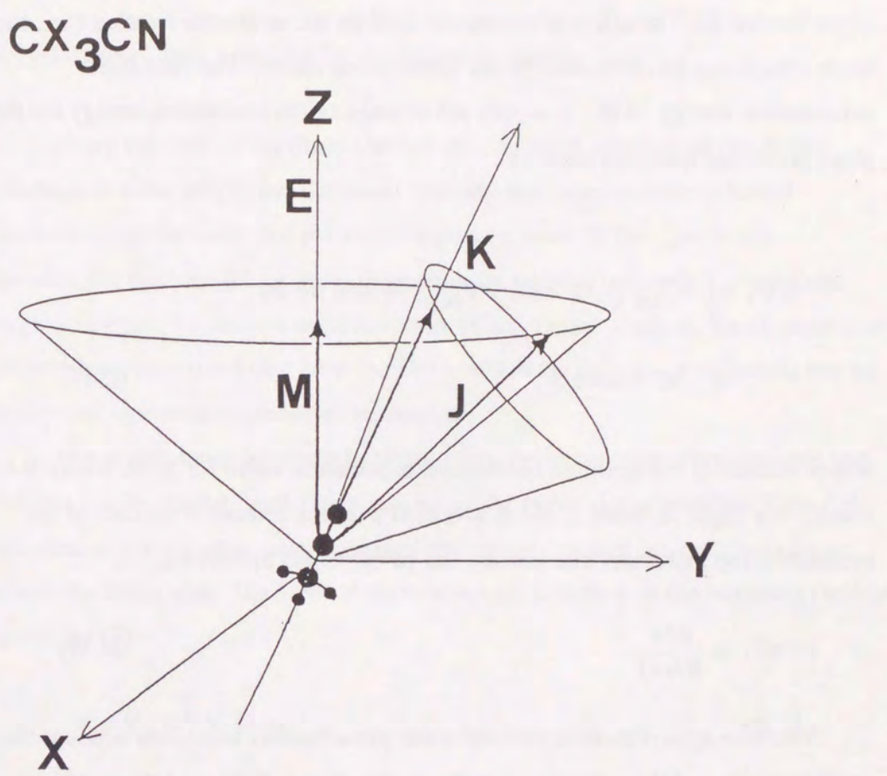

Figure II-3. Rotational behavior of a symmetric-top molecule in the electric field. The total angular momentum precesses around the axis of the electric field E, and the molecular axis precesses around the total angular momentum. The total angular momentum is defined by J, its projection on the molecular axis is defined K, and its projection on the electric field is defined by M.

$$\Psi_{JKM}(\psi,\theta,\phi) = (-1)^{M-K}\left[(2J+1)/8\pi^2\right]^{1/2} D^J_{KM}(\psi,\theta,\phi) \quad , \qquad \text{(II-11)}$$

where D^J_{KM} is the rotational function, i.e., the angular momentum eigenfunction.[4] The effect of an electric field on the molecular rotation (i.e., the Stark effect) can be calculated by the perturbation theory. The first-order perturbation energy ΔW_1 is simply the average of the interaction energy for the given rotational quantum state, i.e.,

$$\Delta W_1 = \int \Psi^*_{JKM} \left(-\mu E \cos\theta\right) \Psi_{JKM} \, d\phi \sin\theta \, d\theta \, d\psi$$

$$= -\mu E < \cos\theta > , \qquad \text{(II-12)}$$

where <cosθ> is the quantum mechanical expectation value for cosθ, where θ is exactly the angle between μ and E averaged over the rotational motion of the symmetric-top molecule. The <cosθ> can be expressed as follows:

$$\langle\cos\theta\rangle = \frac{KM}{J(J+1)}. \qquad \text{(II-13)}$$

The next approximation (second-order perturbation) takes into account the small distortion of the wave function due to the electric field, and the resulting energy is given as follows:

$$\Delta W_2 = \frac{\mu^2 E^2}{2Bh}\left\{\frac{(J^2-K^2)(J^2-M^2)}{J^3(2J-1)(2J+1)} - \frac{\left[(J+1)^2 - K^2\right]\left[(J+1)^2 - M^2\right]}{(J+1)^3(2J+1)(2J+3)}\right\}. \qquad \text{(II-14)}$$

It should be noted that the first-order Stark energy would be generally be much lager than the second-order Stark energy. For the CH_3CN molecule, the first-order Stark energy is larger about a factor of ~1000 than the second-order Stark energy in our experimental condition. Therefore, the second-order energy

is unimportant under this experiments. (The second-order Stark energy becomes to be important in the case of the orientation of the linear molecule or of the strong electric field.)

C. Rotational state selection by the hexapole electric field.

Using the type of the Stern-Gerlach electric field, the sign of the dipole moment is selected.[5] But the beam intensity decreases and the selected molecules are focused on a particular region in space. If the type of the quadrupole electric field is used, the molecular beam is focused on a particular region in space by the second-order Stark effect. In this method, the alignment of molecules are selected (see equation II-14, where the $|M|$ can be selected) but the molecular orientation cannot be selected.[6]

The electrostatic hexapole field can focus the symmetric-top molecules that exhibit the first-order Stark effect and select the molecular orientation. This field consists of six rods alternately charged and equally spaced on a circle centered about the beam axis. The form of the equipotential surface in the hexapole field is given by [7]

$$V = V_0 \left(\frac{r}{r_0}\right)^3 \cos\phi \, , \qquad \text{(II-15)}$$

where the cylindrical coordinates(r, θ, z) are taken such that z axis coincides with the beam axis. The absolute strength of the electric field is given by

$$\left|\vec{E}\right| = \left(\frac{3V_0}{{r_0}^3}\right) r^2 \, , \qquad \text{(II-16)}$$

and does not depend on φ. This expresses the field strength of the electric field inside of a hexapole.

The equation of motion becomes

$$F = m\frac{d^2r}{dt^2} = -\mu\cos\theta\frac{\partial E}{\partial r}$$

$$= -\left(\frac{6V_0\mu}{r_0^3}\right) r\cos\theta$$

$$= -k\,r\cos\theta\ , \qquad \text{(II-17)}$$

where r_0 is the radius of the field assembly, r is the radial displacement of the molecule, V_0 is the rod voltage with respect to the axis, and m is the mass of molecule. By solving equation (II-17), the trajectory of a symmetric-top molecule in the hexapole electric field is determined.[8,9] For molecules with the positive sign of cosθ, the force is directed toward the axis, resulting in harmonic motion. For molecules with the negative sign of cosθ, the molecules are defocused. Solving this equation for r, it is found that

$$r_x = r_{inc}\cos\left[\alpha(x-x_2)/v\right] + (v/\alpha)\,(r_{inc}/x_2)\sin\left[\alpha(x-x_2)/v\right] \qquad \text{(II-18)}$$

for the focused molecules, and

$$r_x = \frac{r_{inc}}{2}\left[\frac{v}{\alpha x_2} + 1\right]\exp\left[\frac{\alpha(x-x_2)}{v}\right] + \frac{r_{inc}}{2}\left[\frac{v}{\alpha x_2} - 1\right]\exp\left[-\frac{\alpha(x-x_2)}{v}\right]$$

(II-19)

for the defocused molecules.

Here, r_{inc} is the radical position at the field entrance, and $\alpha = (k/m)^{1/2}$, v is the stream velocity of molecular beam. Three types of trajectories of molecule in the hexapole field (cosθ is 0, positive, and negative) are schematically shown in figure II-4. By the trajectory calculation, the distribution of cosθ of the molecular beam at the particular region can be determined.

A typical number of trajectories was 1×10^6 and this number was found to

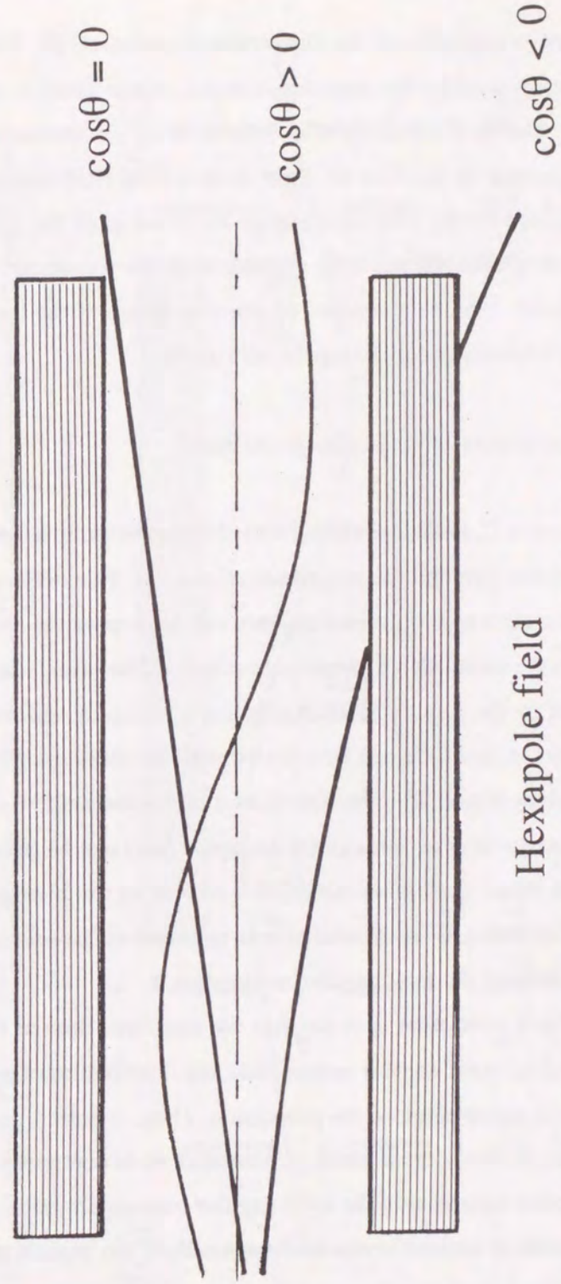

Hexapole field

Figure II-4. Various motion of molecule with the dipole moment μ in a hexapole electric field. In case of μ= 0, trajectory is not changed. In case of μ<0, the molecule defocused out of the hexapole field. In case of μ>0, the trajectory is the harmonic motion.

be sufficient to regard as ensemble of the trajectories as statistical.[9] The experimental parameters used for the trajectory simulation are listed in table II-1 and figure II-5. The velocity distribution of molecules in the molecular beam was experimentally determined by the time of flight method.[10] Boltzmann distribution was assumed for the rotational energy distribution of the CX_3CN molecule. The trajectory simulation is only dependent on the rotational temperature of the beam. It was determined by the simulation of the dependence of the focused beam intensity on the hexapole voltage V_0.

D. Orientational distribution of molecules in the beam.

As shown in section *C*, the molecule is focused or deflected in a hexapole field depending upon the sign and the magnitude of <cosθ>. This deflection using the hexapole field as a state selection filter enables one to prepare the molecular beam which has only the molecules with positive <cosθ>. The orientation of molecules is achieved by the passing adiabatically into a region of uniform field. Finally, the state selected molecule can be oriented with the laboratory frame.[11]

From the trajectory simulation, the distribution of the transmitted molecules with the particular rotational state through the hexapole field can be determined. Figure II-6 shows the result of the distribution of $< \cos\theta >$ by the histograms. In this treatment, the distribution of molecular axis is regarded as the average of the precessional motion around the total angular momentum J.

If the collision time in reaction is larger than the rotational time of the molecular axis around the total angular momentum, the distribution of molecular axis can be regarded as the average of the precession. Then, $< \cos\theta >$ is a good approximation. If the collision time is small or comparative as compared with the rotation of the molecular axis around the total angular momentum, the orientational distribution of molecules should be considered the motion of precession. (The distribution of <cosθ> is not the same as the distribution of the

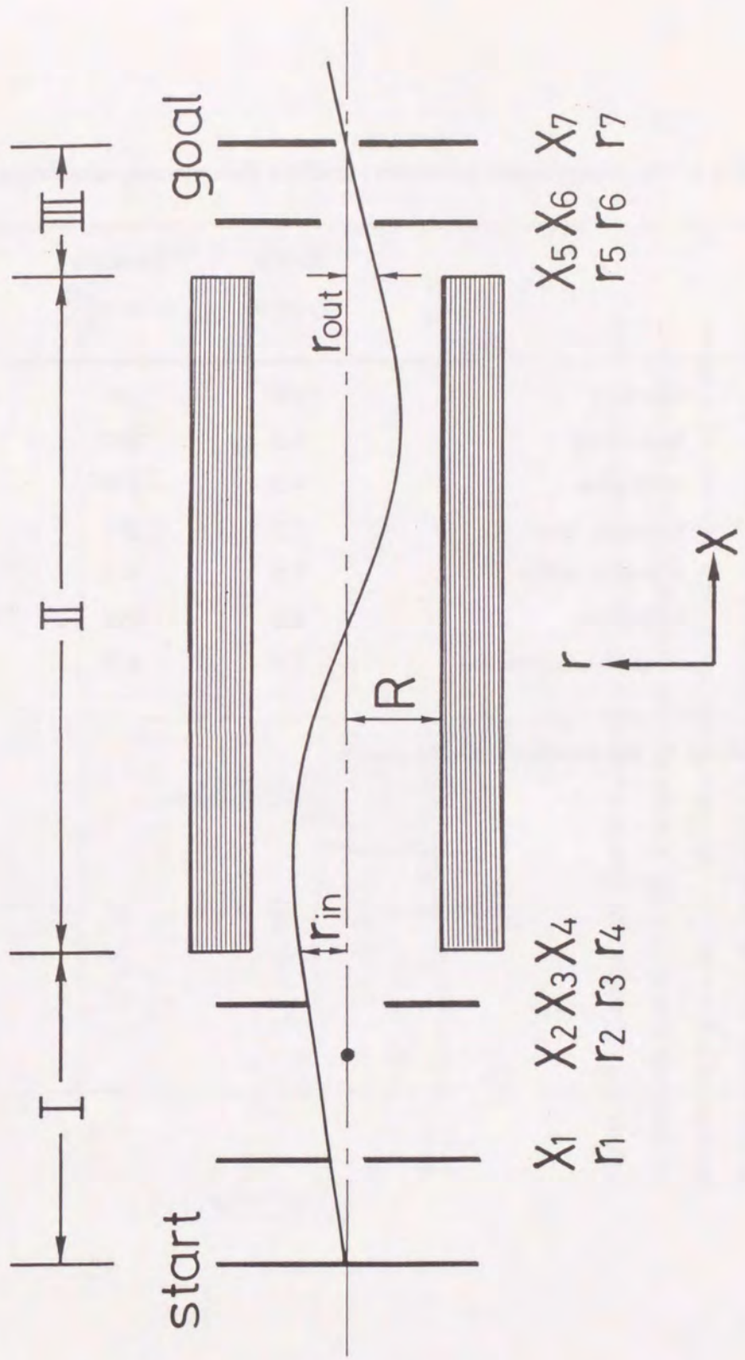

Figure II-5. Experimental setup used to the trajectory simulation.

Table II-1. The experimental parameters used for the trajectory simulation

i		Radius r_i (mm)	Distance x_i (mm) [a]
1	skimmer	0.50	10
2	beam-stop	1.5	187
3	collimator	4.0	230
4	hexapole inlet	7.5	261
5	hexapole outlet	7.5	861
6	collimator	6.0	898
7	crossed beam region	1.5	953

a) x_i is defined by the distance from the nozzle.

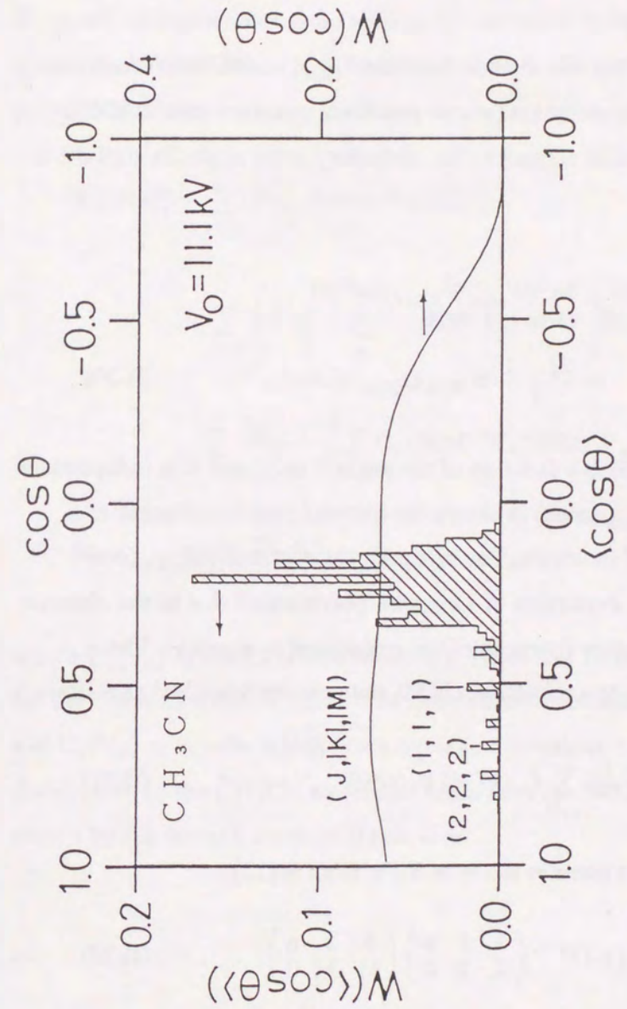

Figure II-6. Classical and quantal distributions of CH_3CN molecular beam after the state selection at 11.1 kV. The set of three rotational quantum numbers in parentheses is given as (J, K, M). The classical distribution, W(<cosθ>), is shown by histograms. Smooth curve shows the quantal distribution function, W(cosθ), calculated by the transformation of W(<cosθ>).

molecular axis.)

In order to calculate the quantal distribution of the molecular axis after the state selection in later case, we consider the distribution of a specific |JKM> state in laboratory frame. For a molecule in state |JKM>, Choi and Bernstein have evaluated as follows.[12]

The quantal probability distribution function P_{JKM}, which determines the probability for finding the molecule (whose rotational quantum state is |JKM>) of a specific orientation with respect to the laboratory polar angle $2\pi \sin\theta \, d\theta$, is given by

$$P_{JKM}(\cos\theta)\, d(\cos\theta) = 4\pi^2 (\Psi^*_{JKM} \Psi_{JKM}) \sin\theta \, d\theta$$

$$= \frac{2J+1}{2} D^*_{JKM} D_{JKM} \, d(\cos\theta) , \qquad \text{(II-20)}$$

where $P_{JKM}(\cos\theta)\, d(\cos\theta)$ is a function of the angle θ only, and it is independent of both ϕ and ψ. The $P_{JKM}(\cos\theta)$ is shown the orientational distribution of a particular |JKM> state of molecule. The orientational distribution$P_{JKM}(\cos\theta)$ must be described by an expansion of Legendre polynomials due to the absence of any azimuthal dependence (because of the cylindrical symmetry). The orientational distribution of a particular (JKM) state can be described as follows:

$$P_{JKM}(\cos\theta) = \frac{(2J+1)}{2} \sum_{n=0}^{2J} C_n(JKM)\, P_n(\cos\theta), \qquad \text{(II-21)}$$

where $C_n(JKM)$ can be written in terms of 3-j symbol as[13] ;

$$C_n(JKM) = (2n+1)\,(-1)^{M-K} \begin{pmatrix} J & J & n \\ K & -K & 0 \end{pmatrix} \begin{pmatrix} J & J & n \\ M & -M & 0 \end{pmatrix} , \qquad \text{(II-22)}$$

where $P_n(\cos\theta)$ is the Legendre polynomials, and coefficients $C_n(JKM)$ are determined as a function of (JKM) values. For the molecule where state selection

of a single |JKM> state is not feasible, the orientational distribution of the molecular beam is a sum over the individual states weighted by the population of each state.

In order to obtain as the expression for the orientational distribution function $W_V(\cos\theta)$ at a given hexapole voltage V, one needs to know the (JKM) rotational distribution $W_V(JKM)$ at V. It is computed from the Monte Carlo trajectory calculation. Thus,

$$W_V(\cos\theta) = \sum_{JKM} P_{JKM}(\cos\theta)\, W_V(JKM) \qquad \text{(II-23)}$$

$$= \sum_{JKM} \left(\frac{2J+1}{2} \sum_n C_n(JKM)\, P_n(\cos\theta) \right) W_V(JKM)$$

$$= \sum_n \frac{2n+1}{2} \left(\sum_{JKM} C_n(JKM)\, W_V(JKM) \right) P_n(\cos\theta)$$

$$= \sum_n \left(\frac{2n+1}{2} C_n(V_0) \right) P_n(\cos\theta) , \qquad \text{(II-25)}$$

where $C_n(V_0)$ is the Legendre Moments. Table II-2 listed the Legendre Moments for the oriented CH_3CN beam. The normalization condition renders $C_0(V_0) = 1$ and $C_1(V_0) = \langle\cos\theta\rangle$ which is the average orientation. Calculated quantal distribution of the CH_3CN molecular beam after the hexapole state selection is shown by the smooth curve in figure II-6.

Table II-2. The Legendre moments for the orientational distribution of the CH_3CN molecule [a)]

	Hexapole rod voltage V_0 (kV)					
	5.5	6.6	7.7	8.8	9.9	11.1
$<C_1>$	0.407	0.354	0.314	0.285	0.262	0.247
$<C_2>$	-0.047	-0.087	-0.108	-0.115	-0.114	-0.109
$<C_3>$	-0.077	-0.655	-0.488	-0.308	-0.013	0.001
$<C_4>$	0.006	0.019	0.025	0.025	0.022	0.018
$<C_5>$	0.012	0.005	-0.003	-0.011	-0.017	-0.021
$<C_6>$	-0.002	-0.007	-0.007	-0.005	-0.002	0.002
$<C_7>$	0.001	0.002	0.004	0.006	0.007	0.007
$<C_8>$	0.002	0.003	0.002	0.001	0.000	-0.001

a) $<C_n>$ stands for the n th Legendre moments.

II-2. Experimental

A. Oriented Molecular Beam Apparatus

The experimental setup is schematically shown in figure II-7.[14] The oriented molecular beam apparatus consists of six differentially pumped chambers. A beam of CX_3CN with 5 ms pulse width is formed by supersonic expansion from a conventional pulsed valve with a 0.8-mm diameter nozzle. The beam is defined with a skimmer and a collimator of 1.01 and 4.0 mm in diameter, respectively. An axial beam-stop of 1.5 mm in diameter was placed in front of the hexapole field in order to remove the unoriented molecules which cannot be focused by the hexapole electric field.[10] After the collimation, the CX_3CN molecular beam enters an electric hexapole field of 60-cm, and the beam was selected owing to $<\cos\theta>$, where $<\cos\theta>$is defined as KM/J(J+1). After passing through a collimator of 6.0-mm in diameter, the beam of the state-selected CX_3CN molecules finally enters the region of a uniform electric field (150 Vcm^{-1}) through a guiding fields. The strength of the uniform field is sufficient to justify the strong field approximation for the CX_3CN molecule.[10,16]

Figure II-8 schematically illustrates the process which the molecules oriented by the hexapole and uniform electric field. At the exit of the hexapole, the molecule orients via the electric field of hexapole as shown in figure (a) but does not orient via the laboratory frame. The molecular orientation via the laboratory frame can be achieved by the adiabatically transformation through the guiding and the uniform field as shown in the figure (b and c). The voltage differences from one field to the next field must be small compared to the spacing between Stark levels to avoid flips in the selected quantum numbers.[11,15] It should be noted the uniform field is tilted for the relative velocity vector which can be determined by the results of the time-of-flight experiment. (see section *C*) Meanwhile, the polarity of the uniform electric field was switched periodically to alter the collisional geometry from the CN-end, the CX_3-end, and the random

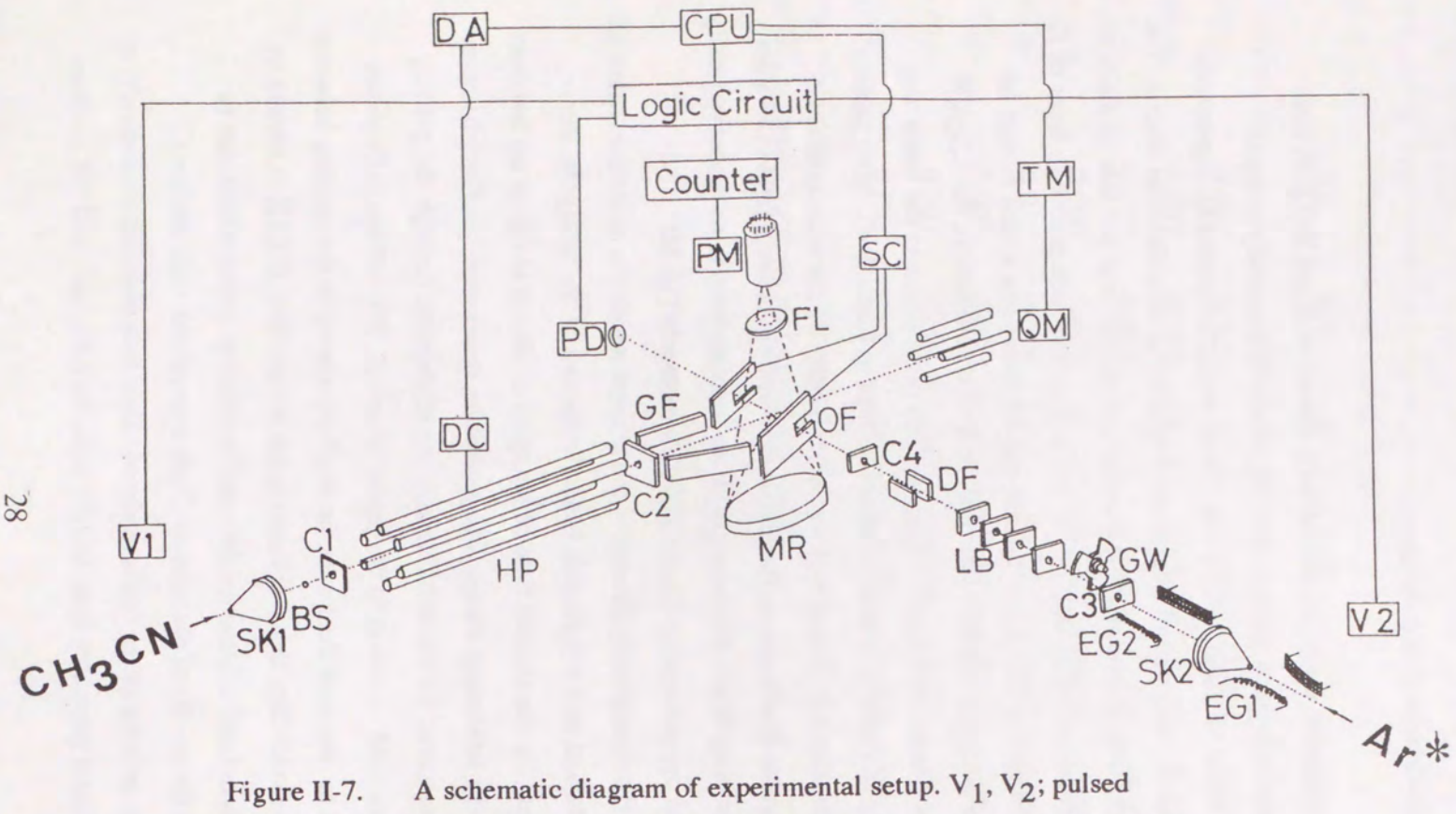

Figure II-7. A schematic diagram of experimental setup. V_1, V_2; pulsed valves, SK_1, SK_2: skimmer; BS: beam-stop, C_1, C_2, C_3, C_4: beam collimators GF: guiding field, HP: hexapole electric field, MR: concave mirror, DF: deflector, LB: light baffles, PM: photomultiplier.

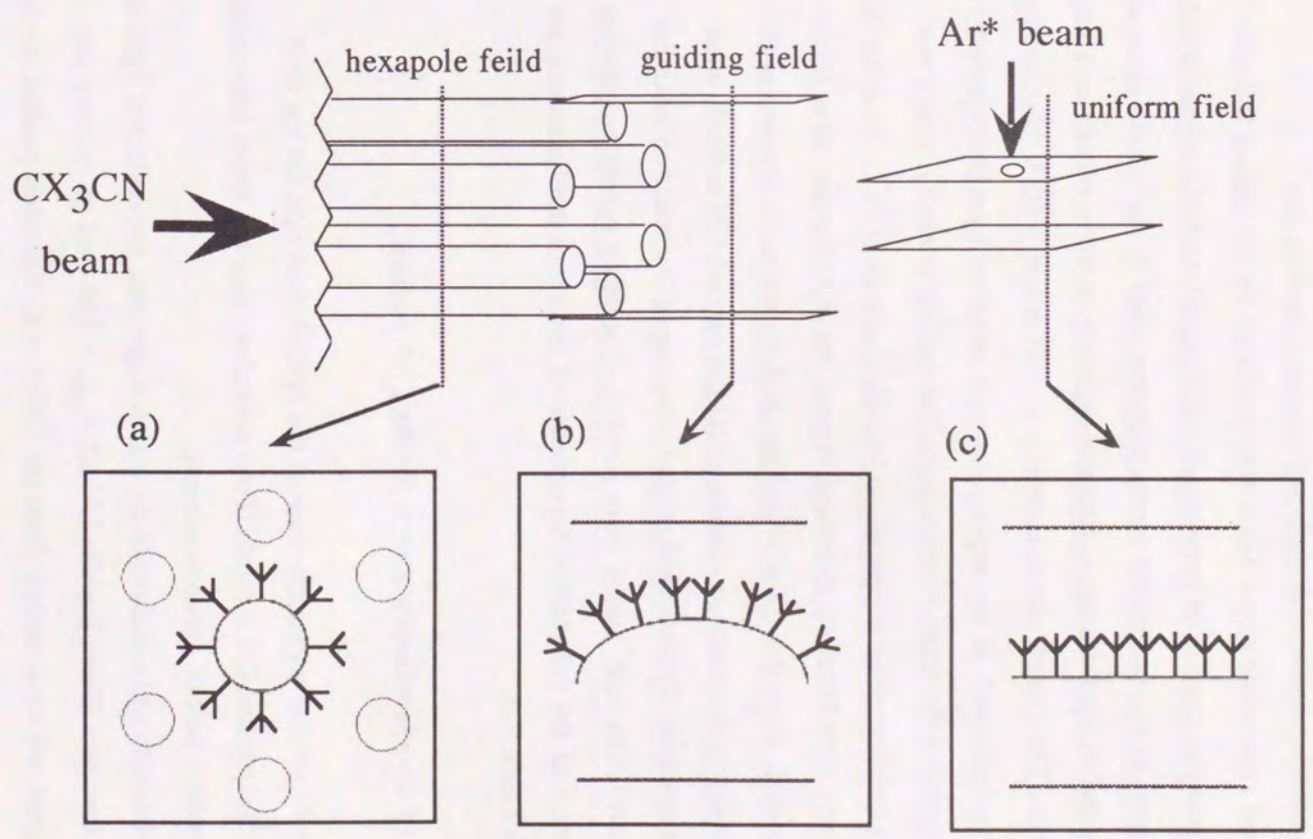

Figure II-8. Pictorial representation of molecular orientation from hexapole to uniform field.

orientations, where the random orientation is the case of the uniform field off. The CX_3CN molecular beam crossed the pulsed metastable argon beam. The stagnation pressure for each molecules were 60 Torr (1 Torr = 133 Pa) in all cases. Neat gases were employed to avoid additional experimental inaccuracy caused by the collision-induced emissions in use of a seeding gas.

The pulsed supersonic argon beam was produced by the pulsed 0.8 mm diameter valve at the stagnation pressure of 125 Torr. Metastable argon atoms, Ar*, were formed by the successive electron impact, first in the nozzle-skimmer region and second in the skimmer-collimator region in order to obtain an intense metastable beam. The typical anode current was 100 mA at + 80 V bias voltage. The ionic byproducts such as the argon ions were removed by a deflector of 400 V/cm before entering the cross beam region. The $Ar(^3P)$ intensity, which was measured by a ceratron, was estimated to be $\sim 10^{16}$ atoms $sr^{-1}s^{-1}$. In order to decrease the stray light from the discharge region, the light baffles were placed in the buffer chamber. Both the CX_3CN and the Ar* beams were crossed at the beam inter-section in the reaction chamber, and the excited CN radicals were formed by the reaction. Typical background pressure of the reaction chamber was 5×10^{-7} Torr when both beams were running. Operating conditions during the measurements of the orientation dependence of the chemiluminescence are summarized in Table II-3.

B. Detection of the chemiluminescence for the CN radical*

Figure. II-9 shows a schematic view of the optical detection for the total emission from the excited CN radicals. Total emission from the beam intersection was collected with a pair of concave mirrors.

In the acetonitrile and acetonitrile-d_3 reaction systems, the collected light is filtered by the low-pass filter (Toshiba UV-33, λ_{cut} = 330 nm) to remove the background signal, which is mainly from the OH(A→X) emission peaked around 308 nm. This was caused by the impurity water in the reagent gas. Energetically,

Table II-3. Experimental conditions

CH_3CN beam	stagnation pressure	P_0 = 60 Torr
	stream velocity	$Vs = 685 \pm 10$ ms^{-1}
	translational temperature	$Ts = 57 \pm 5$ K
CD_3CN beam	stagnation prssure	P_0 = 60 Torr
	stream velocity	$Vs = 661 \pm 10$ ms^{-1}
	translational temperature	$Ts = 57 \pm 5$ K
CF_3CN beam	stagnation prssure	P_0 = 60 Torr
	stream velocity	$Vs = 435 \pm 10$ ms^{-1}
	translational temperature	$Ts = 61 \pm 5$ K
$Ar(^3P)$ beam	stagnation prssure	P_0 = 125 Torr
	stream velocity	$Vs = 650 \pm 10$ ms^{-1}
	translational temperature	$Ts = 45 \pm 5$ K

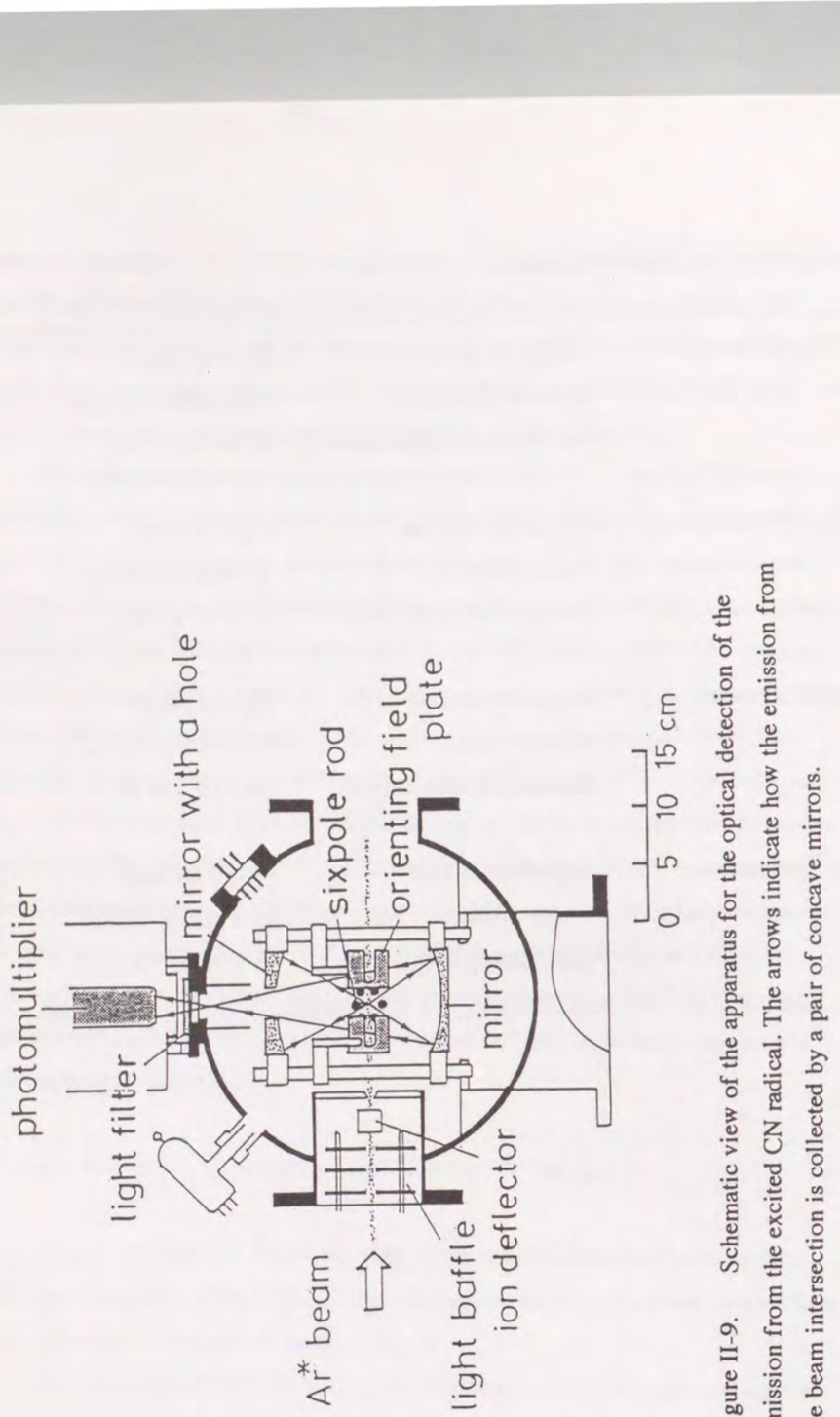

Figure II-9. Schematic view of the apparatus for the optical detection of the emission from the excited CN radical. The arrows indicate how the emission from the beam intersection is collected by a pair of concave mirrors.

both emissions of the CN(A→X) and the CN(B→X) transitions of the cyanide radical could be seen in the reaction of Ar* with acetonitrile[17]; the emission intensity of the former band however turned out to be small under the crossed beam condition. The contribution of the CN(A→X) emission may be within a few percent in the observed emission. The observation of the CN(B→X) emission in the crossed beam experiment with the oriented CH_3CN beam was hardly possible to carry out at lower hexapole voltage because of the poor emission intensity. As a typical emission intensity ~ 0.5 counts/pulse was obtained in the gated photon counting, thus we fixed the hexapole voltage of 11.1 kV where the large intensity of the focused beam is expected.

In the CF_3CN reaction system, the measurements of the orientation dependence of total emission from the excited radicals of CN(B) and CN(A) could be carried out by use of the oriented molecular beam. The CN(B→X) and the CN(A→X) emissions from the beam intersection were isolated by a band-pass filter (389 nm, $\lambda_{1/2}$ = 20 nm) for the CN(B→X) emission and a low-pass filter (Toshiba UV-45, λ_{cut} = 450 nm) for the CN(B→X) emission. The band-pass filter only transmits the CN(B→X) emission, while the low-pass filter transmits the CN(A→X) emission. The experiments were carried out at the hexapole voltage from 6 to 12 kV. The voltage for the hexapole rods was supplied by a dc-dc converter which was controlled by a microcomputer.

The total emission from the crossed beam region was detected by a cooled (-30°C) photomultiplier (Hamamatsu Photonics, R943-02) perpendicularly to the plane of the molecular beams. The signals were amplified and sent to a gated photon-counting system with 2 ms gate width. The background signal due to the stray light (from electron impact for the argon atom or from the emission of the background gas in the reaction chamber) was subtracted every time from the crossed beam signal and the residue was accumulated by a microcomputer (EPSON PC-286VE). Timings for the counter of both pulsed beams and the gating of the counting systems are controlled by a delay pulse unit. The microcomputer generates the master pulse, switches the polarity of the uniform

field, and collects the data.

C. Beam-stop

If the trajectory simulation cannot reproduce the experimental results of the dependence of the beam intensity on the hexapole voltage, the cause is mainly the influence of $(CX_3CN)_n$ clusters included in the beam. In such a case, these species must be removed from the beam intersection.[8] An axial beam-stop of 1.5 mm in diameter was placed in the beam and it was then finally adjusted with an accuracy of 0.01 mm by a two-dimensional translator, monitoring the beam intensity by a mass spectrometer. Figure II-10 schematically shows the focused molecular beam. When the beam-stop is in, the incident beam cannot reach the beam intersection. This beam-stop has the capability of removing 95 % of the incident beam.

Figure II-11 (a) shows the dependence of the CH_3CN molecular beam intensity on the hexapole voltage V_0 when the beam stop is off. The dashed line is a result of Monte Carlo trajectory simulation in which the influence of unfocused molecules is not considered. Figure II-11 (b) shows the dependence of the beam intensity when the beam stop is in. The solid line is the result of the trajectory simulation. When the beam-stop is in, the experimental result can be reappear by the trajectory simulation. It shows the clusters is effectively removed by the beam-stop.

D. Time-of-flight. (TOF)

The velocity distributions of both beams were determined by the conventional TOF analysis.[10] The CX_3CN beam was detected by the quadrupole mass spectrometer, and the metastable argon beam was detected by a ceratron. The accumulated TOF profiles were simulated by a standard two-parameter expression of the velocity distribution for the supersonic beam. The

best-fit convolutions were obtained with those parameters as listed in Table II-3. Figure II-12 shows the observed TOF spectrum of the CH_3CN beam.

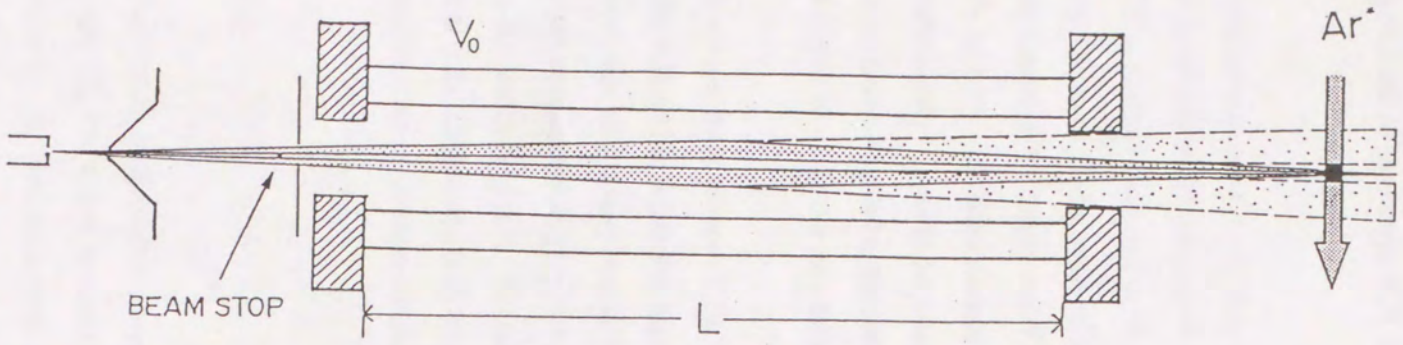

Figure II-10. Schematic view of the focused molecular beam in case of the beam-stop in.

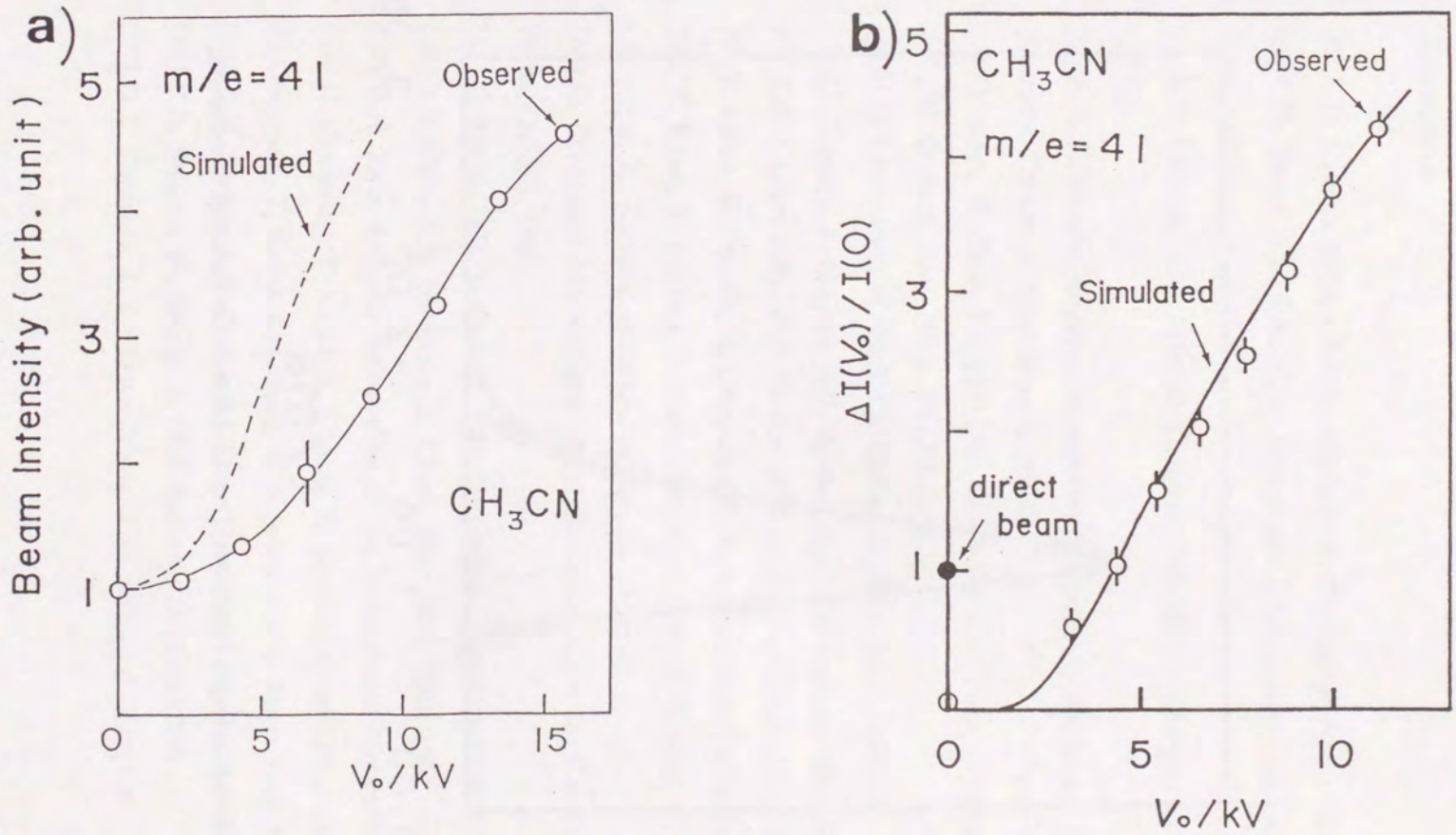

Figure II-11. Dependence of the beam intensity on the hexapole voltage V_0. Solid line is the result of Monte Carlo trajectory simulation. (a) beam-stop out (b) beam stop-in.

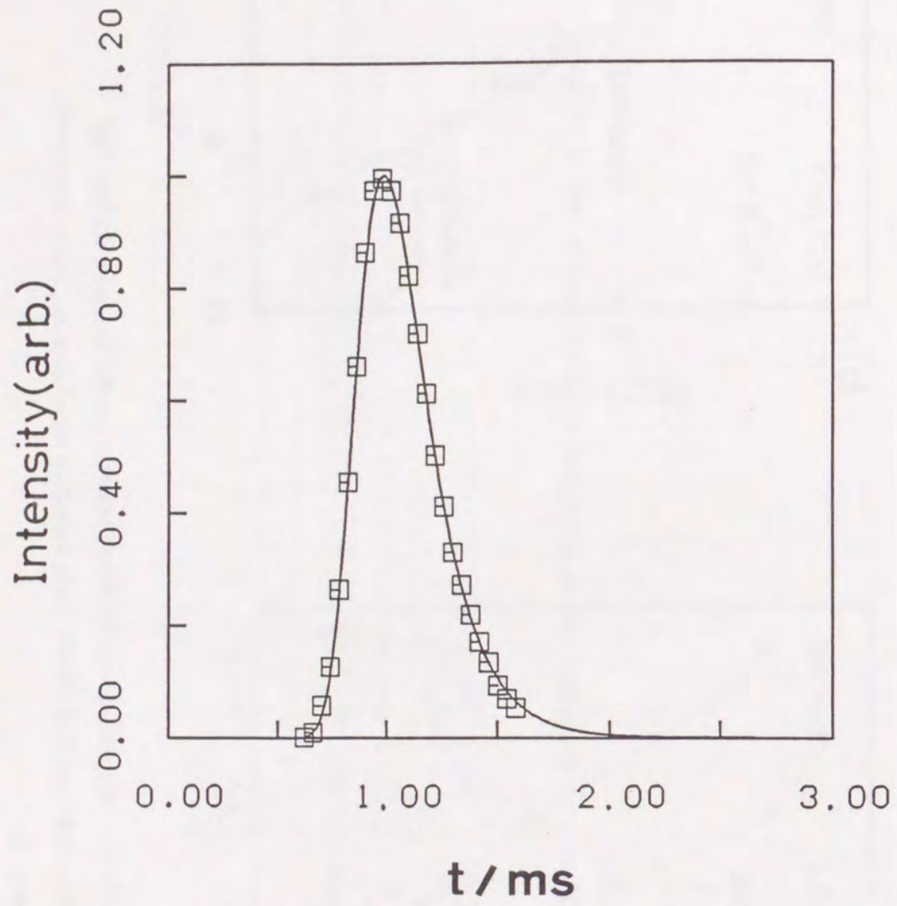

Figure II-12. Time-of flight spectrum. The solid line is the result of simulation.

References

[1] L.D. Landau, E.M. Lifshitz, *Mechanics.* (Pergamon Press, Oxford) (1977)

[2] C.H. Town, A.L. Schawlow, *Microwave Spectroscopy* (McGraw-Hill), New York, (1950)

[3] L.D. Landau, E.M. Lifshitz, *Quantum Mechanics.* (Pergamon Press, Oxford) (1977)

[4] A.R. Edmonds, *Angular Momentum in Quantum Mechanics* (Princeton niversity, Princeton, New Jersey), (1968)

[5] O. Stern, *Z. Phys.* **7** (1921) 249; W. Gerlach, O. Stern, *Z. Phys.* **8** (1921) 110; W. Gerlach, *Ann. Phys.* **76** (1925) 163

[6] H.G. Bennewitz, W. Paul, Ch. Chlier, *Z. Phys.* **141** (1955) 6

[7] J.J. Everdij, A. Huijser, N.F. Verster, *Rev. Sci. Instrum.* **44** (1973) 721

[8] K.K. Chakravorty, D.H. Parker, R.B. Bernstein, *Chem. Phys.* **68** (1982) 1

[9] T. Kasai, K. Ohashi, H. Ohoyama, K. Kuwata, *Chem. Phys. Lett.* **127** (1986) 581; T. Kasai, T. Fukawa, T. Matsunami, D.-C. Che, K. Ohashi, Y. Fukunishi, H. Ohoyama, K. Kuwata, submitted to *Rev. Sci. Instrum*

[10] G. Scoles, ed., *Atomic and Molecular Beam methods.* **Vol 1** (Oxford Univ. Press, Oxford, 1987)

[11] C. Maitz, N.D. Weinstein, D.R. Herschbach, *Mol. Phys.* **24** (1972) 133

[12] S.E. Choi, R.B. bernstein, *J. Chem. Phys.* **85** (1986) 150

[13] R.N. Zare, *Angular Momentum* (Wiley-Interscience Publication) (1988)

[14] H. Ohoyama, T. Kasai, K. Ohashi, K. Kuwata, *Chem. Phys.* **165** (1992) 155; H. Ohoyama, T. Kasai, K. Ohashi, K. Kuwata, *Chem. Phys. Lett.* **136** (1987) 236

[15] D.H. Parker, R.B. Bernstein, *Annu. Rev. Phys. Chem.* **40** (1989) 561

[16] P.A. Steiner, W. Gordy, *J. Mol. Spectry.* **21** (1966) 291

[17] D.H. Stedman, D.W. Setser, *Prog. React. Kint.* **6** (1971) 4

III. Initial Energy Distributions of the Electronically Excited CN Radicals

III-1. Introduction

The observation of the emission spectra of the excited CN radicals should provide the information about the energy distribution of products.[1-10] The photodissociation spectroscopy of CH_3CN, CD_3CN, and CF_3CN have been studied by the vacuum ultraviolet light, and it has been shown that the energy disposal in the vibration of CN(B) was increased as the weight of the methyl group increased.[9] This result shows the initial energy distribution relates to the wight of the methyl group.

In the present study, the reactions of the metastable argon atoms with CX_3CN (X=H, D, and F) were studied by use of the supersonic molecular beams which is suitable for the study of the reaction of the cooled molecular beam under the collision free condition. The energy disposal of the excited CN radical was determined by the simulation of the observed emission spectra. The relationship between the branching of the formation of CN(B) and the weight of the methyl group is discussed in this section.[11] Due to the weak intensity of the oriented molecular beam, examination of the wavelength dependence of the emission using the oriented molecular beam could not be carried out. Randomly oriented molecular beams were employed to observe the emission spectra and the branching of the formed radicals are discussed.

III-2. Experimental

A schematic diagram of the apparatus for the spectral measurement is shown in figure III-1.[12] The apparatus for the spectral measurement consists of the pulsed beam sources of the $Ar(^3P)$ or Ar* atoms and the CX_3CN (X=H, D, and F) molecules without the orientational state selection. The supersonic beam of argon was produced by a 0.8-mm diameter pulsed valve at the stagnation

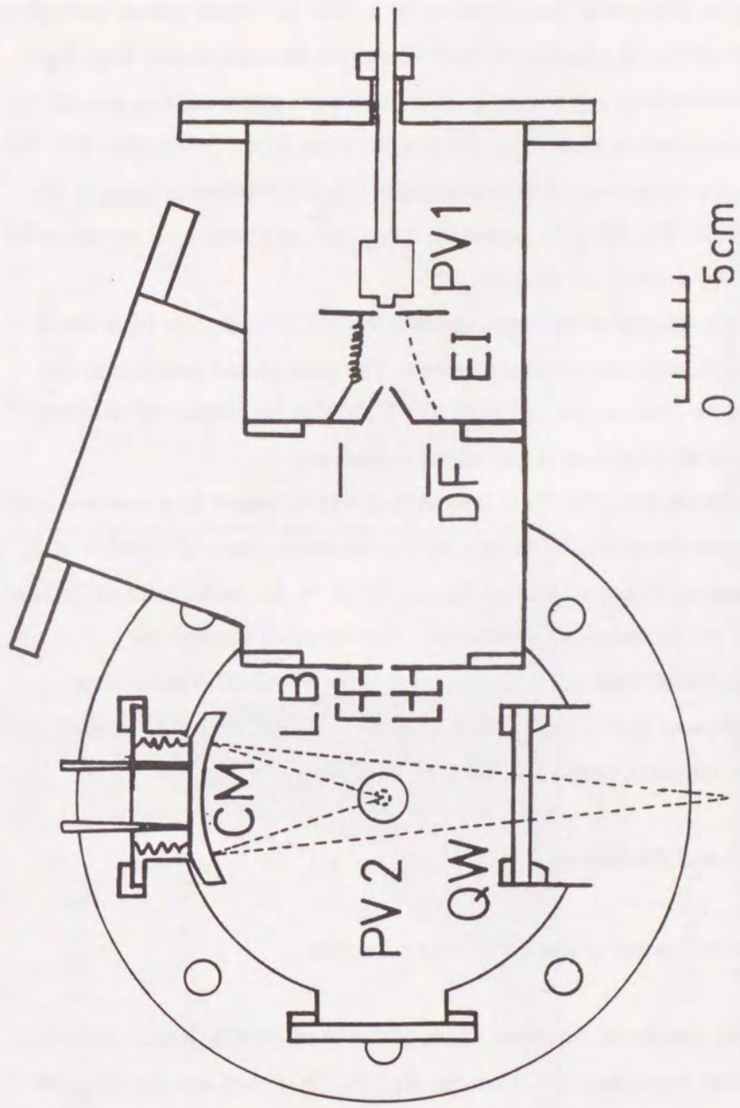

Figure III-1. Cross sectional view of the pulsed molecular beam apparatus. PV1: the pulsed valve for Ar, EI: the electron impact site, DF: deflector, LB: the light baffles, CM: the concave mirror, PV2: the pulsed valve for CX_3CN, QW: the quartz window to the monochromator.

pressure of 150 Torr and the argon atoms were bombarded with electrons from the thoria-coated tungsten filament (0.3 mm inner diameter) in the nozzle-skimmer region. The anode was biased at 80 V. The Ar* beam passes through a series of light baffles in a buffer chamber to remove the undesirable stray light. The byproducts such as argon ions by discharge were removed by a pair of deflection plates with an electric potential of 40 V/cm in the buffer chamber. The metastable argon atom beam crossed with the CX_3CN molecular beam at the beam cross-point. The CX_3CN molecular beam was produced by a pulsed valve at the stagnation pressure of 60 Torr.

The flight lengths to the beam intersection are 30 and 1 cm from the Ar* and the CX_3CN beam sources, respectively. The background pressure in the reaction chamber was maintained at $2x10^{-6}$ Torr with the beams off and $3x10^{-5}$ Torr with the both beams on in the reaction chamber.

The emission from the beam intersection was collected by a concave mirror and imaged onto the entrance slit of a 30 cm monochromator (F number of 3) with either grating blazed at 400 nm for the CN(B → X) emission or at 750 nm for the CN(A → X) emission, respectively. The emission through the monochromator was detected by a photomultiplier (R943-02, Hamamatsu Photonics) followed by a photon-counting system. The experimental system was operated by a microcomputer (SHARP, MZ-2200).

III-3. Results and Discussion

A. The emission spectra of the CN(B→X) transition

Emission spectra of the violet bands ($\Delta v = 0$) of the CN(B→X) transition with the spectral resolution of 1.1 nm for the CH_3CN + Ar* and the CD_3CN + Ar* reactions using a randomly oriented beam are shown by the histograms in figure III-2. The spectra scanned at 0.25 nm interval in the wavelength region from 375 to 395 nm were accumulated up to 1500 times. The intensity of

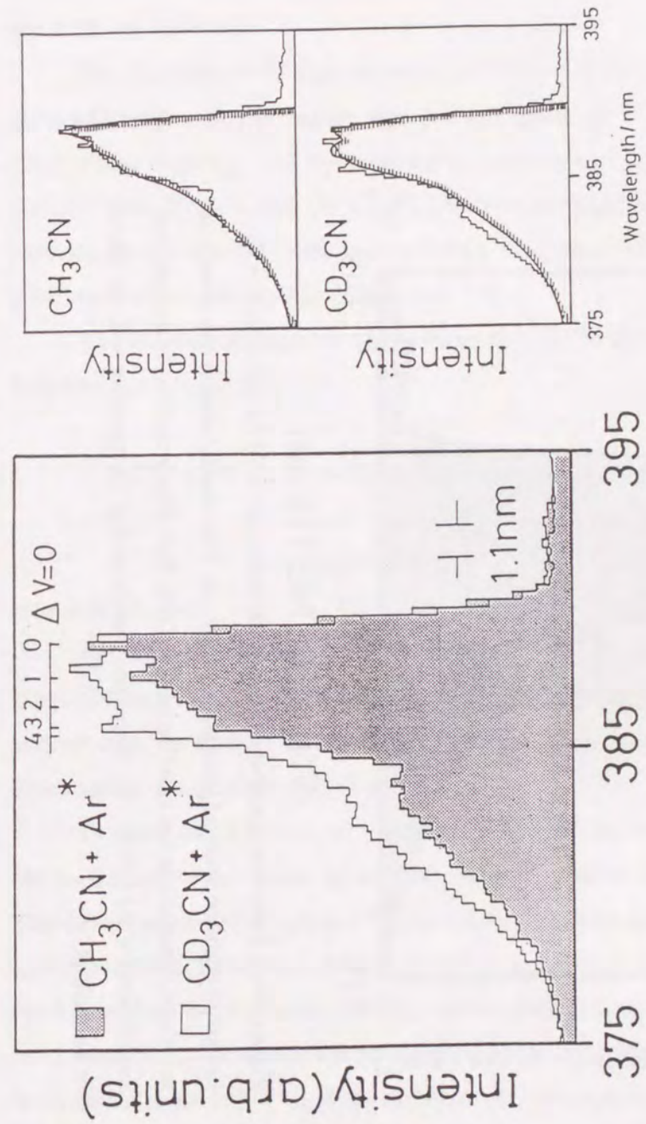

Figure III-2. Violet emission band ($\Delta v = 0$) of the CN(B) radicals with a spectral resolution of 1.1 nm. The estimated standard deviation for intensity is about 5 %. The right panels show the simulated envelopes (the smooth curves) and the observed envelopes of the emission (the histograms).

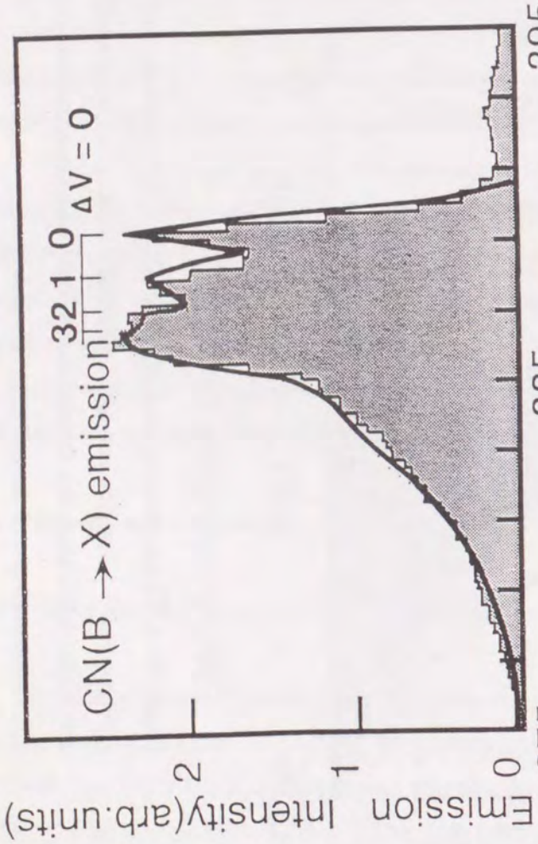

Figure III-3. Emission spectrum of the violet band ($\Delta v = 0$) for the CN(B→X) emission with the spectral resolution of 0.9 nm. The shaded area is the observed emission spectrum in the reaction of CF_3CN + Ar*. The solid line is the spectral simulation for the CN(B→X) emission. The rotational temperature was estimated to be 4200 K.

emission was normalized at 389.0 nm. The emission spectrum of the CN(B→X) transition formed in the crossed-beam reaction of Ar* with CF_3CN with the spectral resolution of 0.9 nm is also show by the shaded area in figure III-3. The emission was accumulated up to 1000 times at each wavelength, and swept with the 0.25 nm interval.

The intensity of the total emission of CN(B→X) increased by the heavy atom substitution in the methyl group. It was found to be $\sigma_H : \sigma_D : \sigma_F = 1 : 2.2 : 4.0$, where σ_H, σ_D, and σ_F stand for the relative emission cross-sections of the CH_3CN, the CD_3CN, and the CF_3CN reaction systems, respectively. First, the increase of the reaction cross-section for the formation of CN(B) by the deuterium substitution is discussed.

The reaction mechanism of the formation of CN(B) is divided into the following two steps[13];

$CX_3CN + Ar^*$ -------> $CX_3CN^* + Ar$ (step i)

CX_3CN^* -------> $CX_3 + CN(B)$ (step ii-a)

-------> $CX_2CN + X$ (step ii-b)

where X=H, or D.

Electronically excited CX_3CN^* is formed at first by the energy transfer from Ar*, and the metastable argon atom is deexcited by molecule(step i). In the second step, the CN(B) radical or the hydrogen atom are produced via the dissociation of CX_3CN^* (step ii-a or b).

Bourene and LeCalve have measured the total deexcitation cross-section of the metastable argon atoms by acetonitrile, and found to be 160 $Å^2$.[14] The deexcitation cross-sections for the ammonia and its deuterate or the methane and methane-d_4 have been measured, and no significant change is found in the total deexcitation cross-section by the deuteration. It is therefore assumed that the total deexcitation cross-section for CD_3CN is almost the same as that for acetonitrile to be 160 $Å^2$ and the difference of the probability of the energy transfer does not expected in (step i).[14]

The cause of the increase of formation of CN(B) in the reaction of acetonitrile-d_3 is due to the dissociation process of CX_3CN in (step ii). The cross section of the CN(B) emission for the CH_3CN + Ar* reaction has been determined to be a few $Å^2$, that is, formation of CN(B) has only a small branching ratio.[11] The major process in the similar reactions such as the reaction of Ar* with ethane or methanol is known to be the hydrogen atomization.[15] The major process of the reaction of acetonitrile with Ar* is estimated to be hydrogen atomization in which the hydrogen atom or atoms of the methyl group is released. It is rational to expect that a larger amount of energy is required to break the C-D bond than to break the C-H bond. Alternately, lowering the frequency of the C-D stretching vibration reduces the rate of deuterium atomization. The branching ratio of hydrogen atomization is lowered by this heavy mass effect. In turn, the branching ratio of formation of CN(B) which competes with hydrogen atomization in the dissociation process (step ii) increased. Namely, the reaction cross-section of formation of CN(B) in the CD_3CN reaction increased as compared with that in the CH_3CN reaction.

Enhancement of the emission intensity in the reaction of CF_3CN with Ar* as compared with the reaction of acetonitrile can be explained as follows. Because of the larger polarizability of the CF_3CN molecule, it is expected that the deexcitation cross-section of Ar* by acetonitrile becomes to be greater than that in the reaction of CH_3CN in (step i).[14] Additionally, the rate of the fluorine atomization may become smaller than hydrogen atomization because of the decrease of the C-F stretching vibration as in the case of the deuterium substitution. As the result, the reaction cross-section of CN(B) increased.

To investigate the relationship between the internal energy distribution of CN(B) and the heavy mass substitution of methyl group, the observed emission spectra in three reaction systems were simulated. The results of simulation are shown by the solid line in each figure. Since the spectral resolution was too poor to resolve the emissions from the higher vibrational states above 7, the band envelope for the $\Delta v = 0$ was analyzed by changing the vibrational populations

from v= 0 to 6.[10] For the rotational population, Boltzmann distribution among the states with quantum numbers up to 120 th and a single rotational temperature for all the vibrational states concerned were assumed. The Franck-Condon factors calculated by Spindler were employed,[16] and the linestrengths were taken from literature.[17] The intensity was convoluted by the slit function, which was determined by using the mercury resonant line at 365 nm.

The vibrational distribution of the CN(B) radicals obtained by the spectral simulations is shown in figure III-4. As seen, those distributions resulted in the Boltzmann distribution. In table III-1, the vibrational and the rotational energy disposal of CN(B) are listed. There is a tendency that the energy disposal in vibration of the CN(B) radical increases as the weight of the methyl group increases. However, that reason is not given successfully. It is of interest that the trend of the higher excitation in the CN(B) vibration as the weight of the methyl group increases seems to agree with the trend in the photodissociation reaction even if the means of excitation is different.[9]

B. The emission spectrum of the CN(A→X) transition

The emission spectrum in the wavelength region from 580 to 620 nm was observed in the reaction of CF_3CN + Ar*. The emission spectrum was shown in figure III-5. In this reaction, the CN(A → X) and the CF_3($1E'$ and/or $2A''_2 \rightarrow 1A'_1$) emissions may appear in this wavelength.[18,19] Although some band peaks in the spectrum could be assigned to the progressions of the CN(A→X) transition, the unresolved broad background in the spectrum would be tentatively assigned to both the CN(A→X) and the CF_3 emissions under the present spectral resolution. In order to estimate the contribution of the emission from the excited CF_3 radical, a spectral simulation was carried out using parameters of the populations of the vibrational states as the simulation of the CN(B→X) emission. The result of the simulation was shown by the solid line in the figure. The contribution of the emission of the excited CF_3 radical was estimated to be less

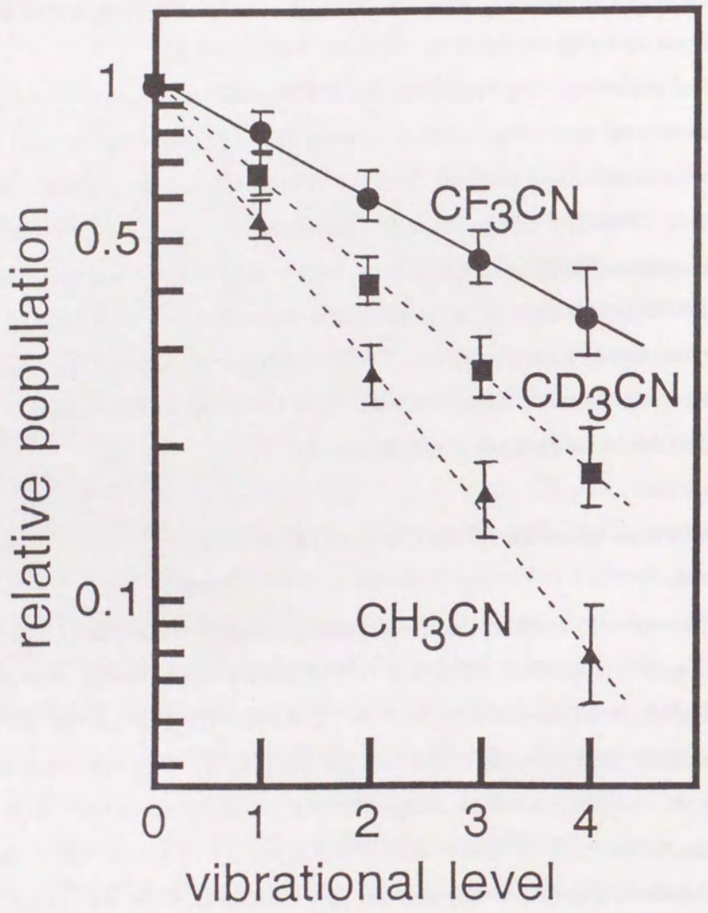

Figure III-4. Vibrational distribution of the CN(B) radical in the reaction of Ar* CH_3CN (triangles), CD_3CN (squares), and CF_3CN (circles). The vibrational distribution resulted in the Boltzmann behavior in all cases. The vibrational temperature were determined to be 6000 K for CH_3CN, 7000 K for CD_3CN, and 10000 K for CF_3CN.

Table III-1. Vibrational and rotational energy disposals in the CN(B) radicals

reactant	f_{vib} / %[a)]	f_{rot} / %[b)]
CH_3CN	12	16
CD_3CN	19	16
CF_3CN	26	12

a) The percentage of the available energy released into the CN(B) vibration.

b) The percentage of the available energy released into the CN(B) rotation.

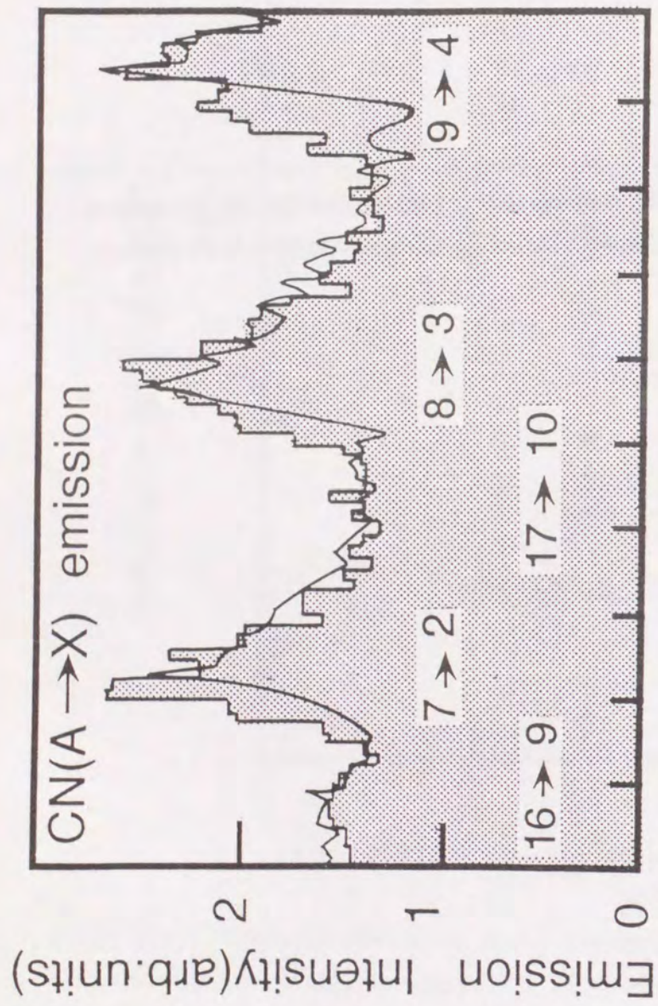

Figure III-5. Emission spectrum of the red band for the CN(A→X) emission with the spectral resolution of 1.1 nm. The shaded area is the observed emission spectrum. The solid line is the spectral simulation for the CN(A→X) emission. The rotational temperature was estimated to be 4000 K.

than 10 % of the total emission. This result shows the branching ratio of the formation of the excited CF_3 radical is small in the reaction of CF_3CN + Ar*.

The intensity of the total emission for the CN(A→X) transition in the reaction of CF_3CN with Ar* was also greater than that in the reaction of CH_3CN. It may be caused by the heavy mass effect in the same way as the formation of CN(B).

C. The emission spectrum from the excited CF_3 radical in the UV region*

In the reaction of CF_3CN with Ar*, the emission for the CF_3 ($2A'_1 \rightarrow 1A''_2$) transition in the UV region is also energetically accessible.[19] Figure III-6 (a) shows the observed UV region emission in the reaction of CF_3CN with Ar*. Figure III-6 (b) shows the CF_3*emission in the reaction of CF_3H with Ar*. These spectra was measured with the resolution of 6.4 nm. The vertical scale of figure a) is magnified five times as compared with that of figure b). As seen, the UV region emission of CF_3* radical in the CF_3CN reaction was not detected under our experimental condition in spite of the energetically accessible. The emission in the reaction of CF_3H with Ar* can be assigned the chemiluminescence for the $2A'_1 \rightarrow 1A''_2$ transition.[19] These experimental results show the branching ratio of the CF_3* radical is very small or zero.

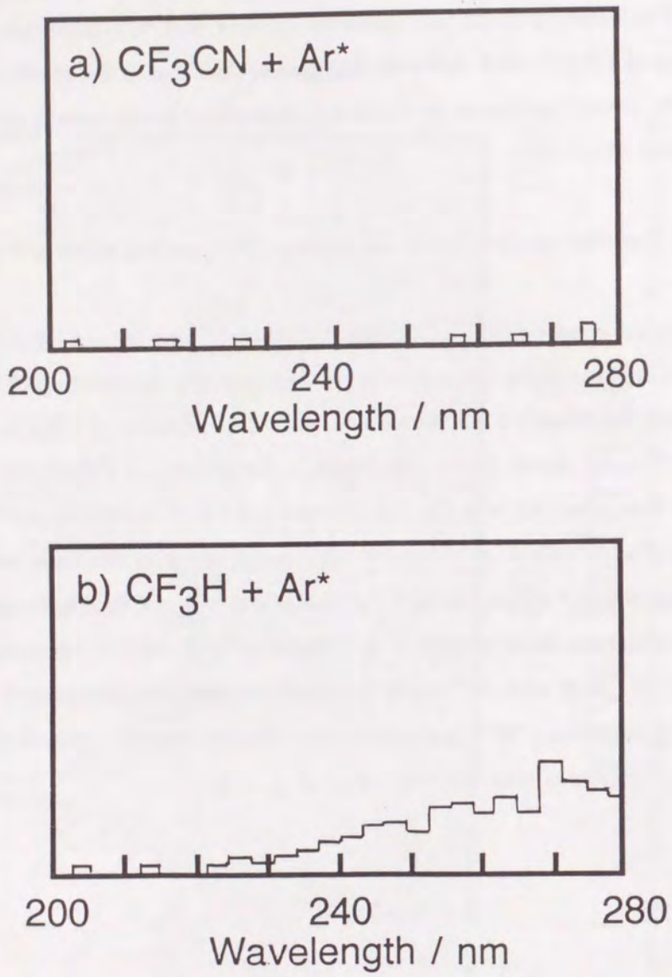

Figure III-6. Emission spectrum from the UV region. (a) In the reaction of CF_3CN + Ar* (b) In the reaction of CF_3H + Ar*. The emission in the reaction of CF_3H + Ar* can be assigned the $CF_3(2A''_2 \rightarrow 1A'_1)$ transition.

References

[1] K.D. Bayes, *Can. J. Chem.* **39** (1961) 1074

[2] H.E. Radford, H.P. Broida, *J. Chem. Phys.* **38** (1963) 644; T. Iwai, M.I. Savadatii, H.P. Broida, *J. Chem. Phys.* **47** (1967) 3861

[3] D.W. Setser, B.A. Thrush, *Proc. Roy. Soc. London A* **288** (1965) 256; D.W. Setser, D.H. Stedman, *J. Chem. Phys.* **49** (198) 467

[4] H. Ito, Y. Ozaki, K. Suzuki, T. Kondow, K. Kuchitsu, *J. Mol. Spectry.* **127** (1988) 283

[5] G. Herzberg. *Z. Physik.* **49** (1928) 512

[6] M.N.R. Ashfold, J.P. Simons, *Trans Faraday. Soc. 2.* **74** (1978) 1263

[7] A. Mele, H. Okabe, *J. Chem. Phys.* **51** (1969) 4798

[8] T. Urisu, K. Kuchitsu, *Chem. Letters.* (1972) 813; K. Suzuki, K. Kuchitsu, *Bull. Chem. Soc. Japan.* **50** (1977) 1449

[9] D.H. Stedman, D.W. Setser, *Prog. Reaction. Kinetics* **6** (1971)

[10] T. Urisu, K. Kuchitsu, *Chem. Phys. Lett.* **18** (1973) 337

[11] K. Tabayashi, K. Shoubatake, *J. Chem. Phys.* **87** (1987) 2404

[12] H. Ohoyama, T. Kasai, K. Ohashi, K. Kuwata, *Chem. Phys. Lett.* **136** (1987) 236; H. Ohoyama, T. Kasai, K. Ohashi, H. Hirata, K. Kuwata, *Chem. Phys. Lett.* **131** (1986) 20

[13] K. Kanda, S. Katsumata, *Spring Symposium of the japanese Chemical Sciety,* (1989) Abstract p255

[14] M. Bourene, J. LeCalve, *J. Chem. Phys.* **58** (1973) 1452

[15] J. Balamuta, M.F. Golde, Y.S. Ho, *J. Chem. Phys.* **79** (1983) 2822

[16] R.J. Spindler, *J. Quant. Spectrosc. Radiat. Transfer.* **5** (1965) 165

[17] G. Herzber, *Molecular Spectra and Molecular Structure 1. Spectra od Diatomic Molecules.* Var Nostrand (1950) 250

[18]M. Suto, N. Washida, *J. Chem. Phys.* **78** (1983) 1007; M. Suto, N. Washida, *J. Chem. Phys.* **78** (1983) 1012

[19] M. Suto, N. Washida, H. Akimoto, M. Nakamura, *J. Che. Phys.* **78** (1983)

1019; N. Washida, M. Suto, S. Nagase, U. Nagahima, K. Morokuma, *J. Chem. Phys.* **78** (1983) 1025

IV. Orientation Dependence of the CN(B) Formation in the Reaction of Ar* with the Oriented CX_3CN (X = H, D)

IV-1. Introduction

An approach using the oriented molecular beam is useful for introducing "orientational selection" in collisional geometry at initial stage of chemical excitation.[1-4] If the oriented molecular beam is used in the study of the reaction of Ar* with molecule, the molecular orbital excited by Ar* can be selected.[5,6]

Acetonitrile, CH_3CN, has a nonbonding orbital which is localized at the CN-end. A large orientation dependence of the formation of the CN radical is expected in the reaction of the metastable atom because it has been shown the nonbonding orbital is more favorable than the sigma orbitals in the electron exchange between the metastable atom and molecule in the study of the Penning ionization electron spectroscopy (PIES).[7] In this section, the effect of the molecular orientation on the formation of the CN(B) radical in the reaction of CH_3CN + Ar* is described.

The electronic state of molecule should be unchanged by the deuterium substitution of the CH_3CN molecule. However, an enhanced CN(B) emission of the B → X electronic transition for the CD_3CN + Ar* reaction as compared with the CH_3CN + Ar* reaction was shown in section III. It was suggested that the branching ratio of the hydrogen atomization channel was decreased by the deuterium substitution and that of the CN(B) formation was increased.[8] To investigate relationship between the enhancement of the CN(B) emission and the molecular orbital, the orientation dependence of the formation of CN(B) was observed in the CD_3CN + Ar* reaction. The experimental results is analyzed by a hard-sphere model and discussed in terms of the interaction between molecular orbitals of CX_3CN and the atomic orbital of Ar*.

IV-2. Experimental

The experimental procedure of the orientation dependence for the measurement of the CN(B) chemiluminescence was described in section II-2. Acetonitrile (Wako Chemical Co., 98% purity in weight) was dehydrated with synthetic zeolite A-3 (Wako Chemical Co.) prior to use, and acetonitrile-d_3 (Aldrich, 99% purity in weight) was used without further purification. The molecular beam intensity was measured by a quadrupole mass sepectrometer, setting on the parent peak (m/e = 41 for CH_3CN, and m/e=44 for CD_3CN).

The measurement of the orientation dependence of the formation of CN(B) was carried out at the hexapole voltage of 11.1 kV because the measurement was carried out under the optimum condition to improve the S/N.

IV-3 Results

A. State selection of the supersonic CX_3CN molecular beam.

For the determination of the rotational temperature, T_r of the molecular beam, the dependence of the beam intensity on the hexapole voltage, V_0 was observed.[9,10] It is shown in figure IV-1. Figure IV-2 also shows the V_0 dependence on the beam intensity of CD_3CN. The effective elimination of the direct CH_3CN beam is demonstrated at $V_0 = 0$ by a beam-stop. The vertical scale is normalized to the direct beam intensity, which is defined as the intensity of the incident beam at $V_0 = 0$ transmitted to the beam intersection in the absence of the beam-stop. The simulated curves in these figures were normalized at the experimental point for 11.1 kV. In these simulations, T_r of the molecular beam is the only parameter.

The shape fit of the focusing curve was found to be rather sensitive to the T_r in the simulation; the inaccuracy was tentatively estimated to be ± 10 K. In the

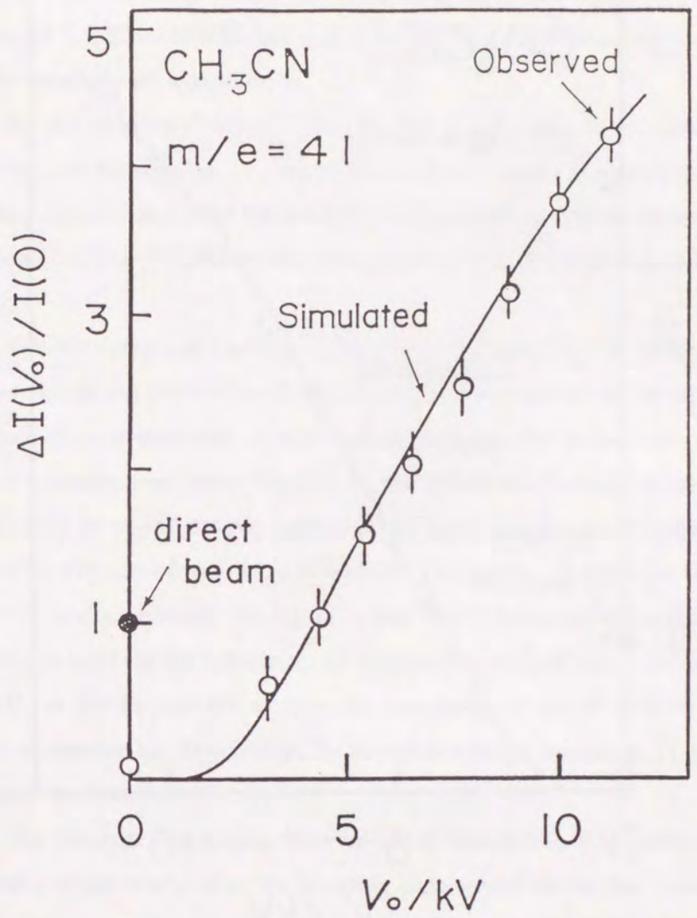

Figure IV-1. Dependence of the beam intensity of CH_3CN on the hexapole voltage V_0. I(0) is the intensity of the direct beam (the filled circle at V_0=0) which includes in part the clusters of CH3CN: the increases of the beam intensity given as $\Delta I(V_0)$ is represented in units of I(0). The solid line is the result of the Monte Carlo trajectory simulation.

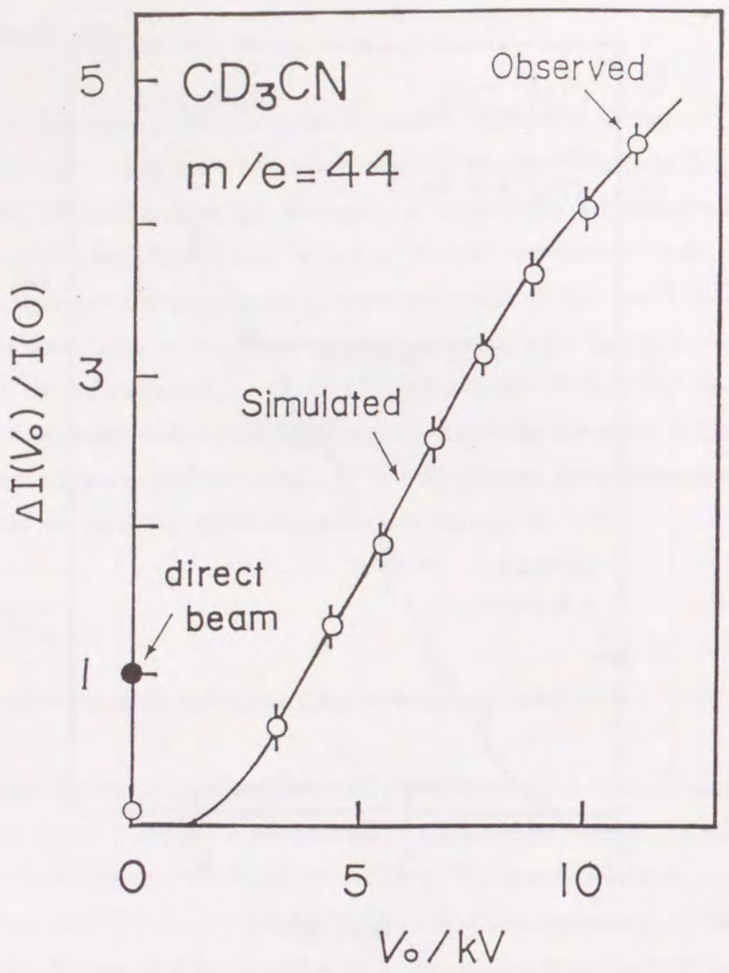

Figure IV-2. Dependence of the beam intensity of CD_3CN on the hexapole voltage V_0. The best-fit for the experimental points is shown with the solid curve.

Monte Carlo trajectory simulation of focusing curve, the T_r of the supersonic beams of CX_3CN were determined to be 57±10 K, and this temperature is equal to the translational temperature.

By use of those rotational temperatures, it is possible to calculate the orientational distribution, i.e., W(<cosθ>), where <cosθ> is defined as KM/J(J+1), of the CH_3CN beam after the hexapole electric field at any given hexapole voltage.[10] The W(<cosθ>) distribution of V_0 = 11.1 KV calculated is shown in figure IV-3.

The histograms of the W(<cosθ>) distribution of CH_3CN in figure IV-3 shows absent the population at <cosθ> = 0 as the result of the beam-stop. A absence of molecules with <cosθ> < 0 is evidently due to the first-order Stark effect. The rotational states like (1,1,1), and (2,2,2) can be easily identified in simulation, however, the populations at the small <cosθ> seem to dominate. The ensemble average of <cosθ> is to be 0.23. The quantal distribution function of W(cosθ) is also shown in the figure, which was transformed from the W(<cosθ>) and this is used for the calculation of the reaction probabilities. It is desirable to take V_0 as low as possible, because the ensemble average of <cosθ> becomes better at smaller V_0. Practically, the hexapole voltage was set at 11.1 kV due to the very weak emission intensity.

The classical and quantal distributions of orientation, W(<cosθ>) and W(cosθ), respectively, after the hexapole state selections for the oriented CD_3CN beam are shown in figure IV-4. The ensemble average of cosθ of the oriented CD_3CN beam is calculated to be 0.24, and this value is almost same as the value of 0.23 for the oriented CH_3CN beam. Therefore, the effect by the nuclear spins of either the hydrogen or the deuterium atoms may be small in the present case.[11] In the calculation of the orientational distributions, the hyperfine interaction term was neglected, but the statistical weight for the nuclear spins was considered.[19]

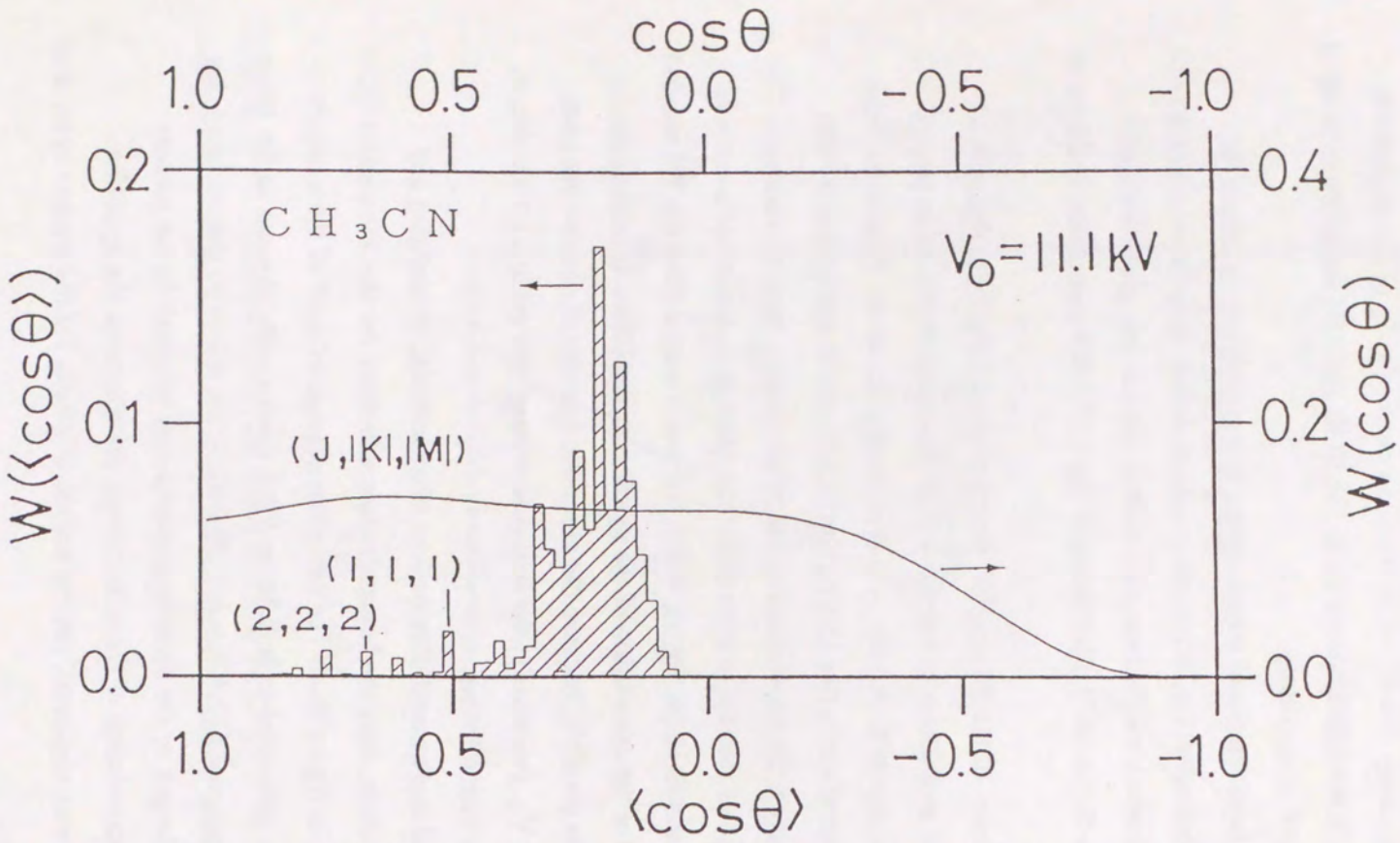

Figure IV-3. The W(<cosθ>) and W(cosθ) distributions of CH_3CN after hexapole state selection at 11.1 kV. The W(<cosθ>) distribution was simulated by $2x10^5$ trajectories. The set of three rotational quantum numbers in parentheses is given as $(J, |K|, |M|)$.

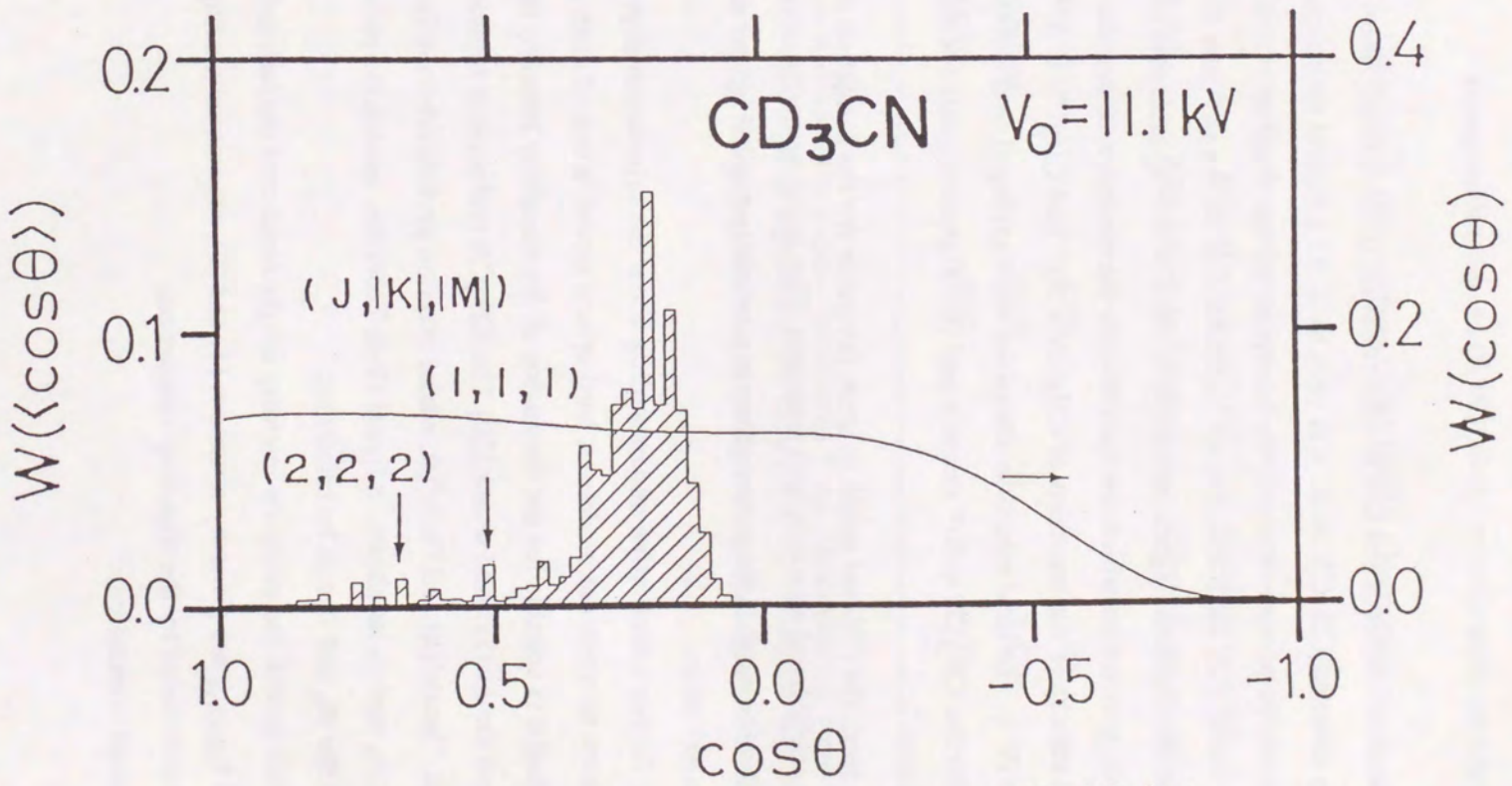

Figure IV-4. The W(<cosθ>) and W(cosθ) distributions of CD_3CN after hexapole state selection at 11.1 kV.

B. Orientation dependences of the CN(B) chemiluminescences

The observation of the CN(B→X) emission in the crossed beam condition with the oriented CH_3CN beam was very hard. As a typical emission intensity of ~ 0.5 counts/pulse was obtained, the hexapole voltage fixed at 11.1 kV where the largest intensity of the focused beam is obtained as shown in figure IV-1.

The accumulated signal intensities of the CN(B→X) emission at the three collisional geometries which are the CN-end, the methyl-end, and the randomly oriented attacks in the reactions of CH_3CN + Ar* and CD_3CN + Ar* are listed in Table IV-1. The total emission intensities were averaged over 44000 pulse signals for the CH_3CN + Ar* reaction and 50400 pulse signals for the CD_3CN + Ar* reaction.

As seen, the CN-end attack is more favorable for the formation of CN(B) than the methyl-end attack in both reactions. This result seems to accord with the chemical intuition that the cyano group can be easily excited by the direct attacks with the Ar* atom.

For further quantitative understanding about the orientation dependence, it is necessary to construct models. A hard-sphere model is one of such simple models and it is suitable for the discussion of the reactivity between the CN-end attack and the methyl-end attack.[20] The CH_3CN molecule is separated into two parts, "heads"(h) and "tails"(t), whose reaction probabilities are independently given as σ_h and σ_t, as shown in figure IV-5. From this model, the relative ratio between the σ_h and σ_t can be calculated.

In this model, the emission intensity for the heads and the tails orientation, I_{CN} and I_{methyl} are given by equations (1) and (2), respectively, using the $W(\cos\theta)$ calculated by the trajectory simulation.

For the head orientation:

Table IV-1. Orientation Dependences of the CN(B) Chemoluminescence [a)]

attacking side	emission intensity for CH_3CN /count pulse^{-1}	emission intensity for CD_3CN /count pulse^{-1}
CN-end attack	0.59	1.59
methyl-end attack	0.44	1.47
non-oriented	0.52	1.52

a) The gate width for the photon counting is 5 ms. Theintensities were averaged over 44000 pulse signals for the CH_3CN + Ar* reaction and 50400 pulse signals for the CD_3CN + Ar* reaction. The estimated standard deviation is within 8%.

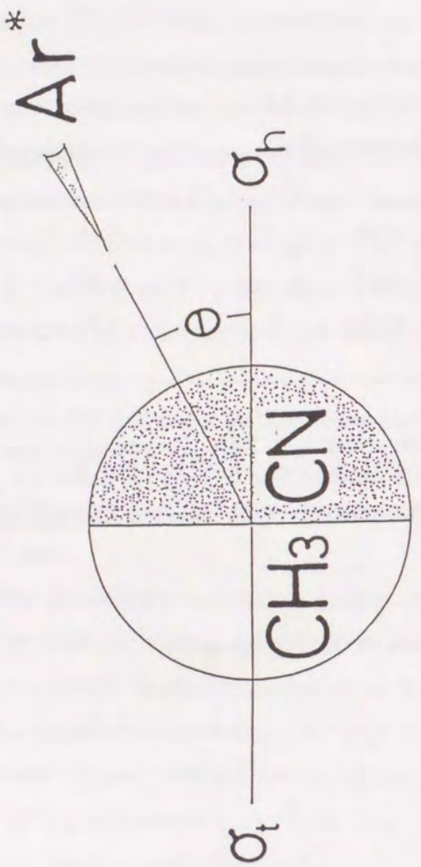

Figure IV-5. Hard-shpere model for the CH_3CN molecule. The molecule is separated into two parts whose reaction probabilities are given by σ_h and σ_t, respectively. The head orientation is identified as the collisional geometry when the $Ar(^3P)$ atom attacks in the CN axis.

$$I_{CN} = \int_{-1}^{1} \left[\frac{1}{2}(1 + \cos\theta)\sigma_h + \frac{1}{2}(1 - \cos\theta)\sigma_t \right] W(\cos\theta)\, d(\cos\theta)$$

(IV-1)

For the tail orientation:

$$I_{methyl} = \int_{-1}^{1} \left[\frac{1}{2}(1 - \cos\theta)\sigma_h + \frac{1}{2}(1 + \cos\theta)\sigma_t \right] W(\cos\theta)\, d(\cos\theta)$$

(IV-2)

The quantity of the interest here is the ratio of those reaction probabilities σ_h/σ_t and this was derived to be 2.9 for the CH_3CN + Ar* reaction and 1.6 for the CD_3CN reaction. These values clearly show a large stereoanisotropy in the CN(B) formation and stating that the CN-end attack is more favorable than the methyl-end attack in both reactions. The relative emission intensities for the randomly oriented CH_3CN and for the randomly oriented CD_3CN were measured simultaneously in the present experiment. The four values of the relative cross section of emission for both reactions can be compared, and the result is illustrated in figure IV-6. The values determined are $\sigma_t(H) : \sigma_h(H) : \sigma_t(D) : \sigma_h(D) = 1 : 2.9 : 3.0 : 4.7$, where the symbols of H and D in parentheses label the system as the CH_3CN and the CD_3CN reactions respectively.

The total cross section for the CD_3CN + Ar* reaction is enhanced as shown in section III. In both reactions the CN-end attacks are more favorable in the formation of the CN(B) radical than the methyl-end attacks. The stereoanisotropy, however, becomes smaller for the acetonitrile-d_3 reaction. This effect of the deuterium substitution would afford some extra information on the reaction branching between the CN formation and the hydrogen atomization in relation to the types of the molecular orbitals.

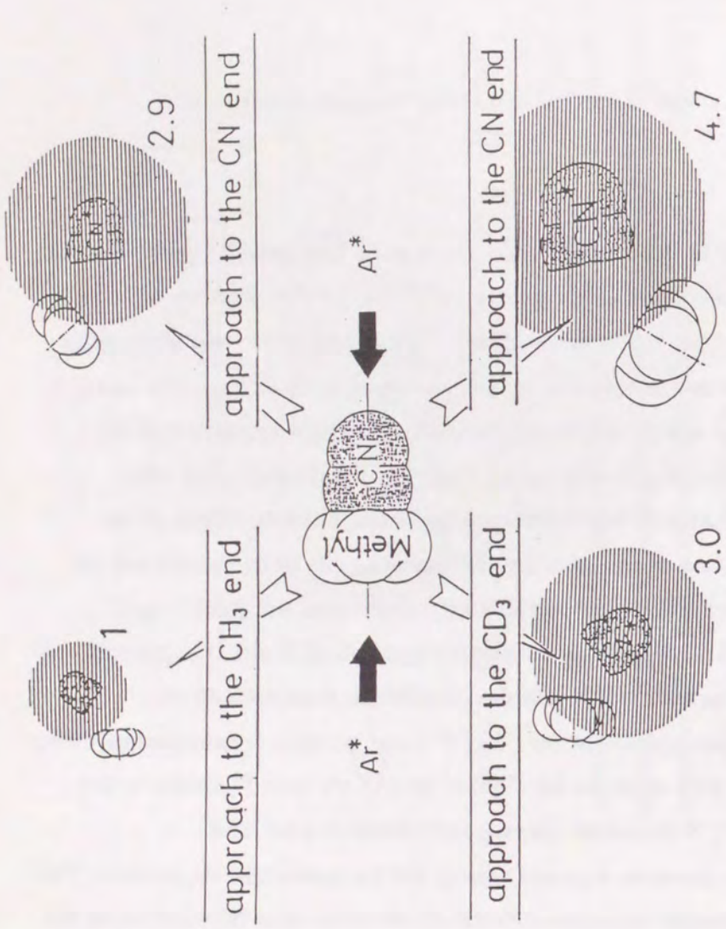

Figure IV-6. Four relative emission cross sections of the formation of CN(B) in the attacks at the methyl-end and at the CN-end of acetonitrile. The areas of the shaded circles stands for the relative cross sections in the four cases.

IV-4. Discussion

The major process of the reaction of acetonitrile with Ar* is estimated to be the hydrogen atomization in which the hydrogen atom of the methyl group is released.[21] The cross section of the formation of CN(B) has been reported to be a few $Å^2$ [13]; the CN(B) formation has only a small branching ratio. Because of this small cross section, the present reaction could occur via a direct collision mechanism with a small impact parameter.[22] The reaction of CH_3CN + Ar* proceeds via the following two steps, as in Penning ionization[23]:

$$Ar(^3P) + CH_3CN \text{ -----> } Ar(^1S) + CH_3CN^* \quad \text{(i)}$$

$$CH_3CN^* \text{ -----> } CH_3 + CN(B) \quad \text{(ii-a)}$$

$$\text{-----> } CH_2CN + H \quad \text{(ii-b)}$$

The collisional electron exchange takes place in step (i). The electron of 4s orbital of the metastable atom is moved out and enters into some orbital of acetonitrile. Simultaneously, an electron of the acetonitrile molecule is transferred into the vacant 3p orbital of the argon atom. The electronically excited acetonitrile molecule was formed and the metastable atom was deexcited in step (i). In step (ii), the CH_3CN^* in the excited state dissociates to give the CN(B) radical. The first step is thought to be initiated by the extent of the orbital overlap between the molecule and the atom. The observed orientation dependences for the formation of CN(B) are tentatively discussed in terms of the interaction between the molecular orbitals of molecule and the atomic orbital of Ar*.

*A. The reaction of the oriented CH_3CN with Ar**

In figure IV-7, the low-lying molecular orbitals of acetonitrile are from the

book of Jorgensen and Salem.[24] The calculated values of energy of the MOs are, as commonly accepted, not so reliable but those assignments and orbital character are useful to discuss. Since the energy difference is small, either the $7a_1$ orbital or the 2e orbital could be the HOMO and the LUMO may be the 3e orbital. The contribution of the molecular orbital in this reaction would be the $7a_1$ and 2e orbitals if the energy of the excitation by the Ar* is payed attention.[25]

In the figure IV-8, the spatial distribution of electron of these molecular orbitals are shown. It has been calculated in the ab initio MO method by Ohno et al.[13] The electron density maps of relevant molecular orbitals for a plane including the C-CN axis is shown by the thin line in the figure. The density of the n-th line from outside (d_n) is $(2.5)(2^n)\times10^{-4}$. The thick line in the figure is illustrated the envelope of the spheres of van der Waals radii of each atoms. The $7a_1$ molecular orbital localizes at the CN-end, and the 2e molecular orbital is rather isotropic in the spatial distribution of electron.

The present analysis with the hard-sphere model states that the Ar* approach in the direction of the cyano group gives more the formation of the CN(B) radical than that in the direction of the methyl-group. It is expected that the nonbonding orbitals are more reactive than bonding orbitals in the electron exchange when molecules contain lone-pair electrons.[13] In the case of the $7a_1$ orbital, the removal of a covalent electron of the C-C bond may accelerate the bond breaking. Thus, the $7a_1$ orbital of molecule is mainly contributed to the formation of the CN(B) radical in the reaction of CH_3CN + Ar*.

*B. The reaction of CD_3CN with Ar**

The stereoanisotropy of the formation of CN(B) becomes smaller for the acetonitrile-d_3 reaction as compared with that for the CH_3CN reaction. In the photodissociation study of acetonitrile and its deuterate, both molecules are thought to be excited to the same electronic states except for the difference in the

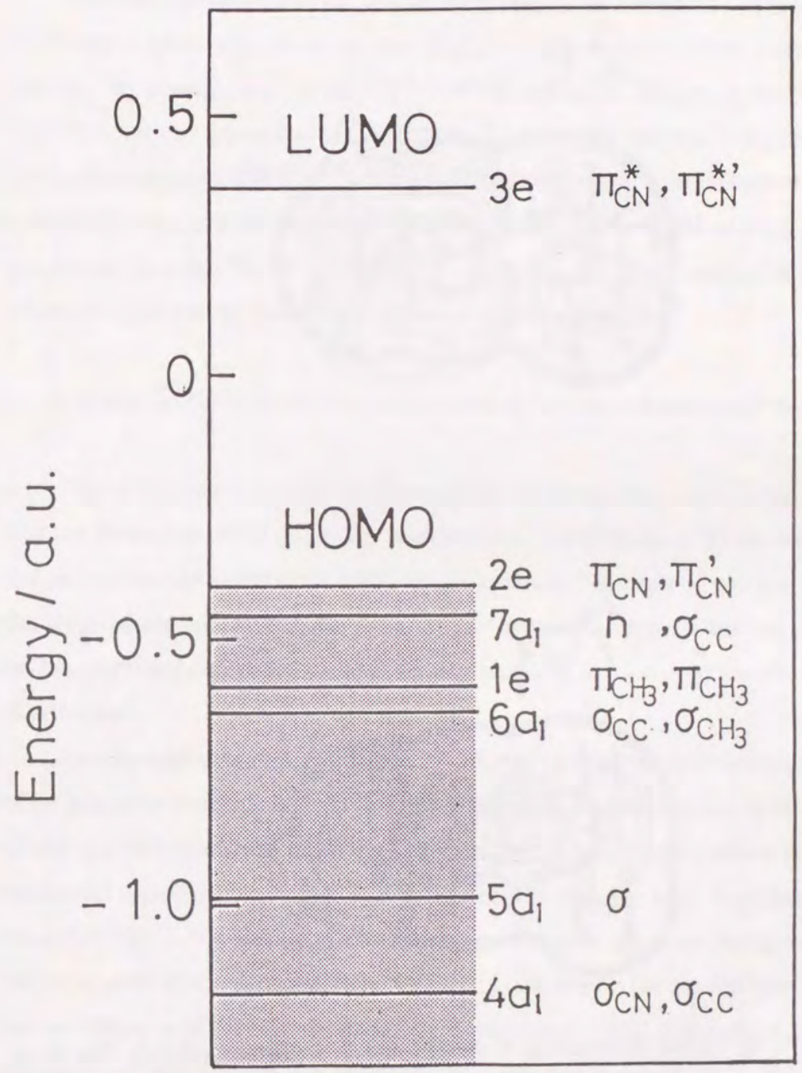

Figure IV-7. The energy diagram for the low-lying molecular orbitals of acetonitrile reproduced from reference [24].

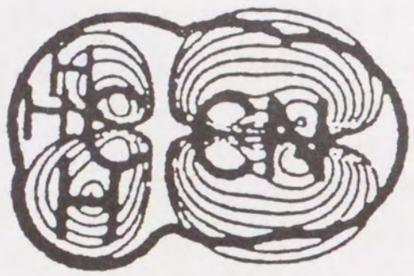

Figure IV-8. Spatial distribution of the $7a_1$ and 2e molecular orbitals. The thick line is shown the envelopes of van der Waals radii of each atoms. The thin line is the electron density maps. The density line of the n-th line from the outside (d_n) is $(2.5)(2n) \times 10^{-4}$ au^{-3}.

internal energy distribution (mainly in vibration).[25]

The opacity function of the CN(B) formation in both reactions in figure IV-9. In the orientation dependence of the CH_3CN + Ar* reaction, it was suggested that the $7a_1$ nonbonding orbital which is localized at the CN group mainly contributes to the formation of CN(B). The increment of the reaction probability for the formation of CN(B) in acetonitrile-d_3 shows a nearly independent behavior for the attacks in two orientations. Therefore, an additional reaction process to form the CN(B) radical has to be considered, and a molecular orbital of an isotropic spatial distribution contributes to this process.

C. Relationship between the molecular orbitals and the branching of reaction

The difference in the stereoanisotropy by the deuterium substitution suggests that the formation of CN(B) has at least two reaction processes. These processes are relevant to the anisotropic and isotropic molecular orbitals of acetonitrile at the stage of the energy transfer from the Ar* atom. The former has been shown as $7a_1$, and the latter could be 2e if we pay attention to its energy and its spatial distribution.

As schematically shown in figure IV-10, one orbital has isotropic and the other has anisotropic character. The minor branching but of interest here is the CN(B) formation and the major branching is the hydrogen atomization.[21] The horizontal quantity gives a measure of the cross section for each branching. The cross section for the hydrogen atomization is shown by the open histograms, and the cross section for the formation of CN(B) is shown by the shaded histograms. In the formation of CN(B), the anisotropic molecular orbital gives rise to the stereoanisotropy, whereas the isotropic molecular orbitals does not give any discrimination for the either orientation. The same enhancement for either the CN-end or the methyl-end attack for the CD_3CN reaction shows that this process should be related to the isotropic molecular orbital as indicated in the figure.

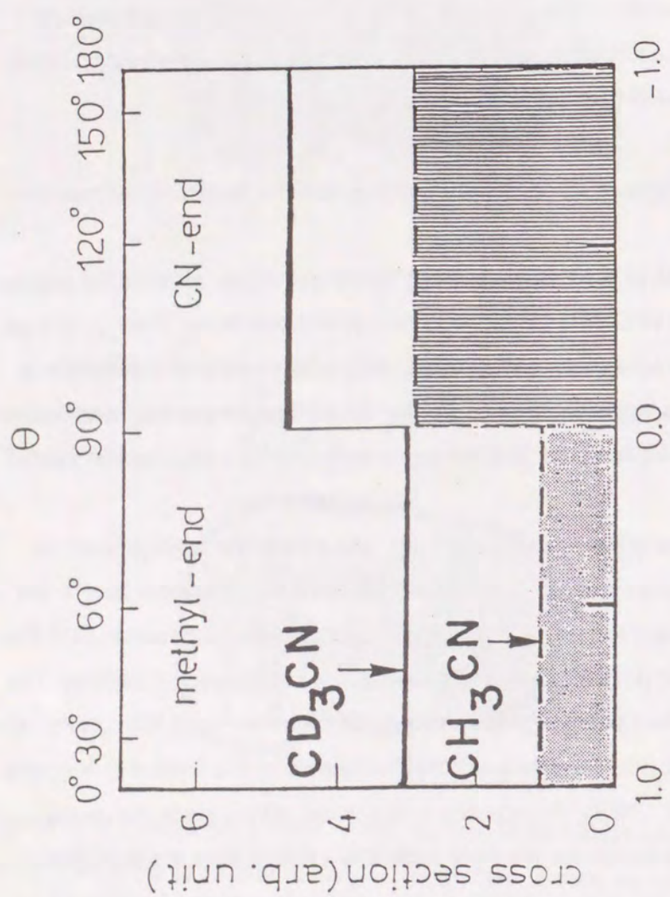

Figure IV-9. Orientational opacity functions for the formation of CN(B) in the CH_3CN reaction (the lower lines) and in the reaction of CD_3CN reaction (the upper lines). Each function is illustrated by the step function calculated from the hard-sphere model.

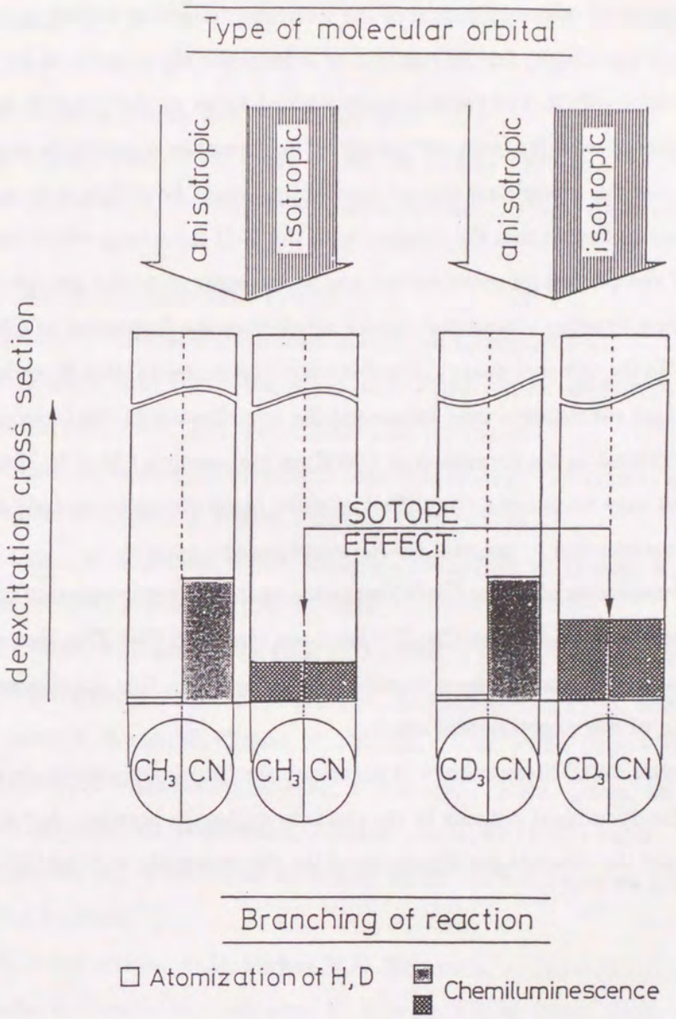

Figure IV-10. Scheme to represent the relationship between the two types of the molecular orbitals (anisotropic and isotropic) and the branching of the reaction to the formation of CN(B) and the hydrogen atomization. The enhancement for the CN(B) formation due to the isotope effect is indicated by the arrows. The open histograms show the cross section for the hydrogen atomization and the shaded histograms mean the cross section for the formation of CN(B) observed in the CN(B) chemiluminescence.

The cause of the contribution of the isotropic molecular orbital in the formation of the CN(B) for the reaction of acetonitrile-d_3 appears to be related to the heavy mass effect. The electronically excited states of the CH_3CN molecule after the energy transfer from Ar* could be the same for acetonitrile and its deuterate, but the vibrational energy distribution could be different to each other. It is rational to expect that the frequency of the C-D stretching vibration reduces the rate of the deuterium atomization, and at the same time the energy redistribution to other vibrational modes accelerates the formation of CN(B). The difference in the internal energy distribution of the excited CH_3CN molecule by the deuterium substitution may be caused the contribution of the isotropic molecular orbital in the formation of CN(B) in the reaction CD_3CN. This explanation may be rather a simplified scheme, but it seems to exclude any uncertain assumption to account for the experimental results.

The enhancement of the CN(B) emission in the photodissociation of CD_3CN as compared with that of the CH_3CN has been observed.[26] This isotope effect was pronounced in the Rydberg transition from 2e to 3p. It is consistent with the explanation of our experimental results.

For more detail discussion, it is necessary the theoretical information in terms of the dynamical process in the electron exchange between Ar* and molecule and the dissociation dynamics of the electronically excited CH_3CN molecule.

References

[1] P.R. Brooks, *Chem. Rev.* **88** (1988) 407

[2] S.R. Leone, *Annu. Rev. Phys. Chem.* **35** (1984) 109

[3] R.B. Bernstein, D.R. Herschbach, R.D. Levine, *J. Phys. Chem.* **91** (1987) 5365

[4] P.R. Brooks, *Science.* **193** (1976) 11

[5] S. Stolte, *Ber.Bunsen-Ges, Phys. Chem.* **86** (1982) 413

[6] D.H. Parker, R.B. Bernstein, *Annu. Rev. Phys. Chem.* **40** (1989) 561

[7] D.W. Setser, *Annu. Rev. phys. Chem.* **27** (1976) 407

[8] K. Ohno, H. Mutoh, Y. Harada, *J. Am. Chem. Soc.* **105** (1983) 4555

[9] A. Mele, H. Okabe, *J. Chem. Phys.* **51** (1969) 4798

[10] T. Urisu, K. Kuchitsu, *Chem. Letters.* (1972) 813; K. Suzuki, K. Kuchitsu, *Bull. Chem. Soc. Japan.* **50** (1977) 1449

[11] K. Ohashi, T. Kasai, D.-C. Che, K. Kuwata, *J. Phys. Chem.* **93** (1989) 5484

[12] H. Ohoyama, T. Kasai, K. Ohashi, K. Kuwata, *Chem. Phys.* **165** (1992) 155; H. Ohoyama, T. Kasai, K. Ohashi, K. Kuwata, *Chem. Phys. Lett.* **136** (1987) 236

[13] K. Ohno, S. Matsumoto, K. Imai, Y. Harada, *J. Phys. Chem.* **88** (1984) 206

[14] K. Tabayashi, K. Shoubatake, *J. Chem. Phys.* **87** (1987) 2404

[14] G. Scoles, Ed. *Atomic and molecular beam methods*; Oxford University Press: **Vol 1** (1988)

[15] K.K. Chakravorty, D.H. Parker, R.B. Bernstein, *J. Chem. Phys.* ***51*** (1982) 1; T. Kasai, K. Ohashi, H. Ohoyama, K. Kuwata, *Chem, Phys. Lette.* **127** (1986) 581; K. Ohashi, T. kasai, K. Kuwata, *J. Phys. Chem.* **92** (1988) 5954

[16] B.D. Kay, A.J. Grimley, *Chem. Phys. Lett.* **127** (1986) 303

[17] S.E. Choi, R.B.bernstein, *J. Chem. Phys.* **83** (1985) 4463; S.E. Choi, R.B. Bernstein, *J. Chem. Phys.* **85** (1986) 150

[18] P.A. Steiner, W. Gordy, *J. Mol. Spectrosc.* **21** (1966) 291

[19] C.H. Townes, A.L. Shawlow, *Microwave Spectroscopy;* McGraw-Hill: New

York, 1955
[20] R.J. Beuhler Jr. R.B. Bernstein, *J. Chem. Phys.* **51** (1969) 5305; G. Marceilin, P.R. Brooks, *J. Am. Chem. Soc.* **97** (1975) 1810; P.R. Brooks, E.M. Jones, *J. Chem. Phys.* **45** (1966) 3449; R.J. Beuhler Jr, R.B. Bernstein, K.H. Kramer, *J. Am. Chem. Soc.* **88** (1966) 5331
[21] J. Balamuta, M.F. Golde, Y.S. Ho, *J. Chem. Phys.* **79** (1983) 2822
[22] K. Kanda, S. Katsumata, *Spring Symposium of the Japanese Chemical Society* (1989) Abstract 255
[23] T. Munakata, Y. Harada, K. Ohno, K. Kuchitsu, *Chem. Phys. Lett.* **84** (1981) 6; J. Perreau, C. Reynaud, G. Lecayon, Y. Ellinger, *J. Phys.* B **19** (1986) 581
[24] W.L. Jorgensen, L. Salem, *The organic chemists book of orbitals* (Academic Press, New Yprk, 1973)
[25] M.N.R, Ashford, J.P. Simosn, *Trans. faraday. Soc. 2.* **74** (1978) 1263
[26] K. Shoubatake,S. Ohshima, A. Hiraya, Y. Matsumoto, K. Tabayashi, *Intern. Conf. on Photochemistry*. Tokyo, August, (1985) Book of Abstract.

V. Orientation Dependence on Branching of Chemiluminescent Channels in the Reaction of Ar* with the Oriented CF_3CN Molecule

V-1. Introduction

Studies on the steric effects in the atom-molecule reactions have been shown that chemical reaction depends on the orientation of reagent.[1-6] When the several products are formed simultaneously in a reaction, orientation of the reactant molecule is one of the dominant factors to determine the branching of reaction.[7-9] The propensity rule of the orbital selection in the various reaction channels is of most interest in the reaction dynamics.

In the study of the orientation dependence in the reaction of Ar* with acetonitrile and the acetonitrile-d_3, the effect of molecular orientation on the formation of CN(B) is dissimilar in these reactions was found. It was explained by the contribution of the isotropic 2e orbital to the formation of CN(B) in the CD_3CN reaction.[10,11]

If the several products are formed in a reaction and the products are detected, it seems to be suitable for the study of the orientation dependence on the reaction branching. The formations of the CN(B), the CN(A), and the CF_3* radicals are energetically accessible in the reaction of Ar* + CF_3CN, and the radicals could be directly detected by the chemiluminescences of the excited radicals. In the section III, it was shown that the branching ratios of the CF_3* formation is small. The formations of the CN(B) and the CN(A) radicals are presented in this thesis. This reaction seems to closely related to the reactions of the Ar* with acetonitrile (see in section IV) and with CF_3H[12] which reaction has been studied in our laboratory, and is considered to be appropriate for the study on the relationship between reaction branching and orientation of the reactant molecule.

The results of the orientation dependences of the chemiluminescences from the CN(B) or the CN(A) radials were analyzed by the hard-sphere model because

of the comparison with the reaction of Ar* with acetonitrile. In spite of the difference of the molecular orbitals between the CF_3CN and CX_3CN (X = H, D) molecules, the ratio of the reaction probability of the CN-end attack and the CF_3-end attack was compared with that in the reaction of Ar* with acetonitrile.

More detailed investigation on a variety of the reaction systems is required to obtain the information about the role of the orientation in reaction dynamics and to understand how the shape of the opacity function can be combined with the chemical shape of molecule. The orientational opacity functions of the formations of CN(B) and CN(A) were observed, and discussed the reaction mechanism of the formation of the excited CN radicals. Additionally, the study of the photodissociation for the CF_3CN molecule by use of the UV-SOR light was carried out in order to compare the chemical excitation by the Ar* with the photodissociation.

V-2. Experimental

The emissions of CN(B → X) and CN(A → X) were isolated by a band-pass filter (389 nm, $\lambda_{1/2}$= 20 nm) for the CN(B → X) emission and a low-pass filter (Toshiba UV-45, λ_{cut} = 450 nm) for the CN(A → X) emission. The band-pass filter only transmits the CN(B → X) chemiluminescence, while the low-pass filter transmits the CN(A → X) chemiluminescence.[13]

In order to obtain the opacity function, the dependences of the hexapole rod voltage, V_0, on the emission intensity should be observed. The V_0 were changed from 6 to 12 kV by the dc-dc converter.[12] The observed emission was accumulated at each voltage until the experimental error stays within 5 %.

V-3. Results

A. Oriented CF_3CN molecular beam

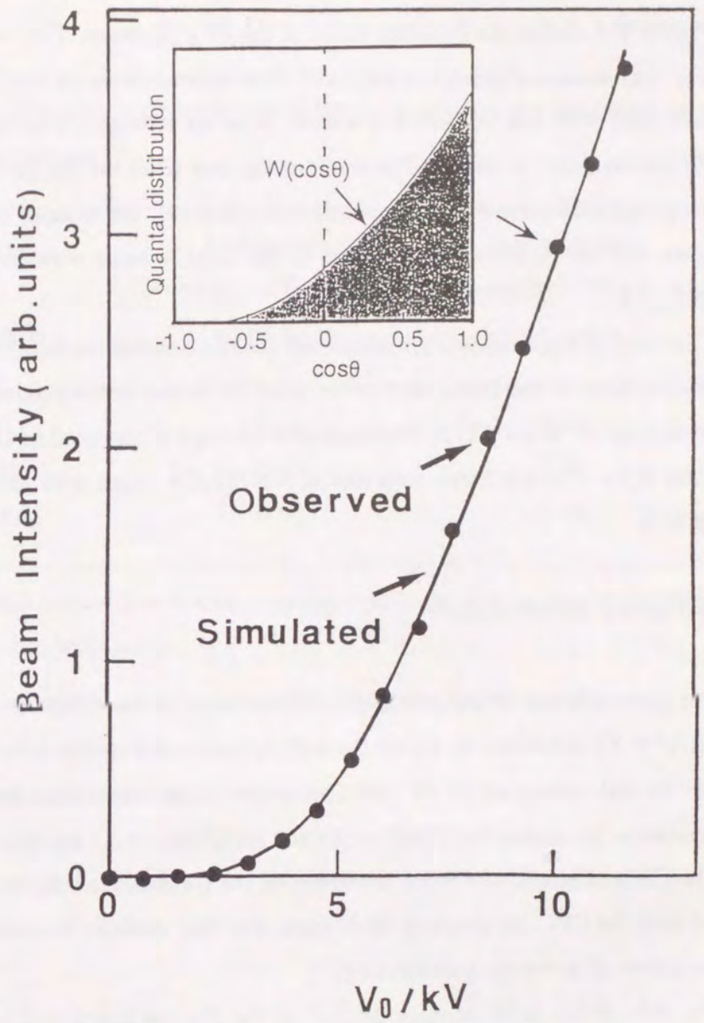

Figure V-1. Dependence of the intensity of the CF_3CN beam upon the hexapole rod voltage. The experimental error bar is smaller than the size of each filled circle. The solid line shows the best fit of the Monte Carlo trajectory simulations with the rotational temperature of 61 ± 5 K. The orientational distribution of CF_3CN at the beam intersection is shown in the inset of the figure. The hexapole rod voltage was 10 kV. The W(cosθ) distribution was simulated with $2x10^3$ trajectories.

Figure V-1 shows the focusing curve of the CF_3CN beam. The beam intensity was measured using a quadrupole mass spectrometer on the $(CF_2CN)^+$ fragment peak with m/e 76, which is known to be the strongest fragment peak of CF_3CN by the electron impact. The result of the best fit of the Monte Carlo trajectory calculations to the observed points is shown by the smooth solid line in the figure, and the rotational temperature of the CF_3CN beam was determined to 61 ± 5 K.[14]

The inset of figure shows the calculated quantal orientation distribution of the CF_3CN beam at the beam intersection after the hexapole state-selection with the rod voltage of 10 kV.[5,15] The ensemble average of the $\cos\theta$ of the CF_3CN beam was 0.55, which is better than that of the CH_3CN beam with the same rod voltage.[10]

B. Hard-sphere model analysis

The determination of the orientation dependences of the CN(B → X) and the CN(A → X) emissions by use of the hard-sphere model analysis were carried out with the rod voltage of 10 kV.[16] The results of the orientation dependences of the emission intensities for CN(B → X) and for CN(A → X) are listed in table V-1. The CN-end attack was more favorable on the formation of the excited CN radicals than the CF_3-end attack in both cases, and this tendency is similar in that in the reaction of Ar* with acetonitrile.[17]

The ratio of the reaction cross section for the CN-end attack to that for the CF_3-end attack was determined to be 1.6 ± 0.2 in the formation of CN(B) using a hard-sphere model which has been used in the reaction of Ar* with acetonitrile so far. This value is almost equal to that for the CD_3CN + Ar* reaction but it is smaller than that for the CH_3CN + Ar* reaction. Similarly, the orientation dependence of the formation of the CN(A) radical was determined and the ratio of the reaction anisotropy in the formation of CN(A) was found to be 1.5 ± 0.2. This value is almost same as that in the formation of the CN(B) radical.

Table V-1. Orientation dependences of the violet and the red emissions of the excited CN radicals.[a)]

attacking side	total emission intensity of CN(B→X) / count pulse^{-1}	total emission intensity of CN(A→X) / count pulse^{-1}
CN-end	0.21	0.12
CF_3-end	0.15	0.09
non-oriented	0.18	0.10

a) The gatewidth of the photon counting was 3 ms. The estimated standard deviations was within 5%.

C. V_0 dependences of the CN(B → X) and the CN(A → X) emissions

To obtain the opacity function, the V_0 dependences on the emission intensity should be measured. In this study, the hexapole voltage, V_0, from 6 to 12 kV was changed.

Table V-2 lists the calculated Legendre moments of the CF_3CN molecules. Figure V-2 shows the orientational distributions of the CF_3CN beam after the state selection at three specified values of V_0 (0, 6, and 12 kV). The inner panel in the figure shows its polar coordinate representation.

Figure V-3 shows the V_0 dependences on the emission intensities of CN(B → X) in three collisional geometries (CN-end, CF_3-end, and random orientation). The experimental points were averaged over 7500 pulses for each orientation at higher V_0 and 25500 pulses at lower V_0. It was found the CN-end attack was more favorable than the CF_3-end attack. The experimental error is within the circles. The vertical scale are normalized to the intensity at 10 kV. The emission for the random orientation have the almost mean values between both orientation. The solid line for the random orientation is the result of the trajectory simulation.

Figure V-4 shows the V_0 dependences of the CN(A → X) emission intensities in three orientations. The CN(A → X) emission intensity was weak as compared with the CN(B → X) emission intensity. Therefore, the lower V_0 cannot be observed. The experimental points were averaged over 36000 at 8 kV and 24000 at other voltage. The experimental error is almost same as that of the measurement of the CN(B → X) emission. The emission intensities for the CN-end attack is the largest in all orientation as same as that for the CN(B → X) emission.

D. Opacity functions for the formations of CN(B) and CN(A)

Table V-2. The Legendre moments for the orientational distribution of the CF_3CN molecule[a)]

	Hexapole voltage V_0				
	6.0	7.0	8.0	10.0	12.0
$<C_1>$	0.623	0.607	0.591	0.555	0.520
$<C_2>$	0.219	0.196	0.174	0.128	0.086
$<C_3>$	0.026	0.013	0.002	-0.019	-0.031
$<C_4>$	-0.005	-0.008	-0.010	-0.009	-0.002
$<C_5>$	0.003	0.003	0.002	0.005	0.008
$<C_6>$	0.003	0.004	0.002	0.002	0.000
$<C_7>$	-0.001	0.001	0.000	0.000	-0.002
$<C_8>$	-0.001	-0.001	-0.001	-0.001	-0.001

a) $<C_n>$ stands for the n-th Legendre moments

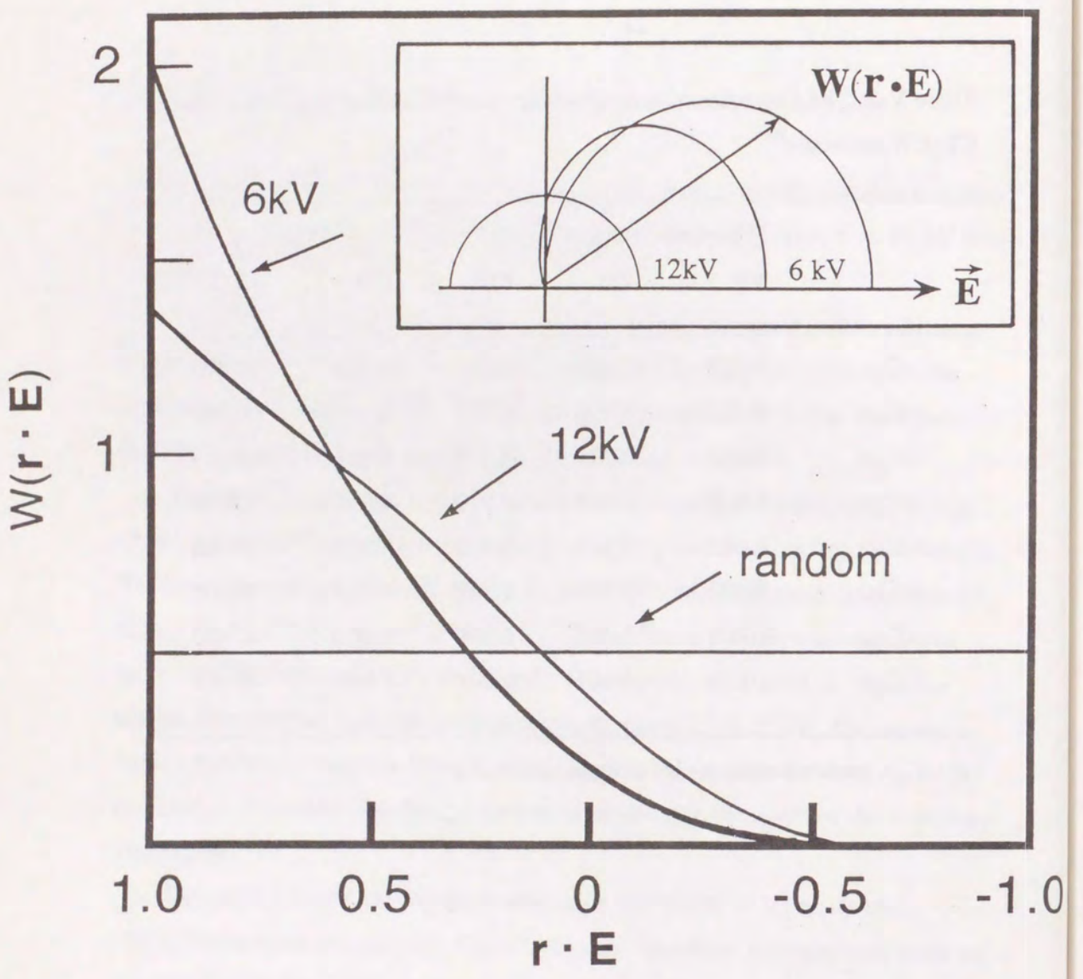

Figure V-2. Determined the quantal orientational distributions W(cosθ) of the CF_3CN beam after the hexapole field at three different V_0. The inner panel shows their polar coordinate representations.

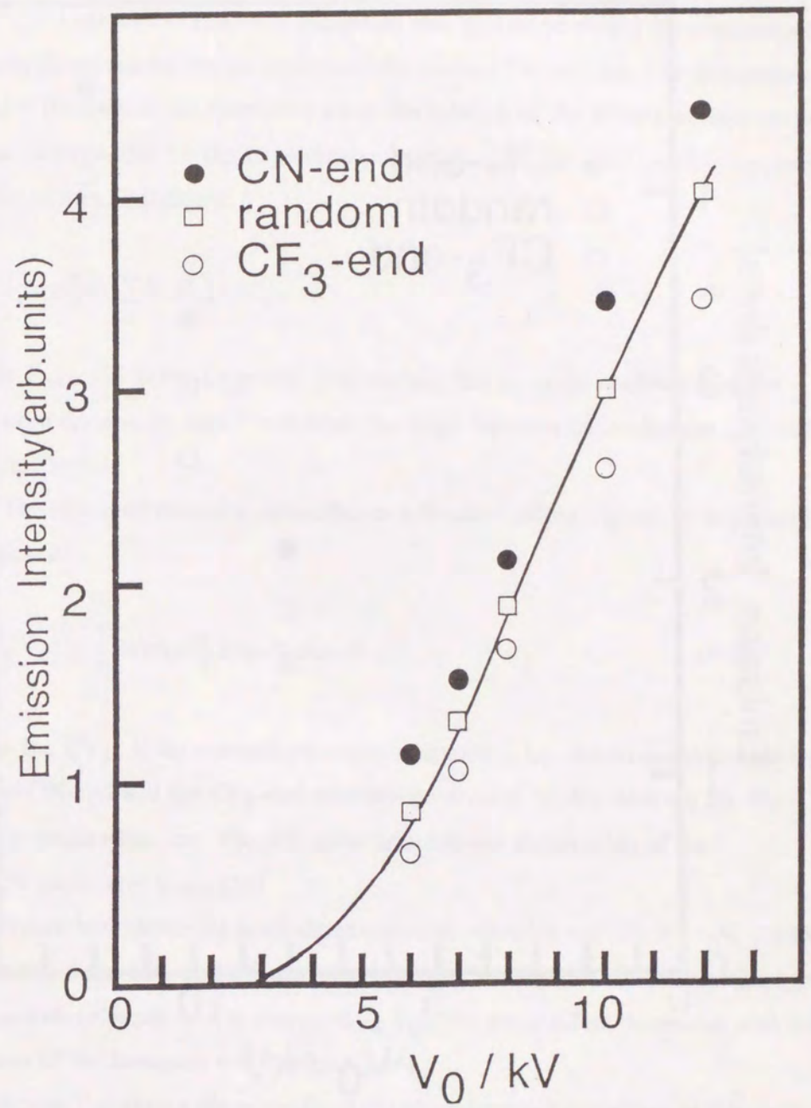

Figure V-3. V_0 dependence of the CN(B→X) emission intensities for the three collisional orientations. The emission intensities for the CN-end attack were found to be significantly lager than those of CF_3-end attack. The emission intensities for the randomly oriented molecules have almost the mean value of those orientation. The solid line is the result of the Monte Carlo trajectory simulation.

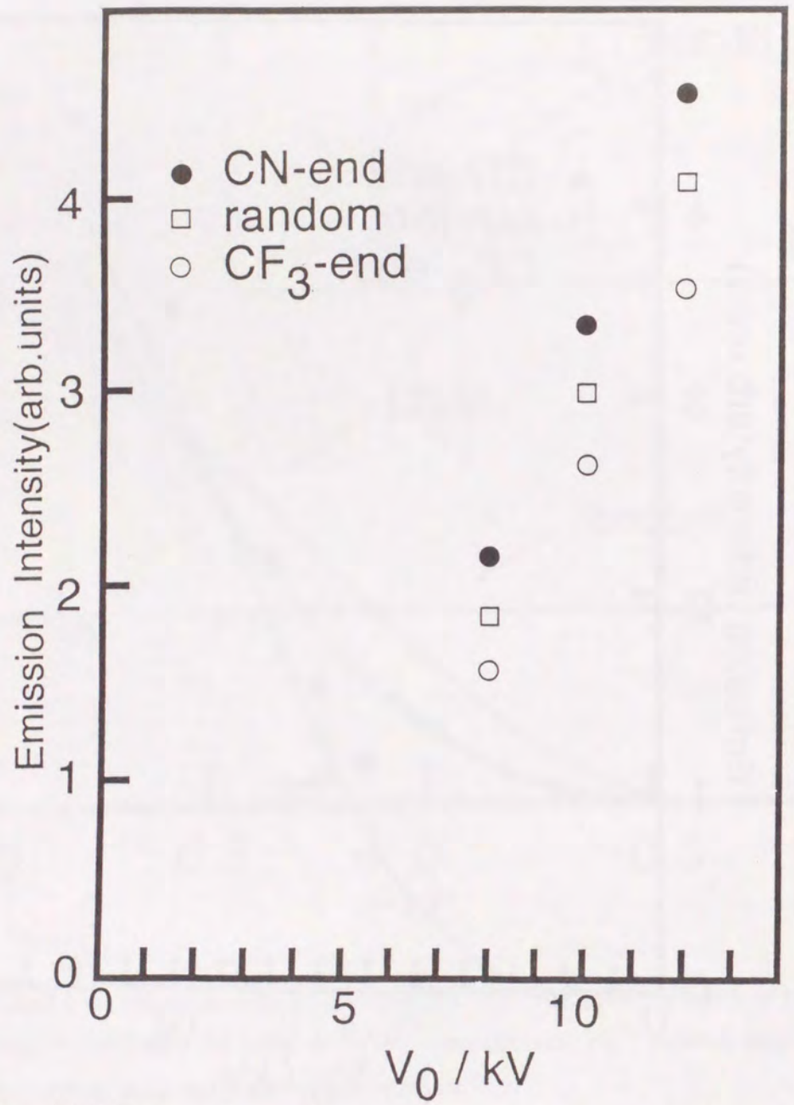

Figure V-4. V_0 dependence of the CN(A→X) emission intensities for the three collisional orientations.

The Legendre polynomial expansion was applied to obtain the orientational opacity functions for the formations of the excited CN radicals. The orientational opacity function is the symmetry about the rotation of the molecular axis, so that it can be expanded by the Legendere polynomials.[18,19] The opacity function can be written as follows:

$$I(\cos\theta) = \sum_n S_n P_n(\cos\theta), \qquad \text{(V-1)}$$

where $P_n(\cos\theta)$ is the Legendre polynomials, the S_n is the coefficient of the Legendre expansion, and θ is defined the angle between the molecular axis and the electric field.

The observed emission intensities as a function of the V_0 can be expressed as follows:

$$I(V_0) = \int_{-1}^{1} W(\cos\theta)\, I(\cos\theta)\, d\cos\theta \ , \qquad \text{(V-2)}$$

where the $I(V_0)$ is the normalized emission intensity, i.e., the emission intensities for the CN-end and the CF_3-end orientations divided by the intensity for the random orientation, the $W(\cos\theta)$ is the orientational distribution of the CF_3CN molecular beam.[20]

Figure V-5 shows the normalized emission intensities of CN(B → X) for the CN-end and the CF_3-end orientations, which are normalized to the intensities for the random orientation at corresponding V_0. The steric effect decreased with the increase of the hexapole rod voltage V_0.[6]

Figure V-6 shows the normalized chemiluminescent intensities of CN(A → X) for the CN-end and the CF_3-end orientations as same as that of the CN(B → X) emission. There is a similar tendency that the steric effect decreased with increasing V_0.

The opacity function was obtained that the experimental points of the normalized chemiluminescent intensities are fitted by equation (V-2), and are

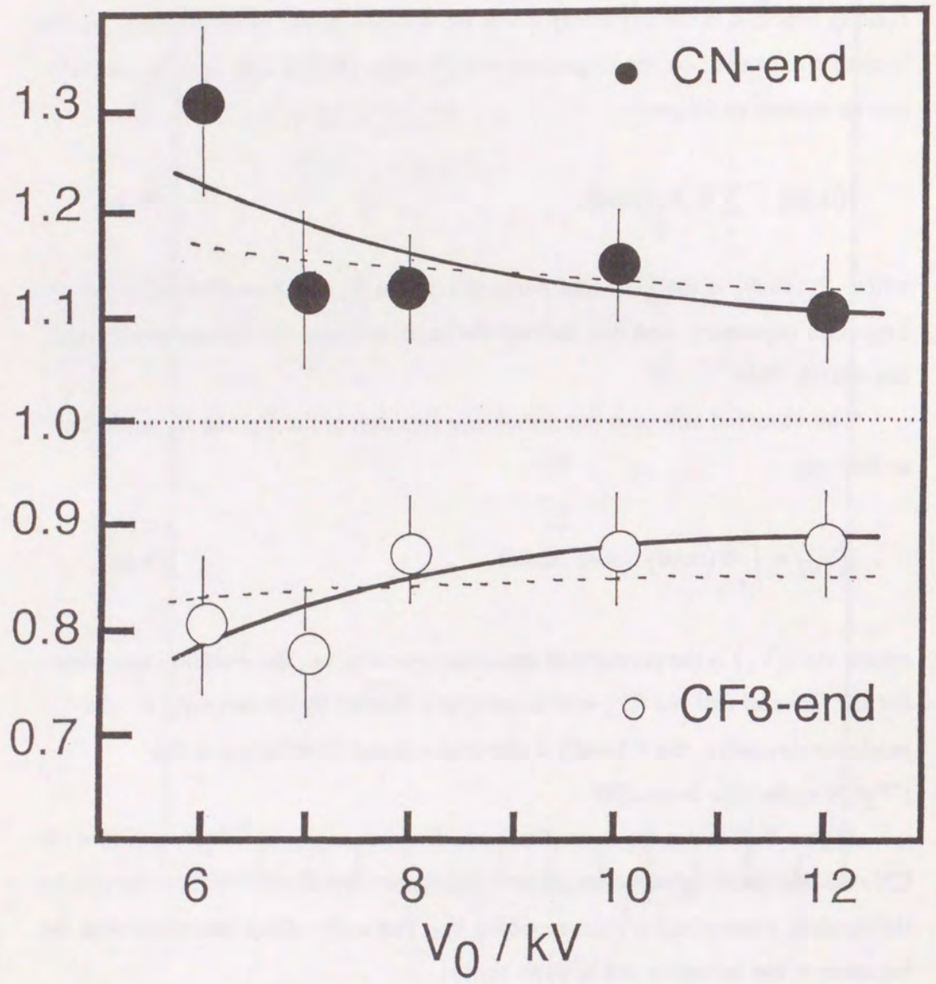

Figure V-5. Normalized CN(B→X) chemiluminescent intensities for the CN-end and the CF_3-end attack, which are normalized to the intensities for the random orientation at the corresponding V_0. Solid line is the result of the Legendre fitting with N = 3, and dashed line is that with N = 2.

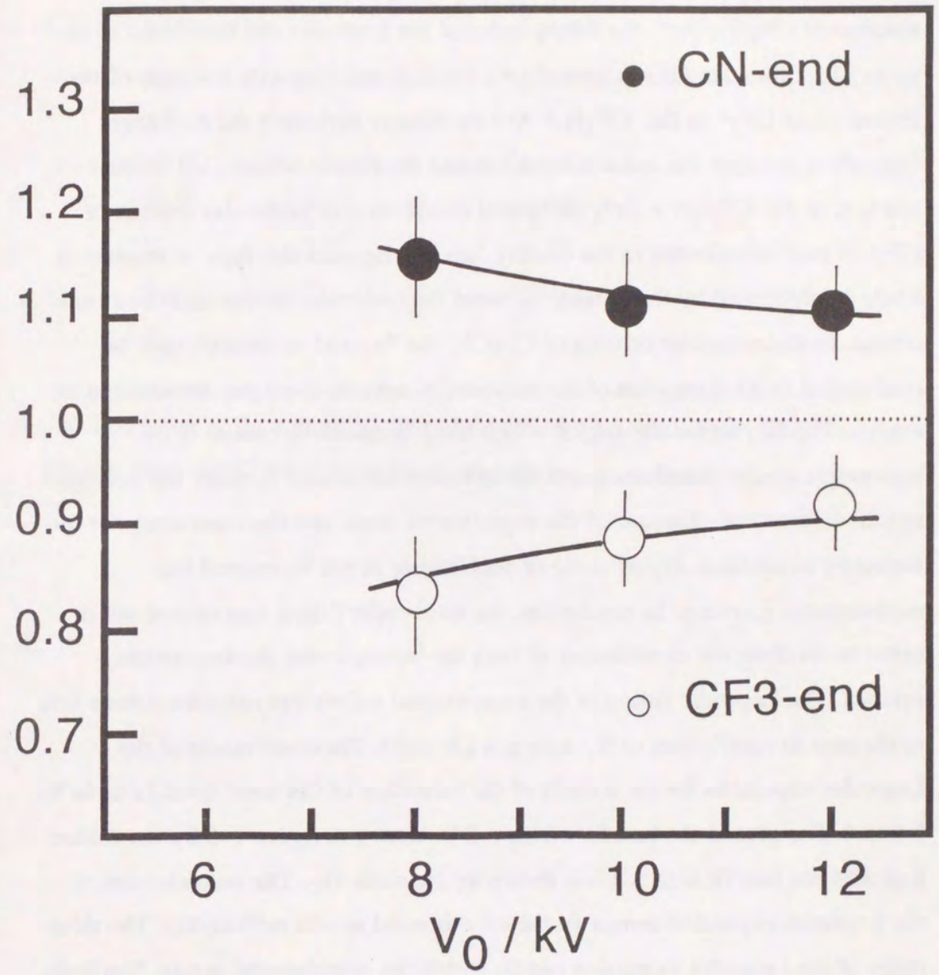

Figure V-6. Normalized CN(A→X) chemiluminescent intensities for the CN-end and the CF_3-end attack, which are normalized to the intensities for the random orientation at the corresponding V_0. Solid line is the result of the Legendre fitting with N = 3.

determined to the coefficient of the Legendre expansion, S_n.[12] Here, it is important to estimate the fitting order of the Legendre expansion.[18] In the reaction of CF_3H + Ar*, the fitting order of the Legendre has been used to be up to fifth-order. And it has been shown the fifth-order opacity function of the formation of CF_3* in the CF_3H + Ar* reaction is attributed the exchange interaction between the molecular orbital and the atomic orbital.[12] In the reaction of the CF_3CN + Ar*, the spatial distribution of molecular orbitals of CF_3CN may be reflected in the opacity function because this type of reaction is likely to proceeded by the overlap between the molecular orbital and the atomic orbital. In the molecular orbitals of CF_3CN, the $7a_1$ and 2e orbitals may be contributed in the formation of the excited CN radicals if we pay attention to its energy. The $7a_1$ molecular orbital which has a nonbonding orbital is the anisotropic spatial distribution and the 2e molecular orbital is rather the isotropic spatial distribution. Because of the experimental error and the inaccuracy for the trajectory simulation, higher order of coefficients might be beyond the experimental accuracy. In conclusion, the third-order fitting was carried out in order to simulate the contribution of both the isotropic and the anisotropic orbitals. The Legendre fitting of the experimental points was calculated three sets of the best-fit coefficients of S_n with n = 1,2 and 3. The coefficients of the Legendre expansion for the I(cosθ) of the formation of CN were listed in table V-3 and 4. The plot of the best fit with n = 2 is shown in figure V-5 by the dashed line, and the best fit with n = 3 is shown by the solid line. The second-order of the Legendre expansion cannot fit the experimental results sufficiently. The third-order of the Legendre expansion can fit within the experimental errors. Similarly, the third-order of the Legendre fitting was carried out for the formation of the CN(A) radical. The result is shown by the solid line in figure V-6.

The orientational opacity function, I(cosθ), of the formation of CN(B) in the case of the n = 3 is demonstrated in figure V-7. The I(cosθ) shows that the CN-end attack is the most reactive and the region of cosθ ~ 0.5 is also favorable in the formation of CN(B). The reactivity of the CF_3-end attack is almost zero.

TableV-3. Coefficients of the Legendre expansion for the I(cosθ) of the CN(B→X) emission

N =	1	2	3
S_0 [a)]	1.00	1.00	1.00
S_1	0.27	0.27	0.28
S_2		0.01	0.01
S_3			1.14

a) The value of S_0 was set as unity because of the normalization requirement for the observed CN(B→X) emission intensities.

TableV-4. Coefficients of the Legendre expansion for the I(cosθ) of the CN(A→X) emission

N =	1	2	3
S_0 [a)]	1.00	1.00	1.00
S_1	0.22	0.22	0.26
S_2		0.03	0.04
S_3			1.21

a) The value of S_0 was set as unity because of the normalization requirement for the observed CN(A→X) emission intensities.

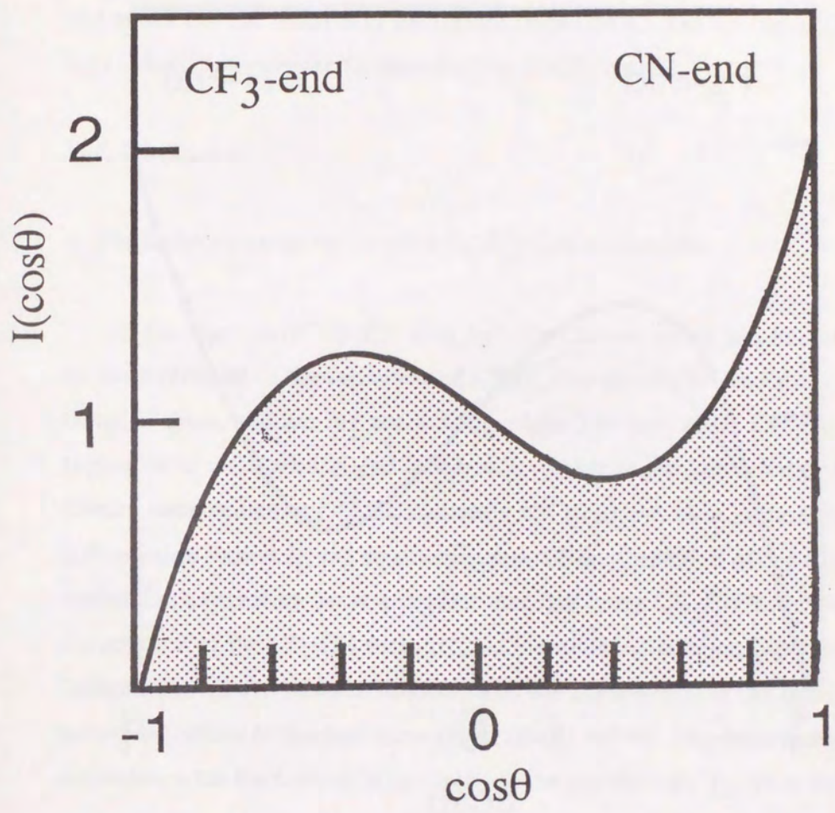

Figure V-7. Orientational opacity function for the CN(B→X) formation which deconvoluted by the Legendre expansion with N = 3.

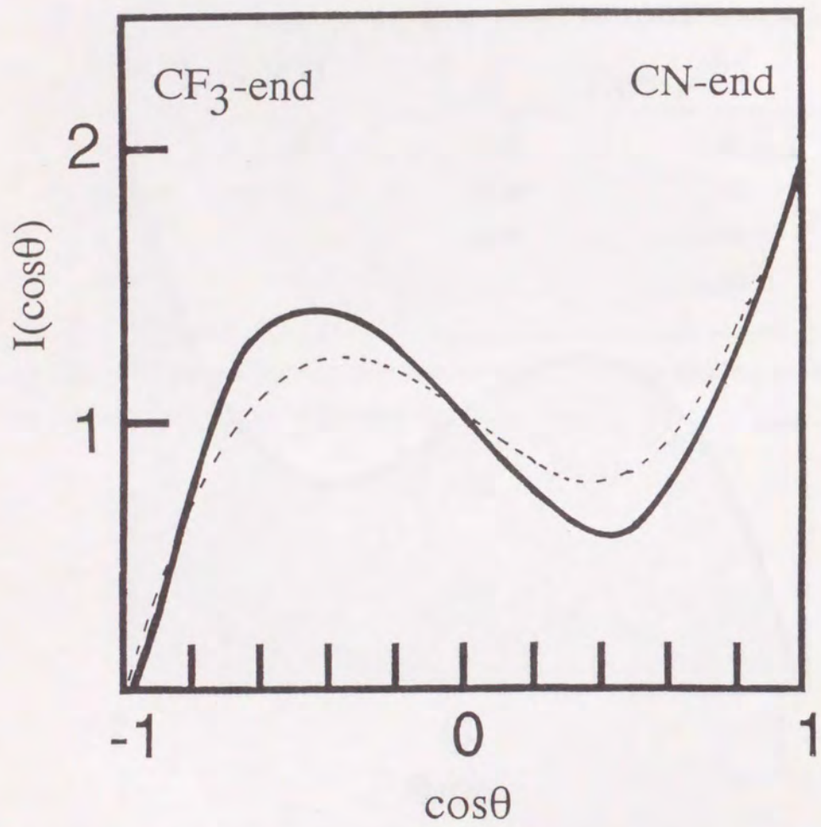

Figure V-8. Orientational opacity function for the formation of CN(A→X) which deconvoluted by the Legendre expansion with N = 3. Dashed line represents the result of the orientational opacity function for the formation of CN(B→X).

The I(cosθ) of the formation of CN(A) is shown by the solid line in figure V-8. The dashed line in the figure is the orientational opacity function of CN(B). The shape of the opacity functions is almost similar to each other. Namely, the CN-end attack is most reactive in the formation of CN(A), and the region of cosθ ~ 0.5 is also reactive in the formation of the CN(A) radical.

V-4. Discussion

A. The comparison to the reaction of Ar with acetonitrile*

In the reaction of CH_3CN with Ar*, the CN-end attack has been shown to be more efficient in the formation of CN(B) than the methyl-end attack by a factor of three, and the $7a_1$ nonbonding orbital localized at the CN-end was suggested to make the CN-end attack be favorable in the formation of CN(B). Similar stereoanisotropy of the formation of CN(B) was seen in the CF_3CN + Ar* reaction, however, the stereoanisotropy of the formation of the excited CN radical in this reaction became smaller than that in the CH_3CN + Ar* reaction. In the reaction of the CD_3CN with Ar*, the dissimilar orientation dependence of the formation of CN(B) has been explained by the contribution of the isotropic 2e molecular orbital to the formation of the CN(B) radical. The observed orientation dependence for the formation of CN(B) in the reaction of CF_3CN + Ar* by the analysis using a hard-sphere model is close to the rather isotropic value of 1.5 for the CD_3CN + Ar* reaction. It was known that the energy of the $7a_1$ and the 2e orbitals of CF_3CN molecule is the almost same.[21]

The formation of CN(B) in the CF_3CN + Ar* reaction, therefore, may contribute the $7a_1$ or the 2e orbitals of molecule. The decrease of the stereoanisotropy in the formation of CN(B) as compared with the CH_3CN reaction is explained due to the additional contribution of the 2e orbital as that in the CD_3CN reaction. More detail discussion will be given from the result of the feature of the opacity function.

The observed stereoanisotropies for the formations of CN(B) and CN(A) in the reaction of CF_3CN + Ar* were almost equal to each other. It suggests that the isotropic and anisotropic molecular orbitals are contributed in the formation of the CN(A) radical in a similar way to that of the CN(B) radical.

B. The feature of the opacity function.

In the reaction of CF_3CN + Ar*, it was suggested that the isotropic and anisotropic molecular orbitals contribute to the formation of the CN(B) and the CN(A) radicals, where the isotropic molecular orbital is the 2e and the anisotropic orbital is the $7a_1$ molecular orbital of CF_3CN. The shape of the 2e orbital is localized around the F atom and the CN bond [22], and the $7a_1$ orbital is localized at the CN-end.

Figure V-9 shows the opacity function of the excited CN formation by the polar coordinate. The dashed line shows the envelope of spheres of van der Waals radii. It clearly shows three reactive regions, that is, the CN-end, and the region around the CN bond and around the F atom. This result could suggest the shape of the opacity function is the reflection of the shape of the $7a_1$ and 2e molecular orbitals of CF_3CN.

It should be emphasized that the selection of molecular orbital can be possible by use of the oriented molecular beam,

C. The reaction branching

The experimental results showed the orientation dependences of the formations of CN(B) and CN(A) are almost equal to each other within the experimental error. Because of the insufficient theoretical information about the potential surface of especially the excited state in this reaction, the qualitative explanation is tentatively provided.

In the previous section, it was suggested that the orientation dependences of

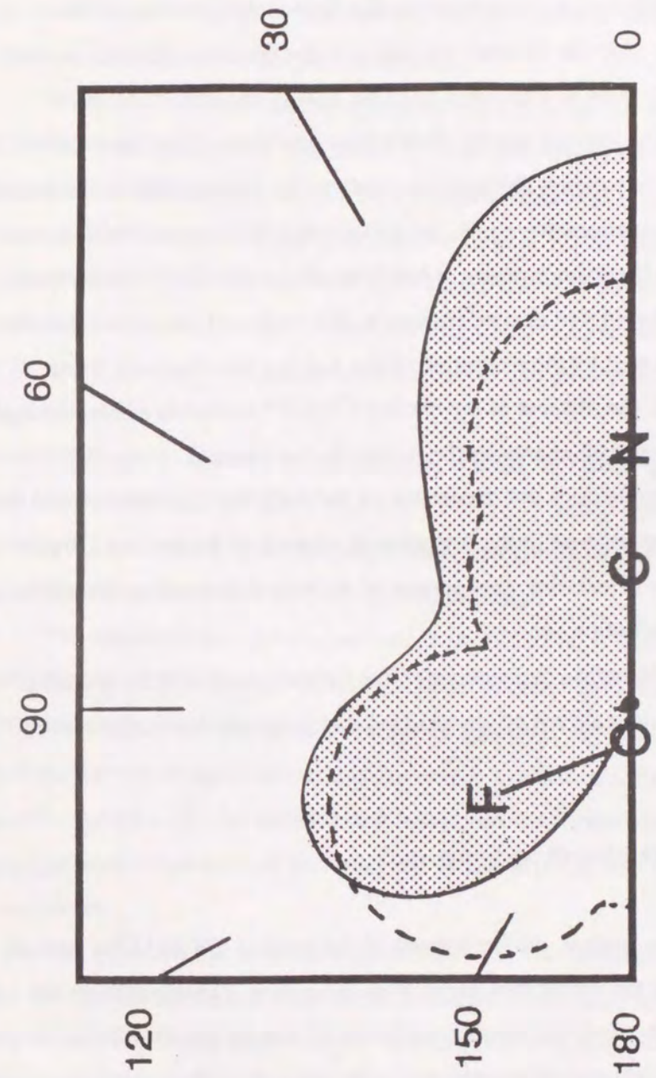

Figure V-9. Opacity function of the excited CN radical formation by the representation of the polar coordinate. Dashed line shows the envelope of the molecular surface which illustrated by van der Waals radii of each atoms.

the formations of the excited CN radicals caused in the excitation process which is the electron exchange between Ar* and molecule. Next objective is to investigation the orientation dependence in the dissociation process of the CF_3CN^* molecule after the electron exchange. If the dissociation time of the excited molecule is short as compared with the energy redistribution in the excited molecule, the internal energy distribution may depend on the collisional geometry, and the orientation dependence exists in the dissociation of the excited molecule. In our experimental results, the dissociation time can not be estimated. However, in photodissociation study, it has been shown the CN(B) radical was formed through a long-lived excited molecule. We tentatively assumed that the excited radicals formed by the excitation of the Ar* are also the long-lived excited molecule. If the lifetime of the excited CF_3CN^* molecule is long enough to redistribute the internal energy in the molecule, the internal energy distribution of the excited molecule does not dependent on the collisional geometry, and there is no orientation dependence in the dissociation process of the excited CF_3CN^* molecule. Thus, the orientation dependence of the radical formation should be originated in the excitation process.

The similar orientation dependence of the formations of CN(B) and CN(A) indicates that both radicals are originated from the same electronically excited state of CF_3CN^*.

D. Comparison with photodissociation study

In the previous section, the formations of the excited CN and CF_3 radicals by the excitation of the metastable argon were described. These products are produced via the electronically excited molecule. However, the excited molecule cannot be assigned because of uncertainty in the amount of the energy deposited in the energy transfer from the Ar*. Even if the means of the excitation is different, the photoexcitation of molecule is interesting in the comparison with chemical excitation after the energy transfer. In the photoexcitation, the state of

the electronically excited molecule can be assigned, so that it may provide some informations into the study of the chemical excitation. In this thesis, the photoexcitation of CF_3CN was studied, and the chemical excitation by the Ar* atom was compared to the photoexcitation.

Figure V-10 schematically shows the apparatus for the photoexcitation of CF_3CN. The light source was used UV-SOR (BL-2A) synchrotron radiation in Institute for Molecular Science.[23] The wavelength region of exciting photon is between 105 and 130 nm and resolution of light is 1.0 Å. This exciting region is almost similar to the excitation of Ar*. The CN(A→X) emission was detected by the photomultiplier through a filter, and the CN(B→X) emission and the $CF_3^*(2A'_1 \rightarrow 1A''_2)$ emission was detected by the photomultiplier through a monochromator.

Figure V-11 shows the absorption spectrum for the CF_3CN molecule and the emission spectra of CN(B→X) and CN(A→X). In the figure, the thick line shows the absorption spectrum, the dashed line shows the CN(A→X) emission and the broken line shows the CN(B→X) emission.

The observed absorption spectrum is no structure. It is a similar result of the reference [21]. Ashfold and Simos has been assigned the absorption spectrum of CF_3CN. It has been shown this absorption spectrum was assigned to the $7a_1 \rightarrow 3s$ and the $2e \rightarrow 3s$ transitions and the $7a_1$ and 2e orbitals of CF_3CN molecule have similar energies.[21] In addition, the broad and very weak absorption around 140 nm has been observed and was assigned to the $7a_1 \rightarrow 3e$ and the $2e \rightarrow 3e$ transitions.

The weak emission in the region of 240 nm was detected and is shown by the thin line in the figure. This emission cannot be detected in the wavelength region of the exciting photon below 110 nm(11.3 eV), and this value is almost same to the energy for the formation of CF_3^* radical. (The dissociation energy of CF_3-CN is 4.9 ± 0.3 eV and the differences between the upper state energy of the UV emission and the ground state of CF_3 radical is 6.4 eV.) We concluded the emission in the region of 240 nm is the emission from the $CF_3(2A'_1 \rightarrow$

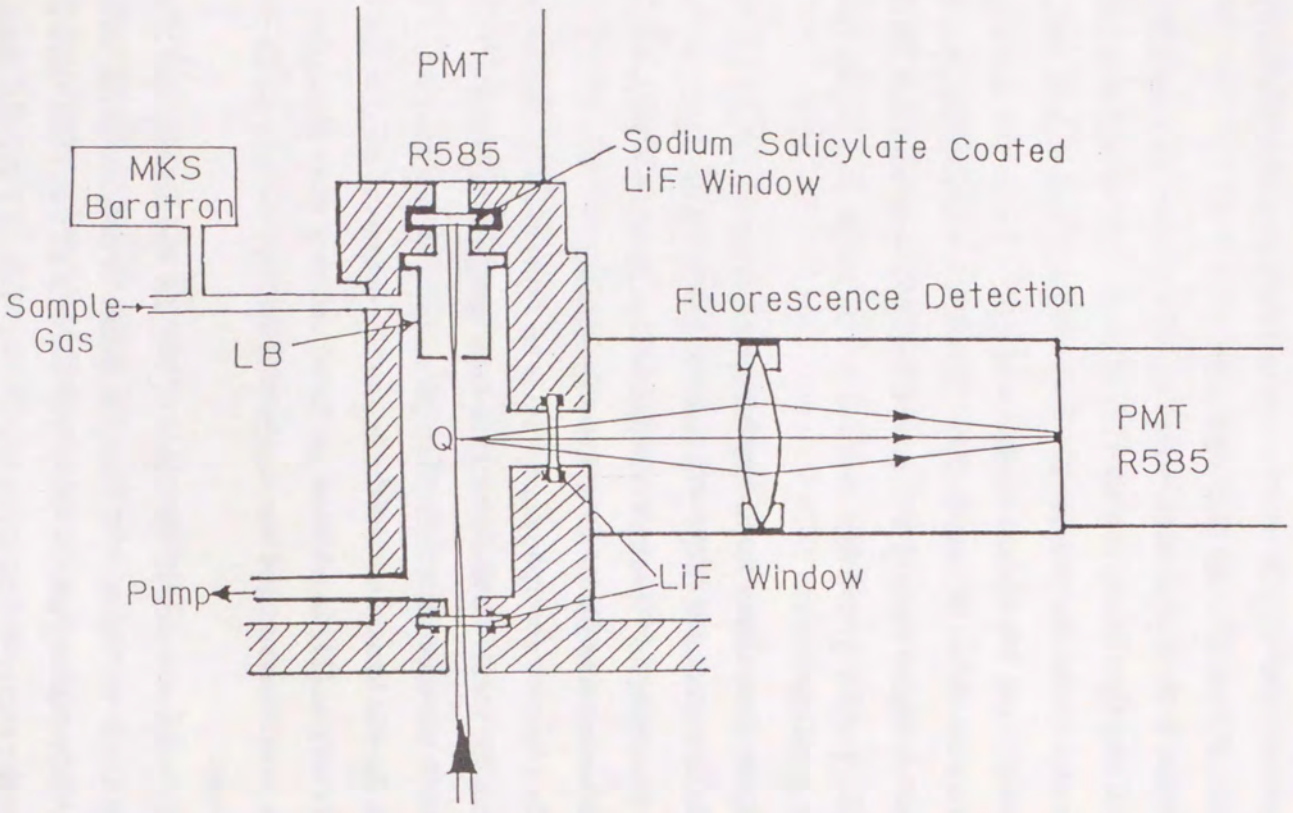

Figure V-10. Apparatus for the photoexcitation experiment.

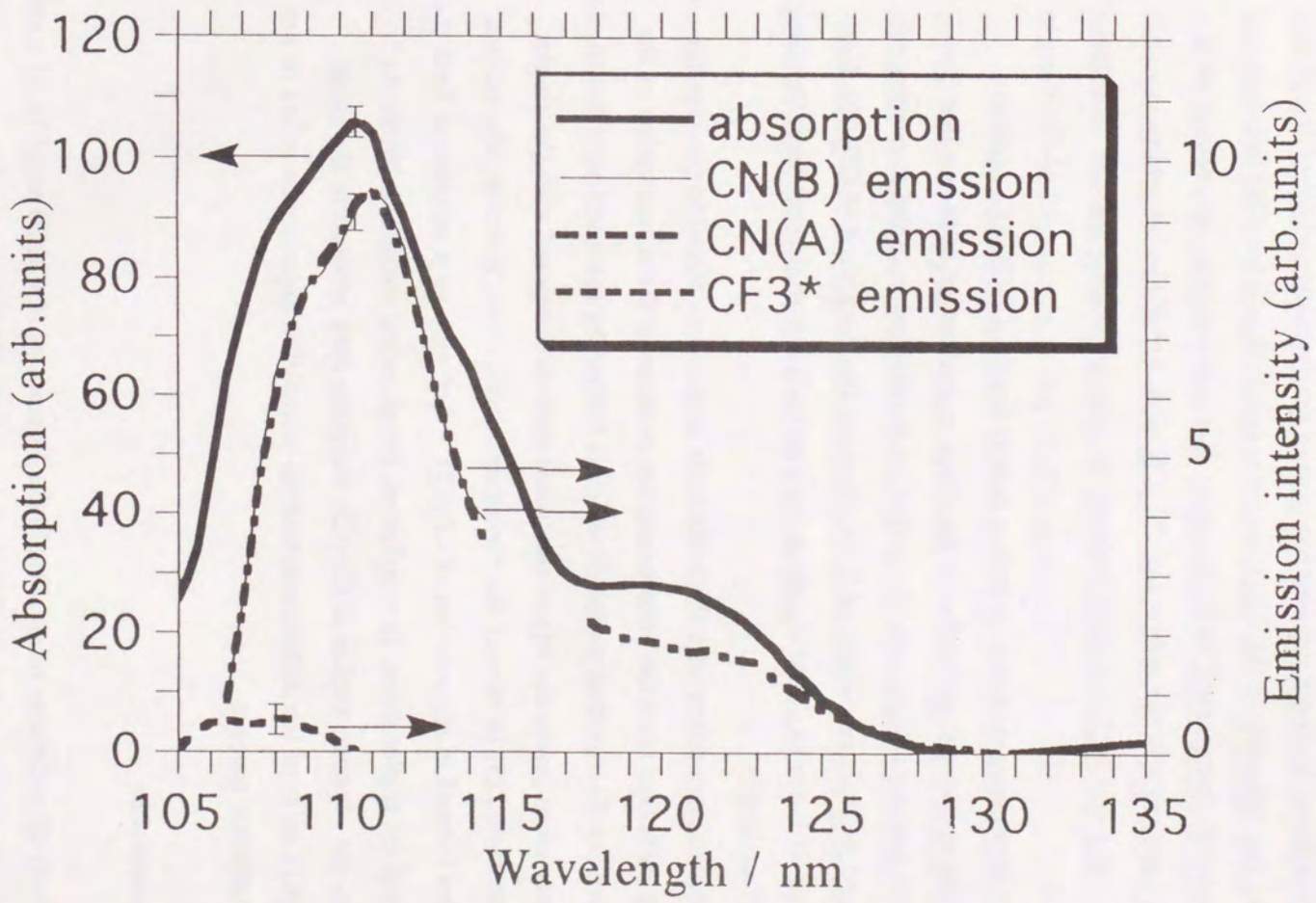

Figure V-11. Absorption and fluorescence excitation spectra of CF_3CN.

$1A''_2$) transition. It shows the reaction path of the formation of CF_3* is opened. However, the intensity of the CF_3* emission is less than a hundred times as compared with that in the CN(B) emission. It is reasonable to be undetected of the CF_3* emission in the reaction of CF_3CN with Ar* if the branching ratio of the formation of CF_3* is similar between the photoexcitation and the chemical excitation.

The dependences of the excitation energy for the CN(B→X) and the CN(A→X) emissions are similar in the shape to each other. It shows that both the CN(B) and the CN(A) radicals in spite of the difference in the symmetry of the formed radical are originated from the same Rydberg state of CF_3CN. It is consistent with our explanation which both radicals are originated from the same CF_3CN* molecule.

Chemical excitation with the metastable atoms is expected to produce the different pathways from the photoexcitation because of the conservation of the spin manifold. The excited molecule which is formed by the reaction of the triplet metastable atom favors the triplet electronic state as compared with the singlet electronic state.[23] In case of the metastable argon atom, however, the excited molecules formed in the reaction of CF_3CN + Ar* may be a mixture of both the singlet and the triplet states. In conclusion, the chemical excitation by the Ar* atom and the photoexcitation of CF_3CN molecule may proceed in the same pathways in spite of the differences that the orientation dependence exists or not in the excitation process.

V-5. Conclusion

Effects of molecular orientation in the formations of CN(B) and CN(A) were studied in the reaction of Ar* with the oriented CF_3CN molecule. The orientation dependence of the formation of the excited CN radical exists in the excitation process by the Ar* atom. The stereoanisotropies for both radical formations in the reaction were almost equal to each other. The values were found to be 1.6 ± 0.2 in the formation of CN(B), and 1.5 ± 0.2 in the formation of CN(A) by the analysis using a hard-sphere model. These values are close to that in the CD_3CN + Ar* reaction, but smaller than that in the CH_3CN + Ar* reaction. The opacity functions for both radical formations were obtained by the Legendre expansion technique. The shape of the opacity function was attributed to the molecular orbitals of the $7a_1$ and 2e of the CF_3CN molecule.

It should be emphasized that the excitation of the particular molecular orbital can be selected using the oriented molecules. In future, the selection of the particular molecular orbital provide the information to the study of the relationship between the molecular orbital and the reaction branching, and it may provide many insights into the control of reaction.

References

[1] R.J. Beuler, R.B. Bernstein, K.H. Kramer, *J. Am. Che. Soc.* **88** (1966) 5331

[2] P.R. Brooks, *Science.* **193** (1976) 11

[3] S. Stolte, *Ber Bunsen-Ges. Phys. Chem.* **86** (1982) 413

[4] R.B. Bernstein, D.R. Herschbach, R.D. Levine, *J. Phys. Chem.* **91** (1987) 5365

[5] D.H. Parker, R.B. Bernstein, *Annu. Rev. Phys. Chem.* **40** (1989) 561

[6] Bernstein Memorial Issue on Molecular Dynamics, *J. Phys. Chem.* **95** (1991)

[7] C.T. Rettner, Z.N. Zare, *J. Chem. Phys.* **77** (1982) 2416

[8] M.S. de Vries, V.I. Srdanov, C.P. Harrahan, R.M. Martin, *J. Chem. Phys.* **77** (1982) 2688

[9] M.S. de Vries, G.W. Tyndall, C.L. Cobb, R.M. Martin, *J. Chem. Phys.* **86** (1987) 2653

[10] T. Kasai, D.-C, Che, K. Ohashi, K. Kuwata, *Chem. Phys. Lett.* **163** (1989) 246

[11] D.-C. Che, T. Kasai, H. Ohoyama, K. Ohashi, T. Fukawa, K. Kuwata, *J. Phys. Chem.* **95** (1991) 8159

[12] H. Ohoyama, T. Kasai, K. Ohashi, *Chem. Phys.* **165** (1992) 155

[13] G. Hertzberg, *Molecular Spectra and Molecular Structure 1. Spectra of Diatomic Molecules.* Var Nostrand. (1950)

[14]G. Scoles, Ed. *Atomic and molecular beam methods.* Oxford University Press: Oxford, **Vol.1** (1988)

[15] S.E. Choi, R.B. Bernstein, *J. Chem. Phys.* **83** (1985) 4463; S.E. Choi, R.B. Bernstein, *J. Chem. Phys.* **85** (1986) 150

[16] R.J. Beuhler Jr. R.B. Bernstein, *J. Chem. Phys.* **51** (1969) 5305; G. Marcelin, P.R. Nrooks, *J. Am. Chem. Soc.* **97** (1975) 1810; P.R. Brooks, J.E. Jones, *J. Chem. Phys.* **45** (1966) 3449; R.J. Beuhler Jr, R.B. Bernstein, K.H. Kramer, *J. Am. Chem. Soc.* **88** (1966) 5331

[17] T. Kasai, D.C. Che, K. Ohashi, K. Kuwata, *Chem. Phys. Lett.* **163** (1989)

246; D.C. Che, T. Kasai, H. Ohoyama, K. Ohashi, T. Fukawa, K. Kuwata, *J. Phys. Chem.* **95** (1991) 8159

[18] S. Stolte, K.K. Charkravorty, R.B. Bernstein, D.H. Parker, *Chem. Phys.* **71** (1982) 353

[19] R.B. Bernstein *J. Chem. Phys.* **82** (1985) 3656; Y.M. Engel, R.D. Levine, *Chem. Phys.* **91** (1984) 167; D. van der Ende, S. Stolte, *Chem. Phys.* **89** (1984) 121; S.E. Choi, R.B. Bernstein, *J. Chem. Phys.* **83** (1985) 4463

[20] S.E. Choi, R.B. Bernstein, *J. Chem. Phys.* **85** (1986) 150

[21] M.N.R. Ashfold, J.P. Simons, *Trans. Faraday. Soc. 2.* **74** (1978) 1263

[22] Y. Fukunishi, private communication.

[23] K. Shoubatake et al., *Ann. Rev. IMS* (1986) P 96; UV-SOR activity report 1984/1985, p 43; K. Shoubatake, S. Ohshima, A. Hiraya, Y. Matsumoto, K. Tabayashi, *Inter. Conf. on Photochemistry.* Tokyo, August, (1985), Book of Abstract.

Acknowledgment

The author is deeply indebted to many people for the work presented in this thesis. The author would first like to thank to express his sincere gratitude to Professor Keiji Kuwata for continuing guidance, encouragement, and helpful advices. The author would like to thank Dr. Toshio Kasai for his many valuable suggestions, encouragement, and his help in the experimental work. The author wishes to thank Dr. Hiroshi Ohoyama for enduring his many questions, and teaching him the skills of the work. The author is grateful to Dr. Hisao Murai for his continuous and heartfelt encouragement.

The author thanks the staff of the machine shop in central workshop, Osaka University, for their fine and laborious work in building the machine. The author is indebted to Dr. K. Shoubatake and Dr. K. Tabayashi for the UV-SOR experiment.